UNIVERSITY OF SOUTHAMPTON

in the
Faculty of Engineering
School of Electronics and Computer Science

Improved Broadband Adaptive Beamformer Performance

by

Neil Tisdale

A thesis submitted in partial fulfilment for the
degree of Doctor of Engineering

January 2010

UNIVERSITY OF SOUTHAMPTON

Abstract

Faculty of Engineering
School of Electronics and Computer Science

Doctor of Engineering

by Neil Tisdale

The protection of wireless communications links against interference is a key concern in mission critical systems. In particular low probability of interception (LPI) systems which operate below the thermal noise floor of the receiver are particularly vulnerable. To protect against interference it is often necessary to include some form of active interference suppression. Broadband adaptive beamforming is one such technique which may be used to suppress interference by spatial and spectral filtering of the signals received by an array antenna. The hardware requirements of adaptive beamforming systems are high in comparison to other approaches. As a result, the total number of adaptable weights realisable in the beamformer may be limited by the size, weight and power constraints of the system. This will limit the degrees of freedom in the beamformer and hence, the interference cancellation capability of the beamformer.

The effectiveness of increasing the number of time-taps in space-time adaptive processors (STAP) as a method of increasing the number of interferers the beamformer can simultaneously cancel in an environment containing a mix of narrowband, partialband and broadband interference is studied. An alternative scheme to free up degrees of freedom in the beamformer is proposed based on frequency-domain excision to pre-filter narrowband interference before it reaches the beamformer. This approach frees up degrees of freedom in the beamformer, which would otherwise be consumed by the narrowband interference, for use in cancelling partialband and broadband interference. To enable the excision filters to identify narrowband interference while allowing partialband and broadband interference to pass through, a novel scheme is presented which produces a frequency mask that varies on a per-bin basis. Eigenanalysis of the beamformer's covariance matrix is used to explore the ability of frequency-domain excision to desensitise the beamformer to narrowband interference while bit error rate (BER) simulations demonstrate the enhanced interference protection the scheme affords an LPI communications link.

Mismatches between the gain and phase responses of the radio-frequency (RF) front-end channels in broadband adaptive beamformers can limit their cancellation performance against higher power partialband and broadband interference. This performance limitation arises from the decorrelation experienced by the received signals across the array due to the interchannel mismatches. In STAP systems this performance limitation may be mitigated by increasing the number of taps per channel in the STAP. However, the computational complexity of adding additional time-taps tends to be high in STAP beamformers. Two new methods of interchannel mismatch compensation are proposed based on efficient frequency-domain methods. Simulations using software models and experiments using a hardware STAP system demonstrate the proposed techniques' ability to improve the cancellation performance where interchannel mismatches are limiting cancellation performance.

Contents

List of Figures

Declaration of Authorship

I, Neil Tisdale, declare that this thesis titled, 'Improved Broadband Adaptive Beamformer Performance' and the work presented in it are my own. I confirm that:

- this work was done wholly or mainly while in candidature for a research degree at this University.
- where any part of this thesis has previously been submitted for a degree or any other qualification at this University or any other institution, this has been clearly stated.
- where I have consulted the published work of others, this is always clearly attributed.
- where I have quoted from the work of others, the source is always given. With the exception of such quotations, this thesis is entirely my own work.
- I have acknowledged all main sources of help.
- where the thesis is based on work done by myself jointly with others, I have made clear exactly what was done by others and what I have contributed myself.
- parts of this work have been published as: [1–3].

Signed: _____

Date: _____

Acknowledgements

I would like to thank Dr. Tom Kazmierski for stepping in to be my primary academic supervisor midway through my studies and for his patience and support given the circumstances. In addition to this my thanks also go to Dr. Stephen Weiss for his contributions during the first half of my studies and for his continued advice even after he had left Southampton University.

During the course of the Engineering Doctorate I have received funding from both the Engineering and Physical Sciences Research Council (EPSRC) and ERA Technology Ltd. (now trading as Cobham Technical Services) without which I would not have been able to undertake this work. Furthermore, I would like to thanks my colleagues at ERA Technology Ltd. for their help and advice along the way, not least, Dr. Duncan Brooks for his support in the role of my industrial supervisor.

Finally, I would like to give heartfelt thanks to my girlfriend and my parents for their support and understanding which have helped sustain me during my studies.

Abbreviations

ADM	Analogue Down-conversion Module
ASIC	Application Specific Integrated Circuit
AWGN	Additive White Gaussian Noise
BER	Bit Error Ratio
BPSK	Binary Phase Shift Keying
C/A	Course Acquisition
CR	Cancellation Ratio
CW	Continuous Wave
DDC	Digital Down Conversion
DFT	Discrete Fourier Transform
DoA	Direction of Arrival
DSP	Digital Signal Processor/Processing
DSSS	Direct Sequence Spread Spectrum
EM	Electromagnetic
FDE	Frequency-Domain Excision
FEC	Forward Error Correction
FFT	Fast Fourier Transform
FPGA	Field Programmable Gate Array
FIR	Finite Impulse Response
GPS	Global Positioning System
GNSS	Global Navigation Satellite System
GSC	Generalised Sidelobe Canceller
IDFT	Inverse Discrete Fourier Transform
IF	Intermediate Frequency
IIR	Infinite Impulse Response

INR	Interference to Noise Ratio
ISR	Interference to Signal Ratio
JTAG	Joint Test Action Group
LCMV	Linearly Constrained Minimum Variance
LMS	Least Mean Square
LPE	Linear Prediction Error
LPI	Low Probability of Interception
LTI	Linear Time-Invariant
MMSE	Minimum Mean Square Error
MVDR	Minimum-Variance Distortionless Response
OFDM	Orthogonal Frequency Division Multiplexing
PLL	Phase-Locked Loop
PN	Pseudo-random Number
PSD	Power Spectral Density
QPSK	Quadrature Phase Shift Keying
RLS	Recursive Least-Squares
MHz	Mega-Hertz
NAVSTAR	Navigation Satellite Timing & Ranging
RF	Radio Frequency
RLS	Recursive Least Squares
SAW	Surface Acoustic Wave
SFAP	Space-Frequency Adaptive Processing
SINR	Signal to Interference plus Noise Ratio
SNR	Signal to Noise Ratio
SMI	Sample Matrix Inversion
STAP	Space-Time Adaptive Processing
STFT	Short Time Fourier Transform
STDFT	Short Time Discrete Fourier Transform
SUCM	Synthesizer Up-conversion Module
TD	Technical Demonstrator
TDL	Tap Delay Line
TFD	Time-Frequency Distribution
ULA	Uniform Linear Array

Symbols

α_l	l^{th} cosine window function coefficient
a_m	Impulse response due to l^{th} antenna element
A_m	Phase shift of m^{th} element
$\mathbf{A}$	Steering vector
$\bar{\mathbf{A}}_{ZB}$	Response vector of STAP to zero-bandwidth signal
$\bar{\mathbf{A}}_{NZB}$	Response vector of STAP to non zero-bandwidth signal
β	Dolph-Chebyshev window coefficient
$\mathbf{b}$	Excision filter window function vector
$\mathbf{B}$	DFT of excision filter window function vector
$\hat{\mathbf{b}}$	SFAP beamformer window function vector
$\bar{\mathbf{B}}$	Matrix of dispersion factors
$\bar{\mathbf{b}}$	Vector of dispersion factors
$\tilde{\mathbf{b}}$	Frequency-domain of Dolph-Chebyshev window function vector
B_g	Bandwidth of interference signal
B_x	Bandwidth of the wanted signal
c	Speed of light
$\mathbf{c}$	Constraint vector of LCMV beamformer with a single constraint
$\mathbf{C}$	Constraint matrix of LCMV beamformer with multiple constraints
$\mathbf{c}_k$	k^{th} column vector of constraint matrix
Δ	Spacing between elements in array
d	Wanted data bitstream
d_z	Decision variables
$\mathbf{D}$	Excision mask
E_b	Energy per bit
$\mathbf{E}_{gg}$	Eigenvectors of the interference signals

$\mathbf{E}_{vv}$	Eigenvectors of the thermal noise
$\hat{\mathbf{F}}$	Constraint response
$\mathbf{F}_N$	$N \times N$ Vandemonde matrix of discrete Fourier coefficients
$\mathbf{f}$	Constraint vector of LCMV beamformer with multiple constraints
$\tilde{f}_k$	Frequency of k^{th} sub-band in SFAP
$\bar{f}$	Constraint value of LCMV beamformer with a single constraint
f_c	Tuned RF frequency of array antenna
f_b	CW frequency
f_g	Centre frequency of interferer
f_k	Square-root of the variance of non-zero bandwidth signal
$\hat{f}_k$	k^{th} constraint frequency
f_s	Sampling frequency
F_u	Weight update rate relative to sampling rate
G	Total number of interference signals
g	Interference signal
G	Number of interference signals
$\hat{\mathbf{G}}$	Desired channel response vector
G_a	Array gain factor
G_b	Beamformer gain
γ	Sidelobe level adjustment coefficient
Γ	Excision function
h_m	Impulse response of the m^{th} channel
H_m	Transfer function of the m^{th} channel
h_p	Impulse response of partialband interference band-limiting filter
K	Number of taps or sub-bands in STAP or SFAP respectively
K_c	Length of sliding window used in closing operation
K_o	Length of sliding window used in opening operation
L_c	Number FIR filter coefficients for channel responses
L_s	Length of the DSSS spreading sequence
L_w	Number of coefficients for cosine window function
λ_i	i^{th} eigenvalue of covariance matrix
$\mathbf{\Lambda}_{gg}$	Diagonal matrix of eigenvalues due to interference
$\mathbf{\Lambda}_{vv}$	Diagonal matrix of eigenvalues due to noise

n_e	Number of bit errors
N	Dimension of Vandermonde matrix containing discrete Fourier transform coefficients
N_b	Number of bits transmitted
N_e	Length of excision filters
N_r	Number of snapshots in ensemble average of covariance matrix
N_0	Noise power spectral density
N_q	Length of channel mismatch filters
M	Number of elements in array antenna
φ	Uniformly distributed random phase
P_g	Power of the interference signal
P_x	Power of the wanted signal
ϕ	Cosine between steering vectors
ψ	Null depth improvement
q_m	Excised signal on the m^{th} channel
$\hat{\mathbf{q}}_m$	Block of excised frequency-domain samples in excision filter on m^{th} channel
$\tilde{\mathbf{q}}$	Vector of excised samples on STAP taps
$\mathbf{Q}_m$	Vector of channel mismatch filter weights for m^{th} channel
ρ_e	Bit error rate
$r_k(l)$	Excision threshold for k^{th} frequency sample of l^{th} block
r_{gg}	Auto-correlation function of interference signal
$\mathbf{R}_{gg}$	Covariance matrix of interference
$\mathbf{R}_k$	Covariance matrix of the k^{th} sub-band of SFAP
$\mathbf{R}_{nn}$	Covariance matrix of interference plus thermal noise
$\mathbf{R}_{\bar{q}\bar{q}}$	Covariance matrix of excised signal
$\mathbf{R}_{\bar{u}\bar{u}}$	Covariance matrix of the STAP tap values
$\mathbf{R}_{uu}$	Covariance matrix of the received signal
$\mathbf{R}_{u\bar{x}}$	Correlation vector of received & reference signals
$\mathbf{R}_{vv}$	Covariance matrix of the thermal noise
s	Spreading sequence signal
σ_v^2	Variance of thermal noise
$\mathbf{S}(f)$	Vector of dispersion factors
S_g	Power spectral density of interferer
θ_x	Angle of arrival of wanted signal x

θ_g	Angle of arrival of interference signal g
θ_{g_i}	Angle of arrival of i^{th} interference signal g_i
T_b	Period of one bit
T_c	Period of one chip
$\mathbf{T}_d(\theta)$	Matrix of inter-element delays
T_s	Sampling period
τ_d	Inter-element time delay
u_m	Signal received by m^{th} element of array
$\mathbf{u}$	Signals received by array elements
$\mathbf{u}_m$	Block of input samples to excision filter on m^{th} channel
$\bar{\mathbf{u}}$	Samples on STAP taps
$\hat{u}_m$	Equalised signal on the m^{th} channel
$\tilde{\mathbf{u}}_m$	Block of overlapped samples in excision filter on m^{th} channel
$\tilde{\mathbf{U}}_m$	Block of frequency-domain samples in excision filter on m^{th} channel
$\breve{\mathbf{u}}_m$	Block of zero-padded samples in mismatch filter on m^{th} channel
$\breve{\mathbf{U}}_m$	Block of frequency-domain samples in mismatch filter on m^{th} channel
v_m	Thermal noise on the m^{th} channel of beamformer
$\mathbf{w}$	STAP beamformer weight vector
$\mathbf{W}$	SFAP beamformer weight matrix
x	Wanted signal
$\hat{x}$	Calibration signal vector
$\bar{x}$	Reference signal
y	Beamformer output
$\hat{\mathbf{y}}_m$	Block of input samples to m^{th} channel of SFAP
$\tilde{\mathbf{y}}_m$	Block of overlapped samples on m^{th} channel of SFAP
$\tilde{\mathbf{Y}}_m$	Block of frequency-domain samples on m^{th} channel of SFAP
$\mathbf{Y}_k$	Block of frequency-domain samples on channels for k^{th} sub-band of SFAP
ϖ	Waveform of a single chip
$\hat{\mathbf{z}}$	Block of partially equalised samples on m^{th} channel
$\mathbf{z}$	Block of equalised samples on m^{th} channel
$\hat{\mathbf{z}}$	Vector of equalised samples on STAP taps

For my Grandfather Trevor Tisdale

Chapter 1

Introduction

Since the earliest days of wireless communications engineers have fought a battle against interference to improve the quality and reliability of communications. As a result, a multitude of technologies have been developed to address this problem. Improvements in the selectivity of the radio frequency (RF) front-ends have helped ensure that out of band signals are removed from the received signal. National and international regulations of spectrum allocation and usage have helped ensure that commercial systems minimise the level with which they interfere with each other. Despite these efforts, wireless systems are still likely to experience interference within the portion of the spectrum which they operate. So called *co-channel interference* can arise from a variety of sources: unlicensed radio equipment, radios operating within public bands of the spectrum, electromagnetic (EM) emissions from electrical equipment, such as microwave ovens, EM radiation from space objects, such as the sun, or intentional attempts to disrupt communications [4]. On the technological level more can be done to deal with these sources of interference by designing additional margins into the link budget of the communications system. In particular, in digital communications systems a judicious choice of modulation scheme, spread spectrum techniques or forward error correction (FEC) can be used to improve the resilience of a communications system to interference. In addition to this, some form of active interference suppression can be included in the radio receiver to remove interference before the signal is demodulated. This may be necessary when the expected interference environment is particularly hostile or if little or no levels of disruption can be tolerated in the communications link.

One particular class of communications system that is particularly vulnerable to interference is low probability of interception (LPI) systems. These typically operate with signal powers that are well below the thermal noise floor of the receiver and use techniques such as direct sequence spread spectrum (DSSS) to obtain a good post-correlation

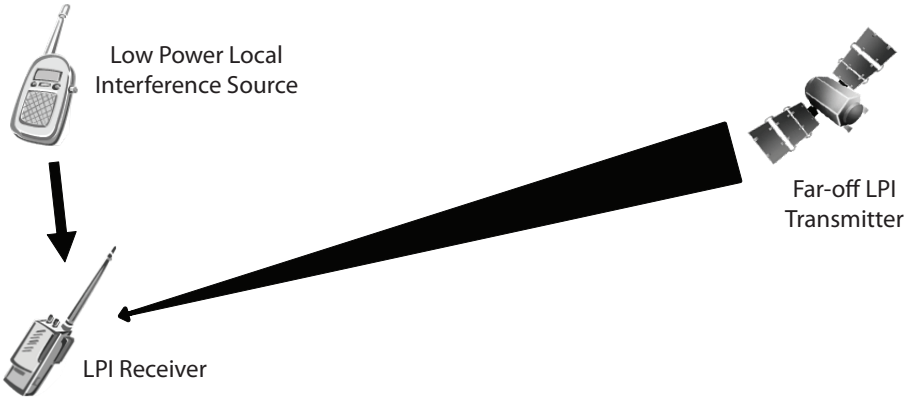

FIGURE 1.1: Illustration of the near-far problem for LPI communications systems

signal to noise ratio (SNR) [5, 6]. An example of this sort of system is the NAVSTAR global positioning system (GPS) [7, 8] which operates at a nominal SNR of -30 dB [9]. In DSSS receivers the despreading of the DSSS signal yields a processing gain G_p in the SNR equal to:

$$G_p = \frac{R_s}{R_d}$$

where R_s is spreading chip rate and R_d is the data rate.

The processing gain affords the DSSS receiver some resilience to interference which is typically expressed in terms of the receiver's *jamming margin* [10]. The jamming margin relates the maximum level of interference the receiver can tolerate given a specified minimum SNR (denoted SNR_r) required to obtain a certain level of performance.

$$(\text{Jamming Margin})_{dB} = (G_p)_{dB} - (L_s)_{dB} - (SNR_r)_{dB}$$

where L_s is the loss of the system (sometimes referred to as implementation loss).

However, by operating at very low signal levels, the jamming margin of LPI systems tends to be small as a significant portion of the processing gain is taken up in ensuring that a suitable post-correlation SNR is obtained [11]. By operating at such low power levels they are susceptible to the so-called "near-far" problem whereby only modest levels of local interference can prevent reception of the wanted signal transmitted from a much greater distance away as shown in Figure 1.1.

Digital adaptive beamforming is an effective method of interference suppression against a variety of forms of interference [12]. An adaptive beamformer consists of a multi-element antenna with an adaptive signal processor which allows the antenna's gain

pattern to be shaped in such a way that nulls can be placed in the direction of interfering signals while steering the mainlobe in the direction of the wanted signal. However, the number of nulls which the beamformer can place in its beam pattern is limited by the degrees of freedom within the beamformer, which in turn, depends on the number of adjustable weights in the beamformer. The cost of adding additional degrees of freedom is typically high, thereby limiting the total number of interference signals the beamformer can simultaneously suppress. With limited degrees of freedom it is important that the adaptive beamformer uses them to most effect by placing nulls in the direction of interference signals that have the most potential to disrupt the DSSS receiver. It is well known that DSSS systems are particularly vulnerable to broadband interference, where the band occupancy of the interference in relation to the DSSS signal is large [13]. While narrow-band interference can also successfully prevent a DSSS receiver from demodulating the wanted signal, particularly when the jamming margin of the system is relatively small [11], it can also be suppressed relatively easily using lower complexity single-channel interference suppression techniques [14]. Therefore, one strategy would be to try to remove narrowband interference using lower complexity techniques prior to adaptive beamforming in order to preserve degrees of freedom in the beamformer.

The aim of this thesis is to consider efficient methods of increasing the interference suppression capacity of broadband adaptive beamformers with a limited number of channels. In particular, in environments in which interference signals of varying band occupancy are present. The focus on beamformers with few channels is with an aim of deployment in small, mobile applications given the relatively high hardware complexity of beamformers. Of particular interest are broadband beamformers such as the space-time adaptive processor (STAP) given their good cancellation performance against non-zero bandwidth signals. While considering methods to improve the STAP's cancellation capacity, consideration will be given to the role of the time taps and the increased degrees of freedom they offer. The problem of reduced cancellation performance against broadband interference due to interchannel mismatches in STAP beamformers is also considered. Efficient methods of compensating for the interchannel mismatches for better broadband cancellation is also explored.

1.1 Research Contributions

The main research contributions presented in this thesis are listed below:

- The limitations of the use of additional time-taps in STAP beamformers in order to increase the number of interference signals which can be simultaneously cancelled

was highlighted. This included deriving the parameters upon which the signal subspace of the STAP's covariance matrix becomes rank 2 when in the presence of a non-zero bandwidth interference signal. Further numerical analysis of the eigenvalues of the covariance matrix was also used to support this investigation.

- The use of frequency-domain excision as a method of pre-filtering narrowband interference prior to beamforming was presented in order to increase the number of simultaneous interference signals which can be cancelled in a mixed interference environment. Factors affecting the performance of this approach were discussed and investigated by simulation.

- A novel algorithm for determining a non-uniform threshold in frequency-domain excision filters was presented. The algorithm makes it possible to selectively identify and excise narrowband interference in the presence of partialband and broadband interference. This is necessary if frequency-domain excision filtering is to be used in an adaptive beamforming system to pre-filter narrowband interference [1, 2].

- Two new methods of efficiently compensating for mismatches between the front-end channels in broadband adaptive beamformers in order to achieve higher levels of cancellation of non-zero bandwidth interference were proposed. Improved performance was demonstrated both by simulation and on a hardware STAP system [3].

Some of the research is supported by a journal publication and 2 conference papers which are listed below:

- N. Tisdale, T. Kazmierski, and D. Brooks. A bandwidth selective frequency domain excision filter for use in front of adaptive array antennas. *Proceedings of the IEEE Military Communications Conference*, pages 1–6, October 2007.

- N. Tisdale, T. Kazmierski, and D. Brooks. Channel mismatch compensation for space-time adaptive processors. In *Proceedings on IEEE Military Communications Conference*, pages 1–7, November 2008.

- N. Tisdale, T. Kazmierski, and D. Brooks. Bandwidth selective filter for the pre-excision of narrowband interference in broadband beamformers. *IET Communications Journal*, 4:201–212, 2010.

1.2 Structure of this Thesis

In Chapter 2 various interference suppression schemes are considered with particular attention being paid to the ability of each technique to protect an LPI DSSS signal from interference. Given the broadband nature of DSSS signals, interference suppression systems with the ability to cancel broadband and partialband interference as well as narrowband interference are of particular interest. Furthermore, the capacity of the various algorithms to cancel multiple sources of interference is discussed.

Having identified in Chapter 2 adaptive beamforming as an approach to interference suppression which can achieve high levels of cancellation against multiple sources of interference, Chapter 3 focuses on efficient methods of increasing the cancellation capacity of broadband adaptive beamformers. The suitability of increasing the number of taps per channel in STAP beamformers as a method of increasing the number of interference sources which the beamformer can simultaneously cancel is explored. An alternative method of increasing the cancellation capacity of an adaptive beamformer by pre-filtering narrowband interference using excision filtering is considered. The effectiveness of this approach at desensitising the beamformer to the presence of narrowband interference is investigated by eigenanalysis of the beamformer's covariance matrix. The performance of this approach in an LPI DSSS system is examined by BER simulation.

Chapter 4 follows on from Chapter 3 by considering the problem of adapting frequency-domain excision filters for use as pre-filters in front of adaptive beamforming systems. In particular, the question of how to identify only narrowband interference in a mixed interference environment is addressed. To this end a novel algorithm is proposed to replace the traditional methods of interference identification used in excision filters. The performance of the algorithm is demonstrated by simulation of the combined excision adaptive beamforming system using the proposed algorithm.

In Chapter 5 the problem of interchannel mismatches between the channels in broadband adaptive beamformers is considered. Mismatches in the responses of the components used in the beamformer's channels prior to digitisation can limit the cancellation achieved against non-zero bandwidth interference. Two new efficient methods of compensating for the interchannel mismatches are presented based on frequency-domain filtering. The improvement in cancellation performance of both of these methods is demonstrated both by software simulation and with a hardware STAP beamformer using a software-in-the-loop approach to implement the algorithms.

Chapter 6 presents the conclusions from this research as well as suggestions for future work which follow on from the work presented in this thesis.

Chapter 2

Interference Suppression

In receiver design theory the matched filter is the optimal receiver, in a minimum mean squared error (MMSE) sense, when the received signal is an additive combination of the wanted signal and Gaussian white noise [15]. Therefore, the matched filter receiver may no longer be optimal when the noise is no longer white, which may be the case when interference is present in the received signal. In DSSS receivers the use of interference suppression to pre-condition, by whitening, the received signal has been shown to be effective at improving the performance of the DSSS receiver [16, 17]. This form of countering the effects of interference is distinct from other approaches which may be used, such as the specialised design of the modulation/coding scheme to improve resilience, as the interference is removed before decoding/demodulation as opposed to simultaneously. Therefore, in the case of the DSSS receiver the objective of the interference suppression system is to whiten the signal.

Various approaches to interference suppression have been proposed in literature and are used in practice. In this chapter some of the key interference suppression techniques used with LPI DSSS receivers are discussed with particular regard to their performance in stressed interference environments i.e. where a number of high power interference signals may be present in the received signal. These have been generalised into two broad categories: single-channel methods and multi-channel methods, owing to the major architectural difference between the two approaches. The chapter ends with a description of the modelling of a DSSS system and the interference signals under consideration, as well as the simulation of signals arriving from various angles in a multi-channel system which employ an antenna array.

2.1 Single Channel Interference Suppression

2.1.1 Time-Domain Interference Suppression

One of the simplest forms of protection against continuous wave (CW) interference is the tracking loop which, using a phase locked loop (PLL), can be used to predict the frequency and amplitude of an interfering CW signal [18, 19]. This information can be used to synthesise a local copy of the interferer which can then be subtracted from the received signal. This method should be capable of cancelling very strong CW interferers with minimal distortion to the wanted signal provided that the instantaneous frequency and amplitude of the CW are accurately estimated. Furthermore, tracking and cancellation of non-stationary CWs, such as swept CWs, should be possible. However, if the PLL fails to lock onto and track the CW then not only will the system fail to suppress the interferer but may also introduce distortion into the wanted signal. Furthermore, the use of a PLL or similar feedback loop to track the CW interference signal limits the scheme to track a single CW, the presence of multiple CWs may lead to instability.

In order to suppress more generalised forms of narrowband interference, linear prediction error (LPE) filtering has traditionally been used in DSSS receivers [14, 16, 20, 21]. LPE filtering uses a prediction filter to predict future values of the received signal based on past values. The LPE filter subtracts the predicted values of the received signal from the actual received signal to form a prediction error signal. Given a sufficiently long filter and wide-sense stationary input the prediction error signal output will be uncorrelated, as such, the LPE filter is often described as having a whitening effect on the signal [22]. This property makes LPE well suited to DSSS systems as the DSSS signal should appear uncorrelated within the period of its spreading code and hence, the predictor will tend not to be able to predict future values of the DSSS signal [23]. By contrast, the interference, assuming it is not spectrally white, will be correlated and as such predictable. Therefore, the received signal can be treated as an autoregressive process where the noise part of the process is given by the LPE filter's output and contains the DSSS signal and thermal noise, while the interference is modelled by the weights of the LPE filter and is thus removed from signal [22]. For an input signal that is wide-sense stationary the optimal weights of the LPE filter are given by the Wiener-Hopf equations [17]. Calculation of the Wiener-Hopf equations requires knowledge of the received signal's autocorrelation function which is not typically known *a priori* and therefore, must be estimated. A number of algorithms have been proposed for solving the Wiener-Hopf equations (and hence estimating the autocorrelation function) and include the Levison-Durbin [24, 25], Burg [26], least mean square (LMS) [27, 28] and recursive least squares (RLS) [29] algorithms. The LPE filter can also be realised as a double-sided

filter by cascading the LPE filter with its time reverse which has the beneficial property of having a zero-phase [16].

The interference cancellation performance of LPE filtering in a stationary environment depends on the length of the filter, the number of interferers and the properties of the interferers. The length of the filter dictates the number of degrees of freedom available to the filter and, therefore, the number of zeros which can be placed in its transfer function [22]. As such the LPE filter is most effective against zero bandwidth interferers, i.e. CW signals, as a single zero can be placed to create an infinitely deep notch at the frequency of each zero bandwidth interferer. Therefore, the number of zero bandwidth interferers the LPE filter can simultaneously suppress is limited by the length of the filter and is not affected by the power of each interference signal [30]. By contrast, narrowband interferers with a non-zero bandwidth theoretically require an infinite number of zeros to be placed in order to fully cancel them [17]. Given that a practical filter will always be finite in length the level of cancellation achieved against a non-zero bandwidth interferer will depend on the filter length and the power of the interferer. However, as the bandwidth of the interferer is increased further it will no longer appear narrowband to the filter and therefore, will exhibit weaker autocorrelation which, in turn, makes it more difficult for the LPE filter to predict and cancel [31]. The performance of the LPE filter can also suffer in situations where the signal to interference plus noise ratio (SINR) is high due to self generated noise in the LPE filter [31]. This arises because the DSSS signal can exhibit small levels of self-correlation resulting in the LPE partially predicting the DSSS signal and attempting to cancel it. This can be improved through the use of decision directed feedback to remove the DSSS signal from the signal [28] or by applying constraints to the filter weight solution [32–35]. For example, a constraint to the solution can be applied to desensitise the predictor to the correlation present in the DSSS spreading sequence or alternatively to introduce an energy minimisation constraint [34, 35].

The relatively slow convergence time of LPE filtering can affect its ability to cancel non-stationary interference. To address this other interference suppression techniques have been proposed, such as the use of time-frequency distributions (TFDs) to estimate the instantaneous frequency of an interferer in combination with a very short finite impulse response (FIR) filter to adaptively notch filter the interference signal [20, 36]. The aim is to utilise the spectral and temporal properties of the TFD kernel function in order to identify and excise highly non-stationary interference signals. The performance of TFD based excision is heavily dependant on the accuracy of the TFD to estimate the instantaneous frequency of the interferer. As such various different TFDs have been considered in literature: Wigner-Ville [36], Choi-Williams [37] and Born-Jordan [38]. In general the TFD relies on the TFD kernel being well matched to a given class of interferer and so one TFD kernel may be better for one type of interference than another.

A stipulation of TFD based excision is that the excision FIR filter must be kept short so as not to degrade the reaction time of the filter [39]. An FIR of 3 to 5 taps is typically used, however this limits the frequency response of the filter and therefore the bandwidth over which the filter can cancel the interference signal. Furthermore, TFD estimation bias will affect its performance, particularly when a shorter filter is used as the notch it will produce is much narrower. Alternatively, Wang and Amin show in [40] that high-order multiplicity filters may be employed instead due to their wider notch frequency response, which they show to be more effective in the presence of TFD estimate bias or when a poor frequency resolution TFD is used. TFD based excision suffers from similar self-noise problems as LPE filtering. However, this can be overcome by estimating the interferer's instantaneous amplitude to determine whether filtering the signal is of any benefit, if not then the filter can be bypassed [41].

2.1.2 Frequency-Domain Excision Filtering

The use of domains other than the time-domain to identify and excise interference has received much attention in the literature [42]. In particular, frequency-domain excision (FDE) which operates in the short-time discrete Fourier transform (STDFT) domain has found application in interference suppression for DSSS signals [43–46]. This is motivated by the ability to easily identify narrowband interference in the frequency-domain over the DSSS signal and receiver thermal noise. A simple threshold test can be used to identify which frequency bins contain interference and the bin's value can either undergo hard excision in the form of zeroing the bin's value or soft excision whereby the bin's magnitude is clipped to a specified level [47–49]. In this way FDE operates in an open-loop manner, thereby avoiding the problems associated with convergence such as slow adaptation rates [50]. Furthermore, as a discrete Fourier transform (DFT) pair is typically used to transform the signals between domains in the STDFT the frequency-domain excision filter can be implemented very efficiently using the fast Fourier transform (FFT).

The threshold used to identify interference in the excision filter is typically a fixed value across all the bins in the DFT against which the magnitude of each DFT record is compared. The value of the threshold can be arbitrarily set by the designer, for example, a fixed level above the estimated noise floor of the receiver, or based on some optimality criterion. In [50], Young presents a method of calculating the optimum threshold value to excise a given portion of the spectrum in the presence of additive white Gaussian noise (AWGN). While in [51] Capozza *et al.* present a method of determining the excision threshold value based on the statistics of the DFT bins. They consider the mean and standard deviation of the power spectral density under normal conditions as well as in the presence of an interferer. They note that under normal conditions the signal energy

is mostly contained within one standard deviation from the mean, however this changes in the presence of interference. Therefore, they propose a method to set the threshold level based on the standard deviation of the received signal.

The process of excising a portion of the received signal's spectrum will have an associated excision loss as a portion of the DSSS signal will also be removed [50]. When a portion of the spectrum is excised which contains little or no energy due to an interferer this is termed *over-excision*. The level of loss experienced will depend on the method of excision used. In [44], Young considers the over-excision loss experienced by a DSSS signal when only the wanted signal and thermal noise are present. He shows that soft excision by clipping experiences a much smaller loss than hard excision by zeroing as the portion of the spectrum excised is increased. This is because the phase information of the wanted signal is retained when the clipping excision method is used, thereby allowing the wanted signal to be recovered, whereas zeroing completely removes the wanted signal in the portions of the spectrum which are excised. Further to this he determines the optimal magnitude to clip to in order to minimise the excision loss when a given portion of the spectrum is excised. However, he does note that the excision loss experienced by clipping to the noise floor as opposed to the optimal clip value are very similar.

One of the main challenges associated with implementing a FDE filter is that of spectral leakage. Spectral leakage is the result of using a finite observation window to ascertain the spectral characteristics of a signal which is infinite in extent [52]. The DFT assumes periodicity of the observed signal beyond the bounds of the observation window. If the signal under observation is not periodic with respect to the observation window, the assumed periodicity of the Fourier transform will generate discontinuities at the window's edges [53]. The effect of these discontinuities on the finite length Fourier transform is the apparent leakage of the signal out across the spectrum. This is most strikingly seen in the Fourier analysis of a complex sinusoid that is not periodic with respect to the observation window. Rather than a Dirac function at the frequency of the complex sinusoid, the spectrum of the signal will exhibit a *mainlobe* at the sinusoid's frequency containing most of the sinusoid's energy, however, energy can be seen to leak out either side of the mainlobe forming *sidelobes*. This impacts upon the performance of frequency-domain excision algorithms as larger portion of the spectrum must be excised in order to sufficiently remove the interferer's energy contained within the sidelobes.

Spectral leakage can be reduced by applying a window function to the signal that de-emphasises the values of the signal near the edges of the observation window prior to transforming the signal into the frequency-domain [53]. This results in higher suppression of the sidelobes and, therefore, better localisation of the interferer's energy in the frequency-domain. This is advantageous to the excision filter as more of the interferer's

energy is removed when the mainlobe is excised leaving less of a residual signal which will contribute to the overall remaining noise level. The choice of window function will determine the power level of the highest sidelobes relative to the mainlobe but the absolute power level of both will depend on the power of the interference signal. Therefore, as the power of the interferer is increased the level of the sidelobes will become more problematic as the power of the residual signal after excision will be raised. In this circumstance excising a larger portion of the spectrum or the use of a window with a higher level of sidelobe suppression may be used to reduce the power which is left in the residual signal. Both these approaches have their disadvantages, in the first case, the excision of a larger portion of the spectrum will result in a reduction in the energy of the wanted signal [54]. In the second case, increasing the level of sidelobe suppression comes at the cost of widening the mainlobe of the interference signal [53]. The reduced spectral resolution of high sidelobe suppression windows results in a higher number of bins which need to be excised per interference signal. Therefore, the most appropriate window to use will depend on the power of the interference signals [55]. A further consideration is that of the loss experienced by the wanted signal due to the attenuation it experiences as a consequence of windowing the received signal. This is termed *processing loss* and the level of loss experienced depends on the shape of the window function. Davidovici and Kanterakis note in [52] that in situations where the level of interference is low the window's processing loss will degrade the receiver's performance. However, Young and Lehnert show in [50] that, by overlapping the blocks of samples by 50% prior to windowing and then adding the overlapped regions after the excised signals have been transformed back into the time-domain, this loss can be reduced to 1 dB or less for a variety of common window functions.

The performance of FDE in the presence of non-stationary interference is dependant on the size of DFTs used in FDE filter as well as the properties of the interferer. In [45] Ouyang and Milstein consider the performance of short-time Fourier transform (STFT) excision against non-stationary interference and as STFTs essentially operate in the same manner as a DFT based excision system utilising both time-domain windowing plus overlap and add the results are of interest. In order to reduce over excision it is desirable to have both good spectral and temporal resolution so that the non-stationary interferer can be well localised in both time and frequency [38]. Unfortunately, there is an inverse relationship between temporal and spectral resolutions that results in one having to be traded off against the other. In the case of the short-time Fourier transform, the longer the observation period, the better the frequency resolution but this is gained at the expense of temporal resolution and vice versa. Ouyang and Milstein note that the correct choice of a windowing function to match the characteristics of the interference

is important in ensuring good spectral resolution and hence, strong cancellation of the interferer.

To overcome the deficiencies of FDE, such as spectral leakage and spectral/temporal resolutions, excisors based on other transforms such as the wavelet [56, 57] or Wigner-Hough [58] transforms have been proposed. The use of the wavelet transform has been shown to be better than FDE in the case of pulsed narrowband interference [56]. However, the complexity of using the wavelet transform is higher than that of FDE as FIR filters are required to implement the forward and inverse wavelet transforms. The use of infinite impulse response (IIR) filters to implement the wavelet transform have also been proposed which can be implemented more efficiently than FIR filters however, numerical instability caused by quantization effects in the coefficients necessitates that care is taken in the implementation of the wavelet transforms using IIR filters [57]. Ultimately, the performance of a particular excision method very much depends on the type of interference encountered and as such, multi-transform systems have also been explored in the literature [59–61]. These systems utilise multiple domains in one system in order to determine which domain best localises the received interference. The identified domain is then used to excise the interference signal. By adapting the domain used these approaches aim to provide better overall cancellation to a wider range of interference types then any single approach on its own. However, the drawback of this is the increased complexity required to support each domain. Furthermore, in the presence of multiple sources of interference of disparate types choosing the most appropriate domain may not be so clear.

2.2 Adaptive Array Beamforming

Advances in the areas of electronic component miniaturisation, integration and processing power have increased the popularity of more computationally complex interference suppression systems such as digital adaptive beamforming. Adaptive beamforming differs from single channel interference suppression in that it uses the combination of a number of signals received from several antennae elements, collectively termed an *array*, to spatially filter signals that are incident upon it. In digital adaptive beamformers this filtering is applied to the signals received by each element after they have been sampled. This is as opposed to analogue adaptive beamformers where the spatial filtering and/or the weight control is processed in the analogue domain. Given the order of progress in electronics most of the beamforming techniques and algorithms started off as fully analogue systems with the weights determined by analogue control loops. As the development of digital electronics has gained pace the discrete-time equivalent of many of

these algorithms were developed to realise fully digital (after analogue down-conversion) beamformers. Fully digital beamformers offer a number of advantages over fully analogue beamformers such as greater flexibility in terms of the beamforming algorithm used and faster adaptation times. Furthermore, the increasing improvements in the performance and efficiency of digital electronics presents many possibilities for realising more compact and higher performance beamforming systems and, as such, only fully digital beamformers will be considered in the rest of this thesis.

Adaptive beamformers are able to spatially filter received signals because a signal impinging upon the array will arrive at each element at fractionally different instances in time due to the spatial separation between the elements within the array. If the elements are assumed to have an omnidirectional response then the signal received by each element in response to a signal will differ only in terms of its relative delay. These relative delays in arrival time of the signal at each element will depend on the signal's angle of arrival relative to the array. By summing together the received signals from each element, a resultant output signal is produced which is the combination of the delayed versions of the received signal from each element. This superposition of the signals from each element has the effect of constructively and destructively interfering to produce varying levels of gain or attenuation dependant of the angle of arrival of the signal. By adjusting the delay experienced by signals arriving at each element the relative delays between these signals are altered resulting in a controllable gain pattern when the response of the array is considered as a whole [62]. In this way the spatial gain pattern of the array can be controlled to give higher gain in one direction, known as *beam-steering*, whilst attenuating signals arriving from another direction, known as *null-steering* or *nulling*. This ability allows adaptive beamforming systems to be able to suppress multiple sources of interference simultaneously while providing gain in the direction of the wanted signal [63].

Control of the relative delays experienced by the signals on each element is typically achieved by a phase shifter, in a digital beamformer this can be implemented as a complex weight as shown in Figure 2.1. However, a phase shift is unable to compensate for the frequency dependence of the array's response to signals which do not arrive at each array element simultaneously. For example, in a linear array, i.e. where the array elements are arranged in a straight line, any signal arriving from an angle other than broadside to the array will produce a frequency dependant response. As a result the cancellation performance of the adaptive beamformer tends to degrade as the bandwidth of an interferer is increased [64]. Therefore, these beamformers show best performance in the presence of narrowband interference and, as such, they are termed *narrowband* beamformers.

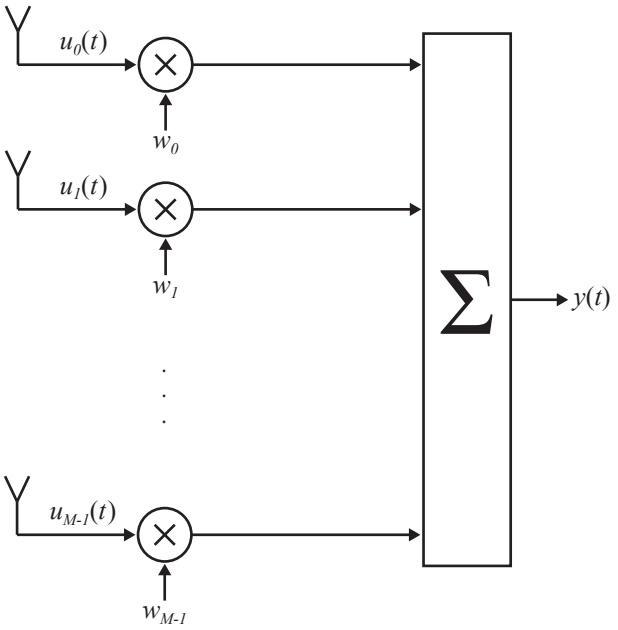

FIGURE 2.1: Dataflow diagram of a narrowband adaptive array

2.2.1 Broadband Adaptive Beamforming

It is well understood that the cancellation performance of narrowband beamformers deteriorates as the bandwidth of the interference signal it is trying to cancel is increased [65]. This reduction in performance occurs because the relative phase response of each element in the array is dependant not just on the angle of arrival but also on the frequency of the received signal. A CW signal is comprised of a single discrete frequency and, therefore, has zero bandwidth, as a result the array only responds at that frequency. By contrast any signal, however narrowband, that has a non-zero bandwidth will be composed of a continuum of frequencies each of which will produce a different relative phase response on each element. This has the effect of making the signal appear to the array to arrive from a range of angles of arrival, the spread of which is proportional to the signal's bandwidth [64, 66]. In other words the non-zero bandwidth signal appears to the array like a continuous series of CW signals arriving from a range of angles rather than one discrete angle. Therefore, the signal appears to be spatially dispersed which is seen in the form of decorrelation of the signal across the array elements. Therefore, to fully cancel the non-zero bandwidth signal the array must place continuous nulls covering the angle range created by the dispersion. With limited degrees of freedom the beamformer must place nulls in directions which will maximise the cancellation achieved over this range of angles.

The problem of broadband dispersion is caused by the approximation of a time delay by a phase shift on each element. In order to improve the broadband cancellation

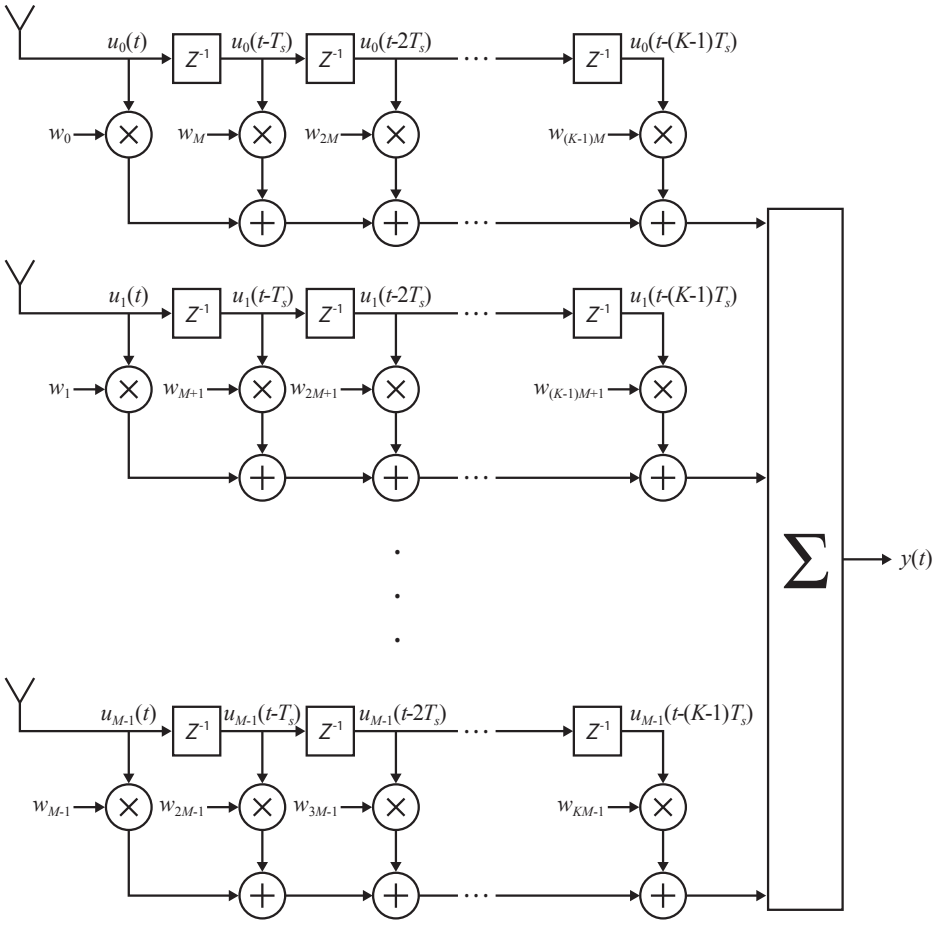

FIGURE 2.2: Dataflow diagram of a space-time adaptive processor

of beamformers Widrow [67] proposed the use of tap delay lines (TDLs) behind each element rather than a single weight which can better approximate the response on each channel to a delay. The inclusion of additional time taps behind each element allows the beamformer to alter its response both spatially and spectrally giving it the ability to remove the decorrelation introduced in response to the non-zero bandwidth signal due to dispersion. A typical implementation of the tap delay line beamformer is the STAP beamformer which, in a digital system, may be realised using M parallel K length FIR filters, where M is the number of elements in the array, and K is the number of time taps per FIR filter as shown in Figure 2.2.

The STAP beamformer has a total of MK adjustable weights giving it $MK-1$ degrees of freedom to steer nulls and/or apply constraints to maintain gain in a given direction at a particular frequency. As well as providing better cancellation against broadband signals, the additional degrees of freedom created by the time taps allow the STAP beamformer to compensate for other impairments to performance such as mismatched RF front-end channel responses or multipath signals [68]. However, the increased number of weights results in increased computational complexity compared with narrowband beamformers.

This includes costs associated with implementing FIR filters instead of a single weight per channel, as well as the cost of the adaptive logic required to adjust the weights. The computational cost of implementing the adaptive algorithm will vary depending on the choice of algorithm used which, in turn, will be driven by the performance requirements of the beamformer, such as convergence time, cancellation performance and numerical stability.

The high computational complexity of STAP beamformers has motivated much research into alternative broadband beamforming systems that aim to reduce the computational cost of such systems. One approach that has been proposed is the space-frequency adaptive processor (SFAP) [69]. SFAP beamformers differ from STAP beamformers in so far as the processing of the received signals is done in the frequency-domain rather than the time-domain. Frequency-domain filtering by fast convolution is mathematically equivalent to time-domain filtering and can be implemented more efficiently when a larger number of taps is required [70]. This is because the application of each weight can be reduced to a single complex multiplication. However, it does require that the signals be transformed into and back from the frequency-domain however, if the FFT is used then the transformations can be implemented very efficiently. Therefore, frequency-domain processing can be of benefit when a large number of bins is required. However, the computational cost of calculating the weights is still large for algorithms whose complexity is proportional to the size of the covariance matrix as the cross-correlations between all the elements and bins still produces an $MK \times MK$ covariance matrix. In response to this sub-optimal, realisations of the SFAP beamformer have been proposed, for example, sub-band beamformers [71]. Sub-band beamforming reduces the problem of beamforming a wide bandwidth by sub-dividing the band into a number of sub-bands via a filter bank such that each sub-band is considered as an independent narrowband channel and therefore, it is assumed, that there is no correlation between the individual sub-bands. Under this assumption the sub-band beamformer can be considered to be K narrowband adaptive beamformers operating in parallel, where the weight for each sub-band on each element is calculated using the cross-correlations between the signals in the same sub-band but on the remaining elements. In the limit, by using the FFT as the analysis and synthesis filter banks to separate and recombine the sub-bands, a critically decimated sub-band beamformer structure can be realised which can be implemented very efficiently. As each sub-band is treated as an independent narrowband channel the complexity of the covariance matrix in the critically decimated sub-band beamformer is K sets of $M \times M$ covariance matrices compared with $MK \times MK$ for the STAP or full SFAP. A comparison of the relative complexities of STAP versus sub-band beamforming is given in [72] where the authors state that if the covariance matrices are formed using LU-factorisation then the number of real operations required per sample

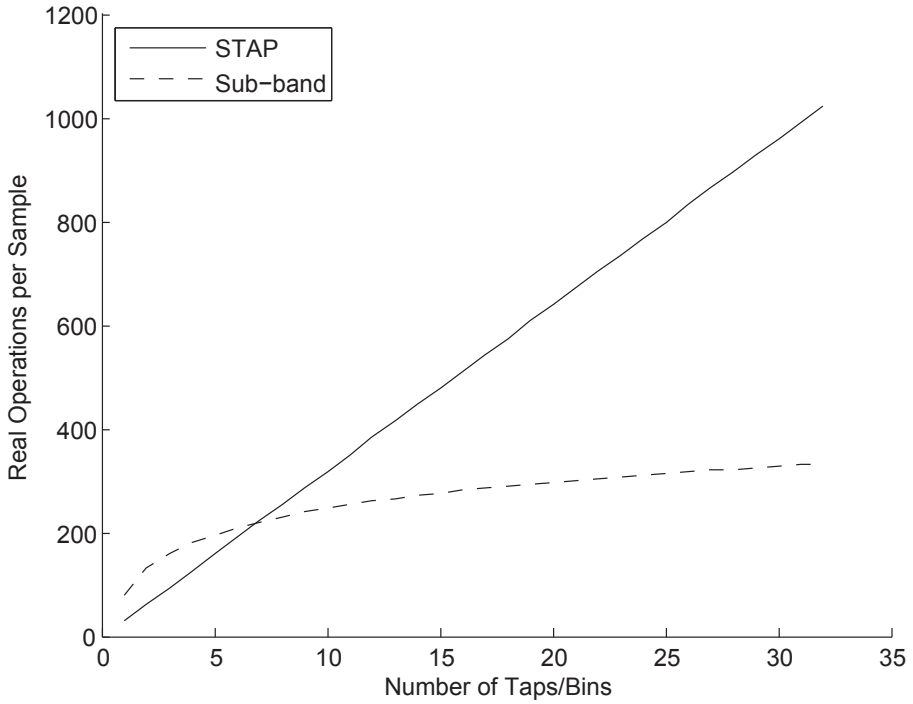

FIGURE 2.3: Relative complexity of a 4 element STAP and sub-band beamformer with a weight update rate relative to the sampling rate of $F_u = 0.001$

for a STAP beamformer with M elements and K taps is $17.33(MK)^3F_u + (8MK - 2)$ and similarly for a sub-band beamformer with a 50% sample overlap is $17.33M^3KF_u + 2((M+1)(2+5\log_2 K) + (8M-2))$, where F_u is the update rate of the weights relative to the sampling rate. The complexity required to calculate the covariance matrix in a real system precludes it from being updated at the same rate as the sampling rate and so the weights tend to be updated at a much slower rate relative to the sampling rate. Figure 2.3 plots the relative complexity in terms of real operations per sample for the two beamformers with a weight update rate relative to the sampling rate of $F_u = 0.001$. This ignores the fact that the FFTs will be most efficiently implemented in the sub-band beamformer when the number of bins is a power of 2 however, the results are sufficiently accurate for comparison between the two beamformers to be made. For a low number of taps/bins the extra processing overhead of transforming the samples between the time and frequency-domains in the sub-band beamformer makes its complexity higher than that of the STAP. However, once the number of taps/bins reaches 8 the complexity of the sub-band beamformer is less than that of the STAP and as the number of taps/bins further increases the complexity of the STAP continues to rise at a much greater rate compared with the sub-band beamformer.

On the surface the critically decimated FFT based sub-band beamformer appears far more efficient compared with the STAP beamformer, particularly for a large number of

taps. However, the use of the FFT to filter the signal into the sub-band leads to sub-optimal performance compared with the STAP beamformer and typically requires many more bins than number of taps in the STAP beamformer in order to show comparable performance [72]. This difference in performance arises because, in using the DFT, the assumption that each sub-band is independent of the other sub-bands is not strictly true [73]. Unless the signals received by the beamformer are periodic with respect to the DFT spectral leakage will occur resulting in the received signals appearing spectrally spread across the bins of the DFT and hence, the sub-bands of the beamformer. Windowing is typically applied to the samples before they are transformed into the frequency-domain in order to reduce this correlation by introducing some suppression of the sidelobes. With a carefully chosen window high levels of sidelobe suppression can be achieved but this is at the cost of increasing the width of the mainlobe. Widening of the mainlobe results in higher levels of correlation between the bins directly neighbouring the bin containing the interference but lower levels of correlation in bins further away. This has the effect of reducing the frequency resolution of the sub-band beamformer thereby increasing the number of bins required and the computational complexity. Alternatively, the performance of the sub-band beamformer can be improved though the use of over-sampled filter banks with frequency responses that are closer to a brick-wall filter than the DFT's. However, this too would result in increased computational complexity due to the oversampling. In general, Fante [72] reports that when performance is taken into account the sub-band beamformer only really becomes more efficient when the number of bins used exceeds 128.

2.2.2 Optimum Beamforming

While the beamformer weights may be manipulated manually or semi-automatically, for example to scan the mainbeam in various directions, this will not yield the most optimum performance from the beamformer in all but the simplest cases. A manually steered beamformer will benefit from the SNR enhancement due to the coherent addition of the signal arriving from the steered direction, in contrast to the uncorrelated noise from each element which does not. However, in the presence of additional signals impinging upon the array which may be deemed as interference, the performance of the steered array may be degraded. In order to achieve optimal performance it is necessary to make use of optimisation theory whereby a performance criterion is specified for which an optimal solution for the weights may be found. A number of optimisation criteria have been suggested in the literature, some of which require *a priori* information to be available to the beamformer such as the direction of arrival of the wanted signal or a reference signal, while others may operate blind. Early works in the area of adaptive beamforming used

the SNR at the output the beamformer as the optimisation criterion; examples of arrays based on this criterion are the celebrated Howells-Applebaum array [74, 75] and Shor array [76]. Both were originally developed as analogue beamformers but the maximum SNR criterion can be readily applied in a discrete-time system. The maximum SNR criterion seems an obvious choice due to its widespread use as a performance indicator in communications systems. In particular, in digital communication systems where the SNR of a received signal may be linked to the probability of bit errors in the demodulated signal stream. The optimum weight set solution for the maximum SNR beamformer is given as follows:

$$\mathbf{w}_{opt} = \mu \mathbf{R}_{nn}^{-1} \mathbf{A} \tag{2.1}$$

where μ is a scalar constant, $\mathbf{R}_{nn}$ is the spatial covariance matrix due to the thermal noise and interference, $\mathbf{A}$ is a steering vector in the direction of the wanted signal.

It can be seen from Eq. (2.1) that, in the absence of interference signals impinging upon the array i.e. $\mathbf{R}_{nn} = \sigma_n^2 \mathbf{I}$, where $\mathbf{I}$ is an identity matrix and σ_n^2 is the variance of the thermal noise on each channel, the weight set is defined by the steering vector and, as such, sets the quiescent pattern of the array. A special case of this beamformer was proposed by Compton [77] and Zahm [78] where the steering vector is set to $\mathbf{A} = \begin{bmatrix} 1 & 0 & \dots & 0 \end{bmatrix}^T$ vector such that the quiescent beam pattern is defined by the radiation pattern of the first element; if omni-directional elements are used then the quiescent pattern of the beamformer will omni-directional. Any signals of sufficient power, including the wanted signal, will prompt the beamformer to produce a null in the direction of the signal such that the signal's power at the output of the beamformer is inverted; for this reason it is known as the power inversion beamformer. This has particular application when the wanted signal is weak in comparison to the noise floor of the system, such as an LPI communications system, where the beamformer is unlikely to try to null the signal. The advantage of the power inversion beamformer is that it is less complicated to implement as it operates blind in so far as it does not require *a priori* knowledge of the direction of arrival of the wanted signal or its statistics. In particular, beam-steered systems, which rely on the generation of the steering vector in order to point the mainbeam in the direction of the wanted signal, are sensitive to the frequency dependent gain and phase distortions present in the antenna array and front-end analogue electronic's responses. To avoid beam-pointing errors, careful calibration or measurement of the system's response is required which adds to the complexity of steered beamformers compared with the power inversion beamformer. Furthermore, the power inversion beamformer with an omni-directional quiescent beam pattern is well suited to scenarios in which the antenna must be able to receive a number of spatially diverse signals, for example from a

number of GPS satellites. However, the disadvantage of this is that the power inversion beamformer does not benefit from the array gain due to the coherent combination of all the elements in the array in the direction of the wanted signal.

The need to specify the steering vector in the maximum SNR beamformer necessitates *a priori* knowledge of the direction of arrival of the wanted signal and the power inversion beamformer is not suitable for the reception of stronger signals. If the direction of arrival of the wanted signal is not known but a suitable reference signal that is sufficiently correlated with the wanted signal can be constructed then the MMSE criterion may be used. Widrow *et al.* show in [67] how the MMSE criterion can be used to adjust the beamformer's weights to minimise the mean square of the difference between the beamformer's output and the desired signal. As alluded to, a reference signal is used in place of the desired signal which is unknown *a priori*. The MMSE solution produces the following weight set:

$$\mathbf{w}_{opt} = \mathbf{R}_{uu}^{-1}\mathbf{r}_{u\bar{x}} \tag{2.2}$$

where $\mathbf{R}_{xx}$ is the covariance matrix due to the received signal, $\mathbf{r}_{u\bar{x}} = E\{\mathbf{u}(t)\bar{x}^*(t)\}$ is the correlation vector between the received signals on each element $\mathbf{u}(t)$ and the conjugate of a reference signal $\bar{x}(t)$, where the conjugate is denoted by the superscript $*$.

As the motivation for using adaptive beamforming is typically for interference cancellation it seems natural to base the optimisation criterion on the output power of the beamformer such that the weight set solution minimises it. This approach is encapsulated in the minimum variance (MV) criterion however, in order to ensure that an all zero solution is not produced, a constraint must be applied to the weight set solution. In linearly constrained minimum-variance (LCMV) beamformers this constraint is linear and is usually used to constrain the gain of the beam pattern in the direction of the wanted signal [79]. The LCMV criterion can be expressed as follows:

$$\min_{w} \mathbf{w}^H R_{uu}\mathbf{w} \quad \text{subject to} \quad \mathbf{c}^H\mathbf{w} = \bar{f} \tag{2.3}$$

where the superscript H denotes the Hermitian transpose of the matrix, $\mathbf{c}$ is the constraint vector and $\bar{f}$ is the constraint value.

The optimal solution to the LCMV problem is given as follows [79]:

$$\mathbf{w} = \frac{\bar{f}^*\mathbf{R}_{uu}^{-1}\mathbf{c}}{\mathbf{c}^H\mathbf{R}_{uu}^{-1}\mathbf{c}} \tag{2.4}$$

A special case of this beamformer is the Capon beamformer [80] where $\bar{f} = 1$ and is often referred to as the minimum variance distortion-less response (MVDR) beamformer as the gain of the mainlobe is unity [79].

The similarity between the weight solutions given in Eq. (2.1) through (2.4) have been noted by a number of authors [81–83]. For example, the cross-correlation vector $\mathbf{r}_{u\bar{x}}$ can be shown to be equivalent to the steering vector used in the maximum SNR solution multiplied by a scalar [68]. Furthermore, the noise covariance matrix $\mathbf{R}_{nn}$ in Eq. (2.1) may be replaced by the signal-plus-noise covariance matrix $\mathbf{R}_{uu}$ used in Eq. (2.2) and Eq. (2.3) as long as there is no mismatch between the look direction vector and the true direction of arrival of the wanted signal [84]. As a result it has been widely observed that the optimum weight set solution for a number of performance criteria ends up being a scalar factor of the Weiner solution [64]. This is important as it shows that a wide class of beamformers may be characterised by the results of a single solution.

One final optimisation criterion of note is an extension of the LCMV which extends the single linear constraint in Eq. (2.3) to multiple linear constraints. In particular, given a broadband beamformer such as the STAP structure shown in Figure 2.2, K linear constraints are defined to constrain the weight set solution to maintain a particular response in a given direction over a specified set of frequencies. This LCMV beamformer with multiple constraints was originally proposed by Frost in [85] however, he made the assumption that the array is aligned to the direction of the wanted signal (or steered electrically or mechanically in that direction) and derived a solution for real only weights. In [64] Compton extends this with a treatment of the more generalised case of a STAP beamformer with complex weights and considers the performance of the beamformer in the non-signal aligned case. The LCMV criterion with multiple linear constraints differs from the LCMV criterion given in Eq. (2.3) in so far as $\mathbf{c}$ becomes $\mathbf{C}$ a $MK \times K$ constraint matrix where each column of $\mathbf{C}$ is a constraint vector, similarly $\bar{f}$ becomes a K length constraint vector $\mathbf{f}$:

$$\min_{w} \mathbf{w}^H R_{uu} \mathbf{w} \quad \text{subject to} \quad \mathbf{C}^H \mathbf{w} = \mathbf{f} \tag{2.5}$$

where $\mathbf{C} \in \mathbb{C}^{MK \times K}$ is the constraint matrix and $\mathbf{f} \in \mathbb{C}^{K \times 1}$ is the constraint vector.

Using the method of Lagrange multipliers Frost derives the optimum steady-state weight set solution to Eq. (2.5) which is given as follows:

$$\mathbf{w} = \mathbf{R}_{uu}^{-1} \mathbf{C} \left(\mathbf{C}^H \mathbf{R}_{uu}^{-1} \mathbf{C} \right)^{-1} \mathbf{f} \tag{2.6}$$

A noteworthy alternative formulation of the LCMV beamformer with multiple constraints is the generalized sidelobe canceller (GSC) [86, 87]. Rather than express the LCMV problem as a constrained optimisation problem, the GSC expresses it as an unconstrained optimisation problem. This means that the constraints on the beam pattern are separated from the calculation of the weight set which minimises the variance of the received signal. This allows for the implementation of the adaptive algorithm to be simplified [88].

Many other solutions to the beamformer weight set problem can be derived using alternative optimisation criteria. For example, Chen *et al.* in [89] derive the weight set solution which maximises the bit error rate (BER) of a binary phase shift keying (BPSK) digital communications system directly rather than indirectly via the SNR or MMSE figures of merit. However the non-linear nature of the demodulation of the BPSK signal required by the algorithm increases the complexity of such algorithms. In [90] the authors exploit self-coherence in the structure of the course-acquisition (C/A) code used by civilian GPS receivers to spatially filter the C/A-code from unwanted interference.

2.2.3 Adaptive Algorithms

The task of computing the optimal weight set solution directly can be computationally intensive given that most of the optimal solutions given in Section 2.2.2 require knowledge of the inverse of the covariance matrix. This assumes that the covariance matrix is known *a priori* which, as the signals incident upon the array and their directions of arrival are typically unknown, is not usually the case. It is also reasonable to expect that those signals and their directions of arrival relative to the array will change over time. As such much attention has been paid in literature to methods of adaptively calculating and tracking the weight set solution.

Perhaps the most straightforward approach to calculating the optimum weight set solution without requiring the covariance matrix to be inverted is by the method of steepest descent [91]. In a wide-sense stationary environment a stationary optimisation surface can be described by the cost function of the optimisation problem. The method of steepest descent traverses the optimisation surface by iteratively adjusting the current weight set based on the gradient of the cost function and a step-size parameter. The algorithm will converge toward a minima which, if there is a single solution to the cost function, will represent the optimal Weiner solution to the minimisation problem. The rate of convergence of the steepest descent algorithm is highly dependant on the eigenvalue spread of the covariance matrix [79]. The presence of high power signals on the array will induce a high eigenvalue spread in the beamformer's covariance matrix which

will adversely affect the convergence performance of the beamformer. Given that the gradient is a function of the covariance matrix knowledge of the covariance matrix is required in order to determine the gradient at a given point on the optimisation surface. The method of steepest descent provides no means of determining the covariance matrix and so it must be known *a priori* or estimated. For this reason it tends not to be used in practice but does form the basis of the computationally less complex LMS algorithm.

The celebrated LMS algorithm avoids the need to know the covariance matrix *a priori* by estimating the instantaneous gradient for a given sample instance [67]. Like the method of steepest descent the LMS algorithm adjusts the weights iteratively but because the instantaneous gradient is used rather than the true gradient the LMS algorithm does not follow the path of steepest descent with respect to the true gradient of the covariance matrix. This arises because the received signals tend to have a stochastic component to them which causes the instantaneous gradient function to vary stochastically. Therefore, the LMS algorithm trades computationally complexity at the expense of convergence rate [92]. However, in environments which are stationary in a wide-sense the instantaneous gradient, averaged over time, will converge towards the true gradient [93]. Therefore, assuming a single minima exists in the cost function and the chosen step-size is suitably small, the weight set solution will converge towards the optimal Weiner solution. However, like the method of steepest descent, the convergence rate of the LMS algorithm is sensitive to the eigenvalue spread of the beamformer's covariance matrix [94].

The generally slow convergence rate of the LMS algorithm together with its sensitivity to eigenspread of the covariance matrix make it unsuitable for systems which require a rapid response to a non-stationary signal environment. As an alternative approach to overcome the convergence rate problem Reed *et al.* [95] [96] proposed the use of sample matrix inversion (SMI) (also referred to as *direct matrix inversion*). In the SMI approach the covariance matrix is estimated by calculating the ensemble average of a number of instantaneous covariance matrices, the result is inverted and the weights calculated directly. Reed *et al.* show that the weight set solution is invariant to eigenspread using the SMI method and that performance to within 3 dB of what would be achieved using the Weiner solution can be obtained if at least $2N_w$ samples sets are used to estimate the covariance matrix, where N_w is the number of adjustable weights. The SMI approach might seem like a retrograde step compared with the LMS and steepest descent algorithm as both direct estimation and inversion of the covariance matrix is required; these are both computationally complex making the SMI method difficult to realise in hardware particularly as the number of weights increases. Although the SMI method is not sensitive to the eigenspread of the covariance matrix in terms of convergence rate, a matrix with a sufficiently high eigenspread will be ill-conditioned

with respect to inversion. This will result in a numerically unstable result if insufficient precision has been used while inverting the matrix.

Direct inversion of the covariance matrix can be avoided by using the RLS algorithm [97]. This is achieved through the application of the matrix inversion lemma which allows the inverse of the covariance matrix to be calculated iteratively as new sample sets become available without directly inverting the matrix. The RLS algorithm converges on a weight set solution which minimises the sum of the squares of the difference between the received signal and the desired signal. The convergence time of the RLS algorithm is comparable with that of the SMI method and, therefore, considerably faster than the LMS algorithm for a large eigenvalue spread in a stationary environment. Furthermore, in common with the SMI approach, the convergence rate of RLS is invariant to the eigenspread of the covariance matrix making it suitable for applications where high interference to noise ratios (INRs) are to be expected. While SMI can be sensitive to the conditioning of the covariance matrix and hence, the numerical precision used within the adaptive algorithm, the RLS algorithm can be implemented using numerically robust approaches such as by QR-decomposition. Furthermore, RLS readily lends itself to parallel implementations in hardware such as on field programmable gate arrays (FPGAs) or application specific integrated circuits (ASICs) [98]. The QR-RLS algorithm [99] in particular can be realised into a highly parallelised systolic array structure [100].

2.2.4 Degrees of Freedom

An important aspect of adaptive beamformers, when used for interference suppression, is the number of interference signals they can simultaneously cancel at a given time. Typically, this figure will be associated with the number of degrees of freedom available to the beamformer [64]. The number of degrees of freedom are in turn dictated by the structure of the beamformer, such as the number of elements within the beamforming array with adjustable weights. In narrowband beamformers there is only one weight per element and, it has already been noted, this affords the beamformer $M - 1$ degrees of freedom. As each degree of freedom can be used to place one null in the beam pattern, in general, each degree of freedom can be associated with the ability to fully cancel a single interferer. This holds true if all the signals incident on the array are uncorrelated and have zero bandwidth i.e. are CWs [101]. Note that the number of signals that can be simultaneously cancelled may exceed the degrees of freedom limitation in some special cases, for example if some of those signals arrive from angles such that they fall within a grating null or steered null (due to a different co-incident signal) of the beamformer's beam pattern. However, this is highly contingent on the distribution of received interference signals and so should not be relied upon. The INR of the CW

signal does not affect the number of degrees of freedom required to fully cancel it; one is sufficient. This manifests itself in the power inversion phenomenon [77] whereby the beamformer will create a null in its beam pattern whose depth will increase with increased INR such that the power due to the interferer at the output of the beamformer is the inverse of the input power.

For signals of a non-zero bandwidth incident on a narrowband beamformer the number of degrees of freedom required to cancel the signal depends on both its bandwidth, power and angle of arrival [101, 102]. This is due to the broadband dispersion effect discussed earlier in which a signal with a non-zero bandwidth will appear as a continuum of signals arriving from a range of angles due to the frequency dependant nature of the array's phase response. Compton [64] notes that as the bandwidth is increased the range of angles over which the signal appears to arrive from increases. When the bandwidth becomes sufficiently wide relative to the spacing of the elements the beamformer will place additional nulls in the beam pattern in order to maximise the cancellation of the interferer, each null requiring a degree of freedom. Therefore, it is possible for a single broadband signal to consume all the degrees of freedom in a beamformer, particularly if it consists of few elements. Zatman explores in [66] the limit of what bandwidth a signal may occupy and still be considered narrowband. To this end, he introduces the concept of the 'effective rank' of a signal's covariance matrix, which he states as the number of its eigenvalues that are larger than 1. Given this definition, he adopts an equivalent two CW model of a broadband signal in order to derive an expression for the second eigenvalue of the two CW model's covariance matrix, thereby defining a precise threshold in terms of the signal's angle of arrival, signal to noise ratio and fractional bandwidth beyond which the signal cannot be considered narrowband. In addition to the interference signal's bandwidth, Gupta [101] has shown how the power of the signal can also affect the number of degrees of freedom used by the beamformer to cancel the signal. He notes that, unlike the power inversion experienced by CW interference with only one degree of freedom consumed, broadband signals will consume an increasing number of degrees of freedom as their INR is increased until all available degrees of freedom have been consumed. At this point the beamformer will begin to shut down as the value of its weights become increasingly smaller.

While narrowband beamformers provide a number of spatial degrees of freedom, broadband beamformers possess additional degrees of freedom by way of time-taps, in the case of STAP beamformers, or sub-bands in SFAP beamformers. As has been mentioned a STAP beamformer with M channels and K taps has $MK - 1$ degrees of freedom and these additional degrees of freedom provide increased cancellation performance against broadband signals [103]. Hence, each broadband signal is said to consume K degrees of freedom [104] and therefore the STAP beamformer is able to simultaneously cancel

$M-1$ broadband interference signals. However, Moore and Gupta [104] point out that like the narrowband beamformer the number of degrees of freedom a broadband signal may consume is dependant on its INR. They show that a broadband signal will consume a minimum of K degrees of freedom but this will increase as the INR of the interferer is increased. In these circumstances the total number of broadband signals the beamformer can simultaneously suppress with be less than $M-1$ [105]. When the bandwidth of a broadband interference signal is reduced such that it is now only a fraction of the signal bandwidth Yeh *et al.* [106] show that the number of degrees of freedom consumed by the partialband interferer reduces such that less than K degrees of freedom are used. This, they note, may allow more than $M-1$ partialband interferers to be simultaneously cancelled. However, as was pointed out by Moore and Gupta, just like broadband interference signals, the degrees of freedom consumed by partialband interferers is also dependant on their INRs. Furthermore, they note the importance of the inter-tap delay in the number of degrees of freedom consumed by partialband interference signals and that signals which meet Zatman's definition of narrowband for a narrowband beamformer can consume more than one degrees of freedom in STAP beamformers due to the dependence on the inter-tap delay (of the TDLs). Lastly, the STAP beamformer finds the maximum potential for the number of interference signals it can simultaneously cancel in the presence of CW interference due to its zero bandwidth. As CW signals have zero bandwidth they exhibit no dispersion across the elements and so only consume one degree of freedom regardless of power. This gives the STAP beamformer the ability to simultaneously cancel $MK-1$ CW interference signals [64].

Finally, it should be noted that constraints placed on the beamformer's solution, for example to maintain gain in a given direction, will consume degrees of freedom and therefore reduce the total number of signals that the beamformer can cancel. In a narrowband beamformer with M elements a single direction constraint will leave $M-2$ degrees of freedom for interference cancellation. In a linearly constrained minimum variance beamformer with multiple constraints the total number of degrees of freedom available for interference suppression will be reduced from $MK-1$ by 1 degree of freedom for each constraint.

2.3 Modelling

In the process of designing and/or evaluating a communications system it is usual to develop a model of that system which can subsequently be used for simulation. In digital communications systems, Monte Carlo simulations [107] are typically used to study the performance of the system. This involves developing the model in a computer simulation

environment such as Matlab [108] and running a number of trials of the system given a random input stimulus and measuring a particular figure of merit to determine system performance. The BER is typically used as the figure of merit in digital communications systems as it gives a direct quantitative estimate of the average error performance of the system. In simulation the BER can be measured by transmitting a random bit sequence and then counting the number of bits which are incorrectly demodulated by the receiver termed *bit errors* and denoted n_e. The bit error rate can then be estimated as $\hat{\rho}_e = n_e/N_b$, where N_b is the total number of bits transmitted. In this thesis all simulations using the BER as a figure of merit were ran until the accumulated error count n_e exceeded 200 bit errors, this bounds the confidence of the estimated BER to within 0.2 of the true BER with a confidence level of 95% [107]. Using the BER as a performance measure in conjunction with Monte Carlo simulations has the advantage that it may be used to measure the performance of the system when portions of the system are not linear and time invariant (LTI) as is the case when magnitude clipping is used in FDE.

Simulation allows the performance of various designs or algorithms to be evaluated and compared without incurring the expense and development time of prototyping each candidate component of the system in hardware. It also allows more control over the testing environment so as to ensure that the parameters of interest may be controlled while unwanted effects are excluded. As the model is a representation of real world processes it is important to ensure that it is sufficiently accurate to provide representative performance results. However, this must be balanced by the danger of overcomplicating the model thereby making analysis of the system too difficult. It is important to understand which processes do not need to be included in the model as they do not produce a sufficiently strong effect as well as those processes that can be decoupled from the model and studied in isolation. To this end the antennae used are assumed to have an ideal omni-directional response and the effects of distortions in the analogue front-ends are omitted in all chapters except for Chapter 5 where they are assumed to be linear.

In this thesis, the focus is on the mitigation of the adverse effects of interference present in the same radio environment and band as an LPI DSSS receiver. Therefore, the main components of the model consist of the transmitted DSSS signal, various forms of additive interference, the channel over which the signals travel and the receiver with some form of active interference suppression. In a real communications channel various processes will contribute to the distortion of the transmitted signal as well as the interference signals. These may include multipath effects, Doppler shift and receiver thermal noise. While all of these phenomena will have an impact on the real world performance of both the interference suppression system and the DSSS receiver, to ensure that the model does not become overcomplicated only thermal noise is considered in this work.

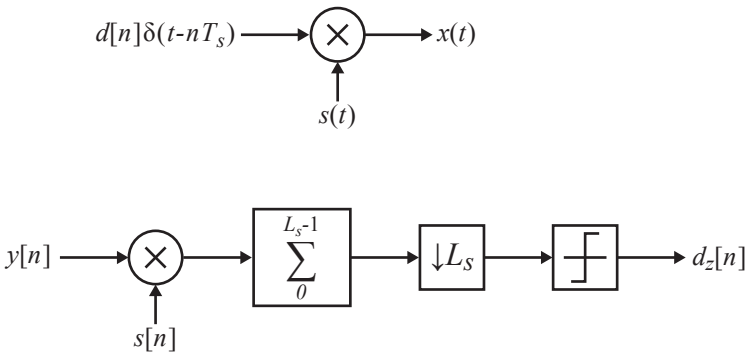

FIGURE 2.4: DSSS transmitter (top) and receiver (bottom)

Receiver thermal noise can be modelled by an additive white Gaussian noise (AWGN) process [109] which is additively combined with the received signal. The remainder of this section details the other components of the system model.

2.3.1 Direct-Sequence Spread-Spectrum Systems

As has already been mentioned in the introduction this work focuses on interference suppression systems for DSSS systems. The reason for this is because of the use of DSSS in secure communications and global navigation satellite systems (GNSS), two areas where interference suppression and anti-jamming are of particular interest. Binary and quadrature phase shift keying (BPSK and QPSK) are the most common forms of data modulation used in conjunction with DSSS. As the theoretical performance of BPSK and QPSK in AWGN is identical only BPSK is considered as these results can be easily extended to QPSK systems. A model of a basic direct sequence spread spectrum communications link with interference suppression is shown in Figure 2.4.

In DSSS systems a binary pseudorandom number (PN) sequence $s[n]$ known as the *spreading sequence* [110] is used to modulate a binary message signal $d[n]$. Each bit of the spreading sequence, known as a *chip*, has a duration of T_c seconds while the duration of each bit in the message signal is $T_b = T_c L_s$ seconds, where L_s is the number of chips in the spreading sequence. The low-pass equivalent of the transmitted signal is given as follows:

$$x(t) = \sqrt{P_x} \sum_{n=-\infty}^{\infty} (2d[n] - 1)s(t - nT_b)$$

where P_x is the average power of the transmitted signal, $d[n] \in \{0, 1\}$ is the n^{th} bit of the transmitted binary data sequence and $s(t)$ is the spreading function formed from an L_s length spreading sequence $s[n]$ such that:

$$s(t) = \sum_{n=0}^{L_s-1} s[n]\varpi_c(t - nT_c)$$

where $s[n] \in \{-1, 1\}$ is the n^{th} chip in the spreading sequence and the function $\varpi_c(t)$ describes the waveform of a single chip, which for this thesis is a rectangular pulse of duration T_c.

2.3.2 Interference Signals

As interference can arise from a multitude of different sources whose characteristics could be equally disparate, it would be impractical to attempt to model them all. Therefore, a generalised set of three classes of interference are considered which are categorised in terms of their band occupancy relative to the wanted signal. Due to the additional complexities involved when modelling non-stationary signals the steady state performance of the systems presented is focused upon, therefore, all signals are assumed to be stationary in a wide-sense. The signals are represented by their low-pass equivalents and as such their frequencies are given relative to baseband. As a number of interference signals may be present at any one time the index i is used to denote the i^{th} interferer.

The first type of interference signal considered is a CW signal which is modelled as a complex sinusoid. Each CW interferer is characterised by its average power P_{g_i}, low-pass equivalent frequency f_{g_i} and phase φ, unless otherwise stated φ is a random value from a uniform distribution over $[0, 2\pi]$. The complex low-pass equivalent of the CW signal is defined as:

$$g_{CW}(t) = \sqrt{P_{g_i}} \exp(j2\pi t f_{g_i} + \varphi) \tag{2.7}$$

The second class of interferer is partialband interferers; Given that intended wanted signal is broadband, due to it being spread by the spreading signal $s(t)$, the beamformer may receive signals with a smaller bandwidth but which are still too wide to be classified as narrowband. Hence, we define partialband interferers as signals of non-zero bandwidth which occupy a portion but not all of the receiver's bandwidth. An example of a partialband signal in the context of a NAVSTAR P-code (precision-code) receiver would be a signal spectrally matched to the NAVSTAR C/A-code signal as the bandwidth

of the C/A-code is 10% the bandwidth of the P-code. To model partialband signals of varying bandwidths a zero-mean complex Gaussian noise process denoted $w(t)$ is filtered by a band-pass filter with an impulse response $h_p(t)$ such that the partialband interferer is given as follows:

$$g_{PB}(t) = \sqrt{P_{g_i}} \int_{-\infty}^{\infty} h_p(t) w(t-\tau) d\tau$$

As the partialband signal will ultimately be sampled the filter response $h_p(t)$ is modelled using a FIR filter. The coefficients of the FIR filter where determined using the Parks-McClellan algorithm to obtain an equiripple band-pass filter such that a pass-band of B_{g_i} centred around the low-pass equivalent frequency f_{g_i} was obtained. In order to ensure that the partialband interference signal is localised well spectrally transition bands of $0.025 f_s$ were specified. To prevent the beamformer from responding to signal energy in the stop-bands at high interference power levels a stop-band attenuation of 100 dB was specified. In order to fulfil this specification the Matlab filter design tool [108] was used to determine a suitable set of filter coefficients resulting in a 247-order FIR filter.

The final class of interferer used is the broadband interference signal which is used to model interference whose bandwidth matches or exceeds that of the wanted signal. This was modelled using a complex Gaussian noise process with zero mean and an average power P_{g_i}. There are many other interference types excluded from this treatment, in particular non-stationary signals such as frequency modulated interferers (e.g. swept CWs) and amplitude modulated interferers (e.g. pulsed signals). Their non-stationary nature makes these forms of interference difficult to analyse and are beyond the scope of this work.

2.3.3 Array Response to Signals

When modelling antenna arrays it is necessary to be able to simulate signals arriving from various directions relative to the array. The spacing between elements within the antenna array will result in each element receiving a time shifted version of each signal where the relative time shifts will depend upon the direction of arrival of each signal and the relative positions of each element within the array. As has been mentioned in Section 2.2, it is these differences in arrival times at each element which the beamformer uses to filter the received signals spatially.

Consider an array of M uniformly spaced antenna elements as shown in Figure 2.5. It should be noted that a variety of different arrangements of the antenna elements may be used and the arrangement of the antenna elements will impact on the performance

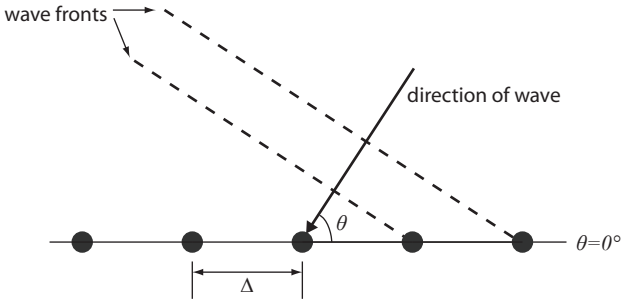

FIGURE 2.5: Uniformly spaced linear antenna array

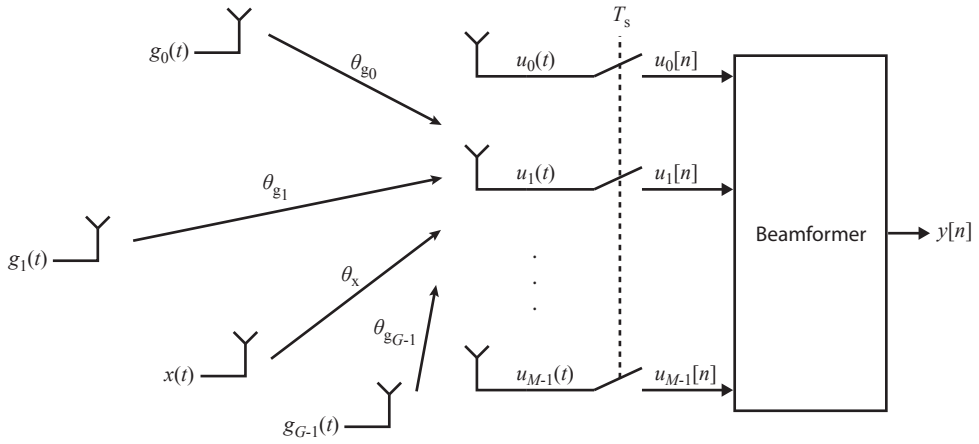

FIGURE 2.6: System model of a beamformer with multiple signals impinging upon the array

of the system. However, the effect of antenna geometry is not the focus of this work and so the linear array with half wavelength spacing between elements is used to provide a suitable model for relative comparisons of system performance. It is common to treat the signals as originating in the far-field from an isotropic source such that the signal's wavefront can be considered planar when it reaches the array.

Impinging upon the array is the wanted signal denoted $x(t)$ from an angle θ_x and G interference signals denoted $g_i(t)$ for the i^{th} interference signal from angles $\theta_{g_i} \forall i$ as shown in Figure 2.6. Each element will receive a superposition of theses various signals which will each differ due to the relative delays in arrival time of each signal at each element. The signal on the m^{th} element is denoted $u_m(t)$ which, for the uniformly linear array (ULA), is given as follows.

$$u_m(t) = x(t - m\tau_d(\theta_x)) + \sum_{i=0}^{G-1} g_i(t - m\tau_d(\theta_{g_i})) + v_m(t) \tag{2.8}$$

where $v_m(t)$ is a white Gaussian noise process with zero-mean, variance σ_v^2 and is identically distributed and independent (i.i.d.) in time and across elements and $\tau_d(\theta)$ is the inter-element time delay due to a signal arriving from an angle θ and is given as follows:

$$\tau_d(\theta) = \frac{\Delta}{c}\cos(\theta) \tag{2.9}$$

where Δ is the spacing between adjacent elements and c is the speed of light in a vacuum.

However, in the simulation of digital systems it is typical to model continuous time signals as discrete-time signals whose sampling rate is either the same as or an integer multiple of the digital system's baseband sampling rate. This is because it is usually only the values of the continuous time signals at the point in time at which they are sampled by the digital system that are of interest; intermediate values are simply not used. This poses a problem in multi-channel systems as the values of each continuous time signal on each channel at each sampling instant will be different due to the relative differences in arrival time of the signal at each element. If each signal impinging upon the array can be described as a closed-form expression then each signal's value can be resolved at the point of sampling with infinite resolution in time; an example of this would be a CW signal. However, it is often necessary to be able to model signals of an arbitrary waveform for which a closed-form expression is not readily available. In this case an alternative strategy may be to over-sample the continuous-time signals in order to produce samples with a time-resolution approaching that necessary to model the time differences between the copies of each signal on the different channels. It is clear that this method could quickly become cumbersome as the over-sampling rate required to achieve a suitable temporal resolution is high. However, if the signals impinging the array are narrowband then they can approximated to CW signals. In which case the interelement time delay $\tau_d(\theta)$ can be expressed as a phase shift where the phase shift experienced by a signal arriving at the m^{th} element from an angle θ is given as follows:

$$A_m(\theta, f) = e^{j2\pi m(f_c+f)\tau_d(\theta)} \qquad m = 0, 1, \ldots, M-1 \tag{2.10}$$

where f is the low-pass equivalent frequency of the incident signal rather than the actual incident frequency of the signal. f_c is the *tuned frequency* of the array and is determined by the spacing Δ of the elements such that $f_c = c/2\Delta$ for half wavelength spacing.

In which case Eq. (2.8) can be re-written as follows:

$$u_m(t) = A_m(\theta_x, 0)x(t) + \sum_{i=0}^{G-1} A_m(\theta_{g_i}, f_{g_i})g_i(t) + v_m(t) \tag{2.11}$$

This model of the received signals is sufficient if the narrowband assumption holds for all the signals incident on the array. However, it is clear that Eq. (2.10) has a dependence on the frequency of the received signal. Therefore, for signals with a non-zero bandwidth the phase shift experienced across the band may not be sufficiently approximated using a single value and, therefore, must be treated as a continuum of values. This can be expressed as a time-domain impulse response for the m^{th} element over the system bandwidth which can be written as follows:

$$a_m(\theta, t) = \int_{-f_s/2}^{f_s/2} A_m(\theta, f) e^{j2\pi f t} df \tag{2.12}$$

By evaluating Eq. (2.12) for each signal impinging upon the array a broadband model of Eq. (2.8) can be written as follows:

$$u_m(t) = \int_{-\infty}^{\infty} a_m(\theta_x, \tau) x(t-\tau) d\tau + \sum_{i=0}^{G-1} \int_{-\infty}^{\infty} a_m(\theta_{g_i}, \tau) g_i(t-\tau) d\tau + v_m(t) \tag{2.13}$$

The signals received by each element, as given by their low-pass equivalents in (2.13), are sampled at a rate $T_s = T_c$. The time sampled signals are denoted by square brackets such that the n^{th} sample on the m^{th} element is given as:

$$u_m[n] = u_m(nT_s) \quad n \in \mathbb{Z} \tag{2.14}$$

The timing of the sampler is assumed to be perfectly synchronised with the timing of the chips of the received DSSS signal as well as there being no frequency offset in the received signal. It is acknowledged that in reality this would not be the case however, the effects of interference on the acquisition and tracking of DSSS signals are not the focus of this work. Therefore, the assumption that if the interference is sufficiently cancelled and suitable algorithms [15] are used for receiver synchronisation then the carrier frequency offset and timing synchronisation errors will be small.

2.3.4 DSSS Receiver

Despreading of the DSSS signal is applied to the sample stream $y[n]$ at the output of the beamformer. The receiver has knowledge of the transmitted signal's spreading sequence $s[n]$ and perfect synchronisation between the spreading sequence $s[n]$ with the received

signal's sequence is assumed during the despreading process. Therefore, the decision variables $d_z[n]$ are given as follows:

$$d_z[n] = \sum_{i=0}^{L_s-1} s[i]y[(nL_s) + i] \tag{2.15}$$

2.4 Summary

In this chapter the current field of active interference suppression for LPI DSSS systems has been explored. The various approaches were categorised into two groups: single-channel and multi-channel based on whether the technique utilised a single antenna or if spatial diversity of the received signals is exploited through the use of an array antenna. It was noted that the ability of multi-channel systems to exploit the spatial diversity of the received signals resulted in a higher interference cancellation capability but at the expense of increased computational complexity. While single-channel systems tend to be less computationally complex than multi-channel systems they are more suited to the suppression of narrowband interference. Finally, the modelling methodology used in this thesis was described, including the simulation of spatially diverse non-zero bandwidth signals arriving at an array antenna.

Chapter 3

Increased Cancellation Capacity in Adaptive Beamformers

3.1 Introduction

In Chapter 2 various interference suppression techniques were discussed with particular emphasis on systems compatible with LPI DSSS signals. It was noted that, in general, multi-channel approaches, such as adaptive beamforming, tend to offer higher levels of protection to LPI DSSS signals compared with single channel methods. This is due to the ability of adaptive beamformers to exploit any spatial diversity between sources of interference and the wanted signal. Crucially, if the wanted signal is uncorrelated with the interference then an adaptive beamformer can achieve high levels of cancellation of the interference signals while maintaining or increasing gain in the direction of the wanted signal. Furthermore, where single channel methods may be defeated by partialband or broadband interference the adaptive beamformer is still usually able to produce a high degree of cancellation, particularly when a broadband beamforming scheme is used such as a STAP beamformer. However, it was noted that this additional protection provided by adaptive beamforming comes at the cost of higher design complexity compared with most single-channel approaches. Therefore, adaptive beamformers tend to be larger in physical design, dissipate more power and have a higher thermal footprint and, as a result, are more limited in terms of where they may be deployed in real-life situations.

Given the differences in the interference suppression capabilities of single-channel and multi-channel systems, as well as their relative complexities, identifying which system is most suitable for a given application can be difficult and will depend on a number of engineering factors. The size, weight and power limitations of the target application must be balanced against the design requirements of how much interference can be tolerated by

the communications system. Clearly, this will also depend on the environment in which the system is to be used, in so far as this may point to the likelihood of encountering interference as well as giving clues as to the properties of the interference, such as spectral occupancy and power level. Unfortunately, it is usually not possible to predict ahead of time what forms of interference may be encountered or the range of interference types may be so broad that it prohibits the use of interference suppression techniques tailored to a subset of interference types. In this circumstance an interference suppression system with the flexibility to cope with a wide range of unknown interference types must be used.

In this chapter, low complexity methods of increasing the number of simultaneous interference signals a broadband adaptive beamforming system can cancel are considered. In particular, methods which avoid the need to increase the number of channels in order to increase the degrees of freedom are of interest. The reason for this is motivated by the complexity involved in adding additional channels to a broadband adaptive beamformer. For example, in a STAP system with M channels and K taps increasing the number of channels will not only increase the computational complexity of the digital processing required to calculate and apply K more weights per additional channel but also add the cost of an additional antenna element in the array, associated cabling and front-end radio frequency (RF) electronics. Increasing the number of time-taps per channel is considered as a method of increasing the cancellation capacity of the beamformer. Increasing the number of time taps per channel avoids the costs associated with an additional RF channel but still adds to the computational load of the digital processing, which must be increased to cope with the calculation and application of M additional weights.

To this end the idea of pre-excising narrowband interference in the frequency-domain prior to the signals reaching the adaptive beamformer is explored. It is assumed that in the most general case the interference environment will contain a mix of narrowband, partialband and broadband interference. In this situation the presence of narrowband interference will occupy degrees of freedom in the beamformer which may otherwise be used in cancelling partialband and broadband interference. In the worst case of an overstressed interference environment the various incident interference signals will exceed the beamformer's available degrees of freedom preventing full cancellation of all the present interference signals. Therefore, if narrowband interference can be cancelled efficiently before reaching the beamformer then it may leave sufficient degrees of freedom in the beamformer to cancel the remaining partialband or broadband interference. Furthermore, this approach may allow for a smaller broadband adaptive beamformer to be used while still maintaining a high interference cancellation capacity, thereby reducing the hardware requirements of the beamformer.

The chapter begins by looking at how the degrees of freedom are consumed within the space-time adaptive processor by analysing the eigenvalues of the beamformer's covariance matrix. In particular the comparative sensitivity of the eigenvalues due to the time-taps versus the weights between channels is examined. A new expression is derived for the second eigenvalue of a STAP beamformer's covariance matrix which indicates the parameters which the temporal degrees of freedom are sensitive to. This can be used to determine when a signal will consumes more than one degree of freedom within the STAP. This is used to evaluate the effectiveness of increasing the number of time-taps as a method of increasing the number of interference signals which the adaptive beamformer can simultaneously cancel.

3.2 Use of Time-Taps to Increase Cancellation Capacity

It has already been asserted that in a design constrained in terms of size, weight and power increasing the number of channels in order to increase the number of interference signals a beamformer can simultaneously cancel is undesirable. As an alternative the number of time-taps in the STAP may be increased as a method of increasing the degrees of freedom in the beamformer with the ultimate goal of increasing the number of interference signals the beamformer can simultaneously cancel. This is based on the assumption that each non-zero bandwidth interference signal incident upon the array will not consume all K degrees of freedom thereby leaving additional capacity in the beamformer to suppress additional interferers [106]. A number of studies have considered the question of what is the optimum balance of taps versus channels in space-time adaptive beamformers. Early works such as those by Rodgers and Compton's [102] consider a 2 element array and what effect varying the number of taps has on the cancellation performance of a broadband interference signal. This work was later expanded upon by Vooks and Compton in [103] who determine the optimum number of taps for an ULA of up to 10 elements. Whereas White [111] questions whether adding more channels or more taps is more effective at improving broadband cancellation performance. However, these studies have focused on improved cancellation performance against broadband interference rather than improved capacity to cancel multiple simultaneous interference signals.

In order to determine how effective increasing the number of time taps is at increasing the cancellation capacity of the STAP it is necessary to understand how the degrees of freedoms which arise from the taps are consumed by various forms of interference. In general the link is made between the bandwidth of and degrees of freedom consumed in the TDLs by a given signal; a narrowband signal consumes 1 degree of freedom while a

broadband signal consumes K degrees of freedom, with partialband signals consuming a value somewhere between the two depending on its bandwidth. So it could be argued that the STAP has sufficient degrees of freedom to cancel $MK-1$ narrowband interferers or M broadband interferers. Unfortunately the situation is complicated by the fact that for non-zero bandwidth signals the degrees of freedom consumed by the signal is not only determined by the bandwidth but other attributes of the signal such as power and angle of arrival as well as the characteristics of the array such as geometry and number of elements [66] [64] [101]. In particular non-zero bandwidth narrowband signals of sufficient power can consume more than 1 degree of freedom while broadband signals of sufficient power can consume more than K degrees of freedom [104]. Moore notes in [104] the difference in sensitivity between taps of the same channel and those of differing channels to interference with a non-zero bandwidth. He provides a limited numerical analysis of the eigenvalues of a STAP beamformer with signals of varying fractional bandwidths impinging upon it. These results show that the bandwidth of the signal relative to the sampling rate of the time-taps has a more dominant effect on the degrees of freedom consumed than the bandwidth of the signal relative to the bandwidth of the array.

In this section the relative sensitivity of the time-taps in the context of degrees of freedom consumed is considered and an expression derived to determine the factors which lead to the temporal degrees of freedom in the beamformer being consumed. To proceed a measure that relates the number of signals received by the beamformer to the consumption of degrees of freedom within the beamformer must be sought. Following the approach of other authors [66] [101] [104] the eigenvalues of the beamformer's covariance matrix are considered for this purpose. Consider a STAP beamformer with M channels and K time taps per channel fed by an M element uniformly-spaced linear array with half wavelength spacing between elements at a centre frequency of f_c. The signal received by the each element of the array is given by each element of the vector:

$$\mathbf{u}(t) = \begin{bmatrix} u_0(t) & u_1(t) & \dots & u_{M-1}(t) \end{bmatrix}^T \tag{3.1}$$

where the superscript T denotes the transpose of the vector.

The signals received by the elements $\mathbf{u}(t)$ are sampled at the sampling rate of the tap delay line f_s such that the signals on the tap delay line taps at the n^{th} sampling interval are as follows:

$$\bar{\mathbf{u}}[n] = \begin{bmatrix} \mathbf{u}(nT_s)^T & \mathbf{u}((n-1)T_s)^T & \dots & \mathbf{u}((n-K+1)T_s)^T \end{bmatrix}^T \tag{3.2}$$

The covariance matrix $\mathbf{R}_{\bar{u}\bar{u}} \in \mathbb{C}^{MK \times MK}$ of the STAP beamformer is given as follows:

$$\mathbf{R}_{\bar{u}\bar{u}} = \mathrm{E}\left\{\bar{\mathbf{u}}[n]\bar{\mathbf{u}}[n]^H\right\} \tag{3.3}$$

where $\mathrm{E}\{\cdot\}$ is the statistical expectation operator.

By making the assumption that all the signals incident on the array are uncorrelated with each other $\mathbf{R}_{\bar{u}\bar{u}}$ can be expressed as the superposition of the covariance matrices of all the signals incident upon the array plus the covariance matrix due to the thermal noise on each channel:

$$\mathbf{R}_{\bar{u}\bar{u}} = \mathbf{R}_{gg} + \mathbf{R}_{vv} \tag{3.4}$$

where $\mathbf{R}_{gg} \in \mathbb{C}^{MK \times MK}$ is the covariance matrix due to all the received signals and $\mathbf{R}_{vv} \in \mathbb{C}^{MK \times MK}$ is the covariance matrix due to the receiver thermal noise. If the thermal noise is the result of an AWGN process and is independent and identically distributed (i.i.d.) in time and across elements then the thermal noise can be approximated to an identity matrix::

$$\mathbf{R}_{vv} = \sigma_v^2 \mathbf{I} \tag{3.5}$$

where σ_v^2 is the variance of the noise and $\mathbf{I}$ is an $MK \times MK$ identity matrix. Note that if channel filtering were applied to limit the bandwidth of the received signal then this approximation would no longer hold true as the cross components between taps of differing sampling instances of the noise covariance matrix will be a function of the reduced bandwidth of the noise relative to the system bandwidth.

The component covariance matrices contributing to $\mathbf{R}_{\bar{u}\bar{u}}$ in Eq. (3.4) can be described in terms of their eigenvalues and eigenvectors which can be found by eigen-decomposition of each matrix [68]. The eigenvalues and eigenvectors due to the thermal noise on each channel form the *noise* subspace of $\mathbf{R}_{vv}$:

$$\mathbf{R}_{vv} = \mathbf{E}_{vv}\mathbf{\Lambda}_{vv}\mathbf{E}_{vv}^H \tag{3.6}$$

where the columns of the matrices $\mathbf{E}_{vv} \in \mathbb{C}^{MK \times MK}$ are the eigenvectors and the diagonal elements of $\mathbf{\Lambda}_{vv}$ are the eigenvalues of the noise subspace.

The eigenvalues of a given covariance matrix $\mathbf{R}$ can be found by solving the characteristic equation of the covariance matrix:

$$\det(\mathbf{R} - \lambda\mathbf{I}) = 0 \tag{3.7}$$

where $\mathbf{I}$ is an identity matrix with the same dimensions as $\mathbf{R}$.

Solving Eq. (3.7) for $\mathbf{R}_{vv}$ yields by inspection the result that the diagonal matrix of the eigenvalues of $\mathbf{R}_{vv}$ must also be an identity matrix:

$$\mathbf{\Lambda}_{vv} = \sigma_v^2\mathbf{I} \tag{3.8}$$

The eigenvalues and eigenvectors due to the signals incident upon the array form the *signal* subspace of $\mathbf{R}_{gg}$:

$$\mathbf{R}_{gg} = \mathbf{E}_{gg}\mathbf{\Lambda}_{gg}\mathbf{E}_{gg}^H \tag{3.9}$$

Again the eigenvalues of $\mathbf{R}_{gg}$ can be found by solving Eq. (3.7). The covariance matrix $\mathbf{R}_{gg}$ contains the beamformer's average response to all the signal incident upon the array. The eigenvalues of the signal sub-space are useful as they indicate how the degrees of freedom in the beamformer are consumed and hence, can be used to determine whether the beamformer has sufficient capacity to cancel all the received signals. Given that $\mathbf{R}_{gg}$ is a semi-definite positive Hermitian matrix its eigenvalues will all be real and non-negative. Furthermore, given that $\mathbf{R}_{gg}$ is Hermitian, the rank of $\mathbf{R}_{gg}$ will be equal to the number of positive eigenvalues associated with $\mathbf{R}_{gg}$. Therefore, each positive eigenvalue gives rise to one linearly independent column in $\mathbf{R}_{gg}$ and hence, a degree of freedom in the weight solution. The number of eigenvalues which are positive will depend on the number of signals incident upon the array as well as the properties of those signals such as bandwidth and power. This also applies to $\mathbf{R}_{\bar{u}\bar{u}}$ as $\mathbf{R}_{vv}$ is a positive definite Hermitian matrix. However, $\mathbf{R}_{\bar{u}\bar{u}}$ is always full rank as the presence of the thermal noise regularises $\mathbf{R}_{\bar{u}\bar{u}}$.

It is well known that a signal of zero bandwidth, i.e. a CW signal, gives rise to exactly one eigenvalue irrespective of power, angle of arrival, array configuration or tap-delay configuration [104]. Therefore, in all cases a CW signal will consume one degree of freedom in the beamformer. This is readily shown by considering the eigenvalues of $\mathbf{R}_{gg}$ when the only signal impinging upon the array is a CW. Consider a CW signal denoted $g(t)$ of the form given by Eq. (2.7) with a low-pass equivalent frequency f_g, power P_g

and arriving at the array from an angle θ_g. The covariance matrix $\mathbf{R}_{gg}$ due to the CW will be given as follows:

$$\mathbf{R}_{gg} = P_g \left(\mathbf{S}(f) \otimes \mathbf{A}(\theta, f)\right) \cdot \left(\mathbf{S}(f) \otimes \mathbf{A}(\theta, f)\right)^H \tag{3.10}$$

where $\otimes$ is the Kronecker product and $\mathbf{S}(f) \in \mathbb{C}^{K\times 1}$ is the response of the time-taps of one channel and is defined as follows:

$$\mathbf{S}(f) = \begin{bmatrix} 1 & e^{j2\pi\frac{f}{f_s}} & \dots & e^{j(K-1)2\pi\frac{f}{f_s}} \end{bmatrix}^T \tag{3.11}$$

and, $\mathbf{A}(\theta, f)\mathbb{C}^{M\times 1}$, termed the *steering vector*, contains the response of the elements of the array antenna to a CW signal arriving from an angle θ with a frequency f and is defined as follows:

$$\mathbf{A}(\theta, f) = \begin{bmatrix} A_0(\theta, f) & A_0(\theta, f) & \dots & A_{M-1}(\theta, f) \end{bmatrix}^T \tag{3.12}$$

where $A_m(\theta, f)$ is the response of the m^{th} element which, for a ULA, is given by Eq. (2.10).

The eigenvalues of $\mathbf{R}_{gg}$ for the CW signal can be found by solving Eq. (3.7) for Eq. (3.10). Inspection shows that $\mathbf{R}_{gg}$ has one single positive eigenvalue which is given as follows:

$$\lambda_1 = P_g MK \tag{3.13}$$

The covariance matrix due to a signal with a non-zero bandwidth incident upon the array will give rise to MK positive eigenvalues. However, only some of these eigenvalues will have a non-negligible value relative to the eigenvalues of the noise and, as such, consume degrees of freedom in the beamformer. Zatman [66] uses the notion of effective rank to quantify the number of eigenvalues with a significant value which he defines as the number of eigenvalues in the signal sub-space whose value is greater than unity. The effective rank of a non-zero bandwidth signal will depend on the properties of the signal, array and time-taps. As a non-zero bandwidth signal may take on any number of forms it is instructive to consider a simple case in which the bandwidth and power are easily related. A suitable model is that of a wide-sense stationary stochastic process with average power P_g whose power spectral density (PSD) S_g is flat over the finite bandwidth B_g as given by the following:

$$S_g(f) = \begin{cases} P_g/B_g & : \quad f_c - B_g/2 \leq f \leq f_c + B_g/2 \\ 0 & : \quad f_c - B_g/2 > f > f_c + B_g/2 \end{cases} \tag{3.14}$$

The covariance matrix $\mathbf{R}_{gg}$ of the non-zero bandwidth signal with the PSD given in Eq. (3.14), can be described in terms of the auto-correlation function $r_{gg}(\tau)$ of the signal $g(t)$:

$$\mathbf{R}_{gg} = \begin{bmatrix} r_{gg}(\mathbf{T}_d(\theta)) & r_{gg}(\mathbf{T}_d(\theta) + T_s) & \dots & r_{gg}(\mathbf{T}_d(\theta) + (K-1)T_s) \\ r_{gg}(\mathbf{T}_d(\theta) - T_s) & r_{gg}(\mathbf{T}_d(\theta)) & \dots & \vdots \\ \vdots & \vdots & \ddots & \vdots \\ r_{gg}(\mathbf{T}_d(\theta) - (K-1)T_s) & \dots & \dots & r_{gg}(\mathbf{T}_d(\theta)) \end{bmatrix} \tag{3.15}$$

where $\mathbf{T}_d(\theta)$ is a matrix containing the relative inter-element delays $\tau_d(\theta)$ for a signal arriving at an angle θ and is defined as follows:

$$\mathbf{T}_d(\theta) = \begin{bmatrix} 0 & \tau_d(\theta) & \dots & (M-1)\tau_d(\theta) \\ -\tau_d(\theta) & 0 & \dots & \vdots \\ \vdots & \vdots & \ddots & \vdots \\ -(M-1)\tau_d(\theta) & \dots & \dots & 0 \end{bmatrix} \tag{3.16}$$

By defining the band-limited stochastic signal $g(t)$ in terms of a PSD its auto-correlation function $r_{gg}(\tau)$ can be determined by invoking the Weiner-Khinchine theorem, such that:

$$r_{gg}(\tau) = \mathrm{E}\left\{g^*(t)g(t+\tau)\right\} = \int_{-\infty}^{\infty} S_g(f)e^{j2\pi\tau f}df \tag{3.17}$$

Solving Eq. (3.17) for each of the elements in Eq. (3.15), the covariance matrix for the non-zero bandwidth signal can be written as follows:

$$\mathbf{R}_{gg} = P_g\bar{\mathbf{B}}(B_g,\theta) \cdot (\mathbf{S}(f) \otimes \mathbf{A}(\theta,f)) (\mathbf{S}(f) \otimes \mathbf{A}(\theta,f))^H \tag{3.18}$$

where the dot operator indicates the Hadamard product of the matrices either side of the operator and $\bar{\mathbf{B}}(B,\theta)$ is a matrix containing the dispersion factors applied to the steering vector due to the bandwidth of the signal and is defined as follows:

$$\bar{\mathbf{B}}(B,\theta) = \mathrm{sinc}(B \begin{bmatrix} \mathbf{T}_d(\theta) & \mathbf{T}_d(\theta)+T_s & \dots & \mathbf{T}_d(\theta)+(K-1)T_s \\ \mathbf{T}_d(\theta)-T_s & \mathbf{T}_d(\theta) & \dots & \vdots \\ \vdots & \vdots & \ddots & \vdots \\ \mathbf{T}_d(\theta)-(K-1)T_s & \dots & \dots & \mathbf{T}_d(\theta) \end{bmatrix}) \quad (3.19)$$

Unless the effective rank of $\mathbf{R}_{gg}$ is small, finding a closed-form solution to the eigenvalues of $\mathbf{R}_{gg}$ in Eq. (3.18) may not be possible and numerical methods must be used. However, if the analysis is limited to non-zero bandwidth signals with an effective rank of no more than 2 then analytic methods of determining the eigenvalues may be used. To this end a rank 2 approximation of the non-zero bandwidth signal may be made using two CW signals as proposed by Zatman in [66]. In the rank 2 model 2 CW signals of equal power are used to approximate the covariance matrix of a broadband signal. As the covariance matrix of the 2 CWs is limited to a rank of 2 the approximation is only valid while $\lambda_3 \approx 0$, therefore only the first two eigenvalues may be determined. However, this is sufficient to study the relative sensitivity between the weights on the taps of the same channel and weights of differing channels as well as the parameters upon which they depend.

The eigenvalues for two uncorrelated CW signals can be expressed in the form of a quadratic equation [112], furthermore when the two CW signals are of equal power then the expression can be simplified to the following:

$$\lambda_{1,2} = MP_g\left(1 \pm |\phi|\right) \quad (3.20)$$

where ϕ is the cosine of the angle between the steering vectors of the two CWs.

In order for the two CW signals to correctly represent the broadband signal, Zatman notes that the first and second moments of the instantaneous spectrum of the two CWs must correspond with the first and second moments of the broadband signal. This is achieved by placing the two CWs at the frequencies $f_c \pm f_k$ in the spectrum where f_k is the square-root of the variance of broadband signal which, for a rectangular PSD, is given as:

$$f_k = \frac{B_g}{2\sqrt{3}} \quad (3.21)$$

Given Eq. (3.21) and that the angle of arrival of the two CWs is θ_g then ϕ is given as follows:

$$\phi = \frac{1}{M}\mathbf{A}(\theta_g, -f_k)^H \mathbf{A}(\theta_g, f_k) \tag{3.22}$$

By expanding and then simplifying Eq. (3.22) and putting the result together with Eq. (3.20) Zatman produces an expression for the second eigenvalue of a broadband signal incident on a ULA with half-wavelength spacing:

$$\lambda_2 = MP_g \left(1 - \text{asinc}_M \left(\frac{\pi B_g \cos(\theta_g)}{f_c\sqrt{3}}\right)\right) \tag{3.23}$$

where asinc() is the aliased sinc function (known also as the Dirichlet function or periodic sinc function) [113] and is defined as follows:

$$\text{asinc}_N(x) \triangleq \frac{\sin\left(\frac{Nx}{2}\right)}{N\sin\left(\frac{x}{2}\right)} \tag{3.24}$$

3.2.1 Rank 2 Model of non-zero Bandwidth Signals in STAP Beamformers

To extend the 2 CW model for non-zero bandwidth signals to a STAP beamformer the effect of the addition of the time-taps on the eigenvalues of $\mathbf{R}_{gg}$ must be taken into account. To this end consider an M element ULA with half wavelength spacing between elements as per Zatman's model. However, rather than one adaptive weight per element there are K adaptive weights forming a tap delay line with a sampling period T_s between taps. The expression for the first and second eigenvalues of the STAP's covariance matrix due to 2 equal power uncorrelated CWs is almost identical to Eq. (3.20), differing only by a factor of K to account for the additional weights:

$$\lambda_{1,2} = MKP_g\left(1 \pm |\phi|\right) \tag{3.25}$$

The effect of the time-taps on each channel of the STAP must be included in the calculation of $|\phi|$ therefore, rather than use the steering vector a response vector for the values on each tap must be determined.

Taking the response of the taps from Eq. (3.11) and the response of the elements of a ULA with half-wavelength spacing as given by Eq. (3.12) the response vector for all the taps of the STAP is given as follows:

$$\bar{\mathbf{A}}_{\text{ZB}}(\theta, f) = \mathbf{S}(f) \otimes \mathbf{A}(\theta, f) \tag{3.26}$$

Taking Eq. (3.22) ϕ can be calculated by determining the inner product of the response vector given by Eq. (3.26) for each CW of the rank two model.

$$\phi = \frac{1}{MK}\bar{\mathbf{A}}_{ZB}(\theta, -f_k)^H \bar{\mathbf{A}}_{ZB}(\theta, f_k) \tag{3.27}$$

Expanding Eq. (3.27) reveals that it can be expressed as the product of two geometric series, the first as a result of the elements, the second as a result of the time taps as follows:

$$\phi = \frac{1}{MK}\left(\sum_{m=0}^{M-1} e^{jm4\pi f_k \tau_d(\theta_g)}\right)\left(\sum_{n=0}^{K-1} e^{jn4\pi f_k/f_s}\right) \tag{3.28}$$

where $\tau_d(\theta)$ is the inter-element time delay as given by Eq. (2.9).

Inspecting Eq. (3.28) the geometric series can be simplified such that:

$$\phi = \frac{1}{MK}\left(\frac{e^{j4\pi M f_k \tau_d(\theta)} - 1}{e^{j4\pi f_k \tau_d(\theta)} - 1}\right)\left(\frac{e^{j4\pi K f_k/f_s} - 1}{e^{j4\pi f_k/f_s} - 1}\right) \tag{3.29}$$

By factoring out the linear phase term $e^{j2\pi f_k(\tau_d(\theta)(M-1)+(K-1)/f_s)}$ in Eq. (3.29) then $|\phi|$ can be expressed in terms of the aliased sinc function:

$$|\phi| = \text{asinc}_M(4\pi f_k \tau_d(\theta_g))\,\text{asinc}_K(4\pi f_k/f_s) \tag{3.30}$$

Substituting the frequency offset f_k from Eq. (3.21) into Eq. (3.30) yields $|\phi|$ for the STAP case:

$$|\phi| = \text{asinc}_M\left(\frac{\pi B_g \cos(\theta_g)}{f_c\sqrt{3}}\right)\text{asinc}_K\left(\frac{2\pi B_g}{f_s\sqrt{3}}\right) \tag{3.31}$$

The 2^{nd} eigenvalue can thus be found by substituting Eq. (3.31) into Eq. (3.25) as follows:

$$\lambda_2 = \frac{MKP_g}{2}\left(1 - \text{asinc}_M\left(\frac{\pi B_g \cos(\theta_g)}{f_c\sqrt{3}}\right)\text{asinc}_K\left(\frac{2\pi B_g}{f_s\sqrt{3}}\right)\right) \tag{3.32}$$

The similarities between Eq. (3.32) and Eq. (3.23) are evident. However, the addition of time taps in the STAP beamformer adds an additional aliased sinc function term in $|\phi|$. The extra term demonstrates the second eigenvalue's dependence on the signal's

bandwidth relative to the sampling rate of the taps but also on the number of taps in the delay lines. By inspection of Eq. (3.32) when $B_g = 0$ both aliased sinc functions are equal to unity resulting in a zero valued second eigenvalue which is as expected for a zero bandwidth signal. For the second eigenvalue to become positive it is necessary for the value of one of the aliased sinc functions to be less than unity. If $f_s < f_c$ then as B_g increases the aliased sinc function due to the time taps will be the first to reach this point. In a typical radio application $f_c >> f_s$, therefore the time taps will always have the dominant effect on the second eigenvalue. In fact, given the condition $f_c >> f_s$, for the aliased sinc function due to the element spacing to respond, the signal would have to violate the rank 2 model approximation as the model is only valid if $\lambda_3 \approx 0$. Therefore, the aliased sinc function due to the element spacing can be assumed to be unity and Eq. (3.32) can be simplified to the following:

$$\lambda_2 = \frac{MKP_g}{2}\left(1 - \text{asinc}_K\left(\frac{2\pi B_g}{f_s\sqrt{3}}\right)\right) \tag{3.33}$$

Eq. (3.33) shows that the second eigenvalue is only dependant on the signal's bandwidth relative to the sampling rate, its power, the number of taps and the number of elements. This agrees with Moore's observation that the eigenvalues of a STAP beamformer's covariance matrix are more sensitive to the signal's bandwidth relative to the sampling rate than the signal's bandwidth relative to the element spacing.

3.2.2 Numerical Results

To study the sensitivity of the STAP's time-taps to a non-zero bandwidth signal a STAP beamformer attached to a ULA with $M = 4$ elements is considered. The inter-tap sampling rate relative to the tuned frequency of the array is $f_s/f_c = 0.025$ to simulate a 40 MHz bandwidth centred at 1.6 GHz as may be found in a NAVSTAR GPS receiver. The non-zero bandwidth signal arrives at the array from an angle $\theta_x = 45°$ and the signal's power P_g and normalised bandwidth B_g/f_s are both varied. Initially, the validity of Eq. (3.33) was confirmed by comparing the results produced using the expression with simulated results. Figures 3.1(a) and 3.1(b) plot these values for both cases using a STAP with $K = 2$ and $K = 10$ taps per channel respectively. In both cases the plots show that the theoretical value produced by Eq. (3.33) closely matches the simulated values. The results produced mostly closely match the simulated values when the number of taps per channel K is small as is shown in Figure 3.1(a). With a larger number of taps the predicted value of λ_2 deviates slightly from the simulated values as the normalised bandwidth of the signal is increased. From Eq. (3.33) it is clear that the value of λ_2 is linearly proportional to the signal's power. This is confirmed by

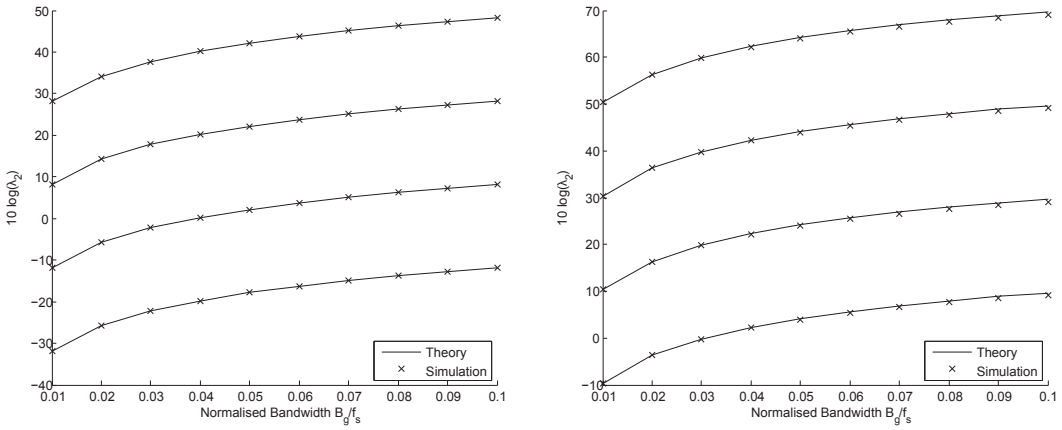

(a) $K = 2$ (b) $K = 10$

FIGURE 3.1: Simulated and theoretical values of 2^{nd} eigenvalue of $\mathbf{R}_{gg}$

the simulated results in both figures and demonstrates that by increasing the signal's power the normalised bandwidth at which the effective rank of the signal increases from 1 to 2 decreases. As a result, signals of the same normalised bandwidth can appear narrowband or partialband to the beamformer depending on their power.

Eq. (3.33) also shows a dependence on the number of taps per channel. Figure 3.2 plots the 2^{nd} eigenvalue for the same scenario however, this time the number of taps is varied while the signal's power remains fixed at $P_g = 30$ dBW. In the same way that increasing the signal's power increased the second eigenvalue so does increasing the number of taps. However, rather than a linear relationship between the two, the increase of the second eigenvalue shows an exponential decay with an increased tap number. This shows that adding an additional tap per channel will increase the sensitivity of the time-taps to the normalised bandwidth of the signal. Therefore, the normalised bandwidth at which the signal becomes rank 2 is decreased such that a signal which may have appeared narrowband to the STAP will now appear partialband due to the increase in the number of time taps. This is more marked for STAPs which have fewer taps per channel to begin with, as the number of taps per channel is increased the sensitivity to the addition of new taps is decreased. These effects should be kept in mind when considering ways of increasing the number of degrees of freedom available to the STAP, particularly with a view to increasing the number of simultaneous interference signals the STAP can cancel. The increased sensitivity of the time-taps to the normalised bandwidth of the signal highlighted here suggest that the degrees of freedom due to the time taps will be more readily consumed by partialband signals. To confirm this it is necessary to consider the remaining eigenvalues due to the non-zero bandwidth signal.

It is also instructive to consider the behaviour of the remaining eigenvalues of $\mathbf{R}_{gg}$. As

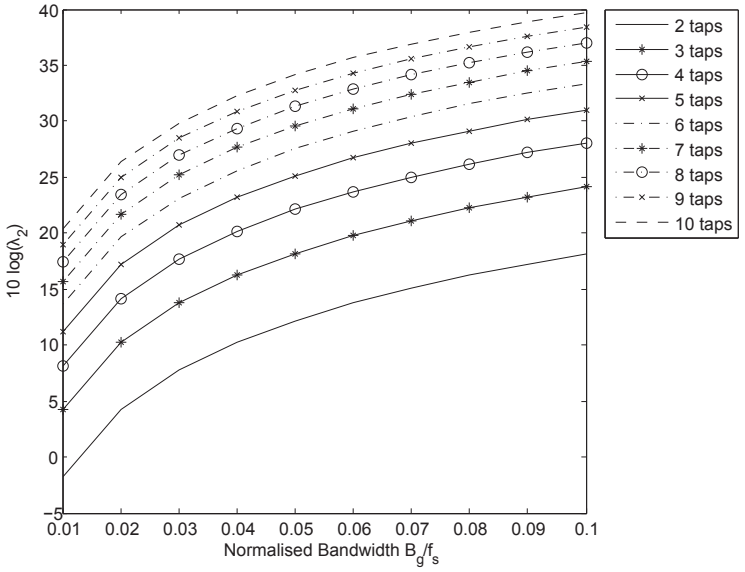

FIGURE 3.2: 2^{nd} eigenvalue of $\mathbf{R}_{gg}$ for a variable number of taps per channel, $P_g = 30$ dBW

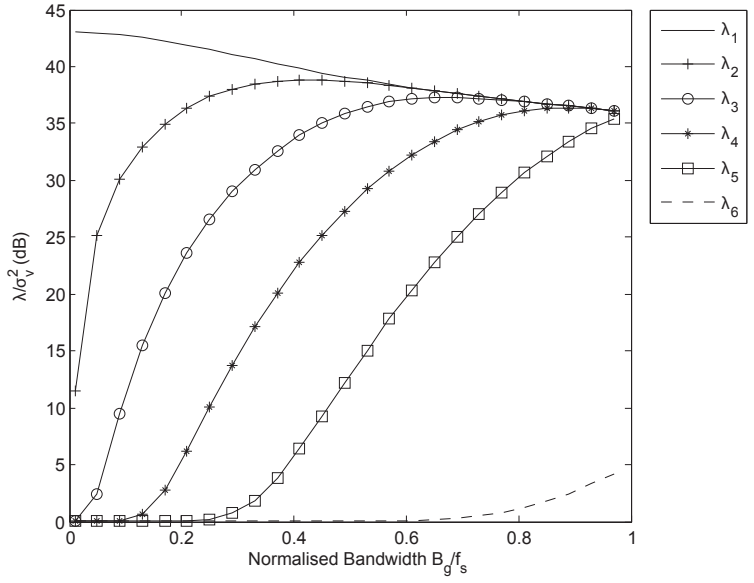

FIGURE 3.3: First 6 eigenvalues of $\mathbf{R}_{\bar{u}\bar{u}}$, $P_g/\sigma_v^2 = 30$ dB and $K = 5$

mentioned previously it is necessary to resort to numerical methods to calculate the remaining eigenvalues by solving Eq. (3.7). Instead of calculating the eigenvalues of the signal only, the eigenvalues of the signal plus the thermal noise are calculated to ensure that the covariance matrix is not ill-conditioned. Hence, rather than calculating the eigenvalues directly from $\mathbf{R}_{gg}$ they are instead calculated from the covariance matrix $\mathbf{R}_{\bar{u}\bar{u}}$ given in Eq. (3.4) where the covariance matrix due to the thermal noise is given in Eq. (3.8) with $\sigma_v^2 = 1$.

Figure 3.3 plots the first 6 eigenvalues of the covariance matrix for the signal used in

Figure 3.2 and a STAP with $M = 4$, $K = 5$, $f_s/f_c = 0.025$. The first 5 eigenvalues are due to the delay between time taps whereas the 6^{th} eigenvalue is due to the spacing between elements. This highlights the relative sensitivity of the time-taps compared with the elements as the first 5 eigenvalues are more closely grouped than the 6^{th} eigenvalue due to $f_s << f_c$. By inspecting the plot of the 5^{th} eigenvalue, the normalised bandwidth at which the effective rank of the signal equals the number of taps per channel, and therefore, has consumed all the degrees of freedom due to the taps on one channel, can be deduced. In this scenario the signal need only occupy approximately a third of the sampling bandwidth of the STAP to have consumed all the degrees of freedom due to the time-taps.

Given that the K^{th} eigenvalue is indicative of all the degrees of freedom due to the K taps on one channel being consumed by the signal, and hence the signal appearing broadband to the beamformer the K^{th} eigenvalue is considered now in isolation. Figure 3.4(a) plots the 5^{th} eigenvalue over a range of normalised bandwidths for various interference signal to noise ratios of the non-zero bandwidth signal. The plot shows that as the INR of the signal is increased, the normalised bandwidth at which the signal appears broadband to the beamformer decreases. Therefore, the ability of the beamformer to utilise spare degrees of freedom due to the time taps will depend not only on the number of incident signals and their normalised bandwidths but also their INRs. For example, Figure 3.4(a) indicates that a signal with $P_g/\sigma_v^2 = 40$ dB will consume 5 degrees of freedom while only occupying just over one fifth of the sampling bandwidth of the STAP. In Figure 3.4(b) the number of taps per channel K has been varied and the INR fixed at $P_g/\sigma_v^2 = 30$ dB, as the number of taps per channel is being varied the K^{th} eigenvalue is plotted. The plots indicates that as additional taps are added to each channel the normalised bandwidth of the signal at which it will consume K degrees of freedom is increased. However, for each additional tap added per channel, the increase in the normalised bandwidth at which the signal appears broadband decreases as more taps are added. So a broadband interferer will always consume K degrees of freedom regardless of the number of taps per channel. Furthermore, the normalised bandwidth at which all K degrees are consumed will typically be much less than the full bandwidth of the system.

In summary, the number of simultaneous interferers which the STAP can cancel depends on the number of degrees of freedom available to it. These are determined by the number of adjustable weights in the STAP which is given by the number of taps per channel K and the number of channels M. Of equal importance are the properties of the interference signals incident upon the array which will affect the number of degrees of freedom consumed within the STAP by each interference signal. If the only signals incident upon the array have a zero bandwidth then the number of interferers which the STAP can simultaneously cancel will be maximised. However, if some of the signals

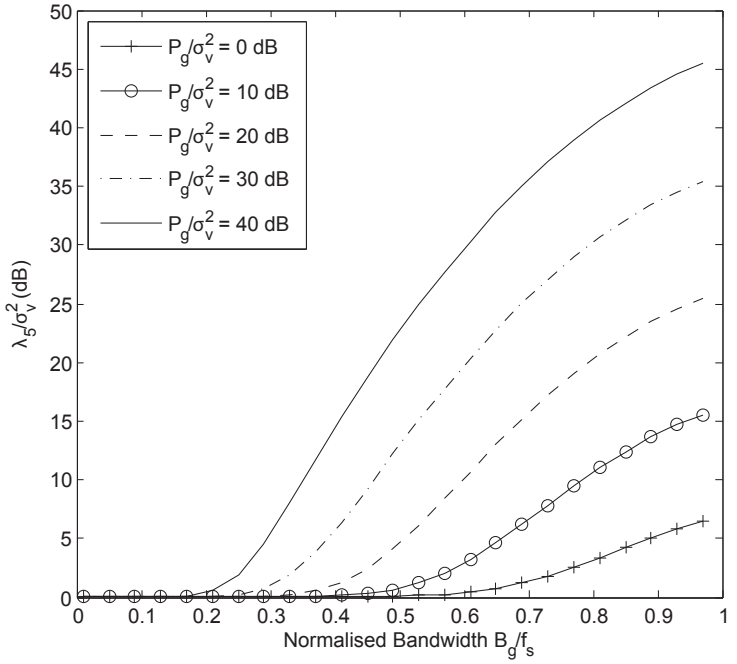

(a) 5^{th} eigenvalue

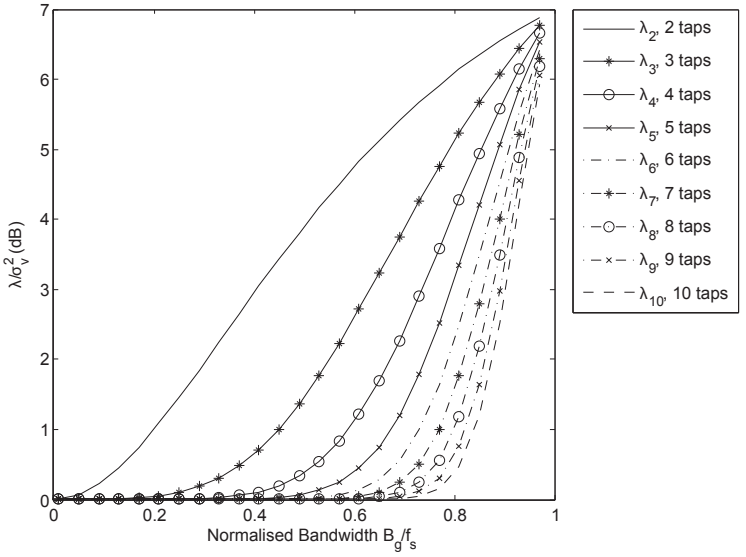

(b) K^{th} eigenvalue

FIGURE 3.4: Eigenvalues of $\mathbf{R}_{\bar{u}\bar{u}}$ variable INRs and numbers of taps

incident upon the array have a non-zero bandwidth then they have the potential to consume more than 1 degrees of freedom per non-zero bandwidth interferer, thereby reducing the total number of interference signals which can be simultaneously cancelled. In a STAP beamformer this is exacerbated by the higher sensitivity of weights of the same channel compared with weights between differing channels. The effectiveness of increasing the number of time-taps per channel as a method of increasing the number of interference signals a STAP can simultaneously cancel relies on each interference signal incident upon the array not consuming all K degrees of freedom per channel. However, the results presented have shown how readily these degrees of freedom are consumed by non-zero bandwidth interferers, particularly as the INR of the interferer is increased.

3.3 Pre-filtering of Narrowband Interference in Beamformers

The problems associated with adding extra time-taps as a method of increasing the number of signals a beamformer can cancel motivates the search for alternatives. Noting that narrowband signals can be efficiently cancelled using single channel interference suppression systems it is proposed that the interference cancellation problem be divided into two discrete and independent stages: the first stage consists of a filter on each of the beamformer's channels which removes narrow-band interference received by each array element, while the second stage is made up of a broadband adaptive beamformer used to remove the remaining partialband and broad-band interference (see figure 3.5). The filters on each channel operate independently of each other and independence is maintained between the pre-filtering and the beamforming stages to minimise the complexity of the design. Given the stipulation that the interference environment contains a mix of narrowband interference as well as partialband and/or broadband interference, the removal of narrowband signals prior to beamforming should free up degrees of freedom in the adaptive beamformer. This could be used to enhance the interference suppression capability of an existing adaptive beamformer design or to reduce the size of the adaptive beamformer design while still maintaining a high interference cancellation capability.

Frequency-domain excision filtering was chosen as the method of narrowband interference pre-filtering because narrowband interference can be readily identified in the frequency-domain. The open-loop nature of the interference identification and removal process in frequency-domain excision lends itself to modification for the purposes of selective narrowband pre-filtering. Many of the other candidate forms of narrowband interference suppression discussed in Chapter 2 are simply unsuitable in this regard. For example, linear prediction error filters operate by decorrelating the received signal with

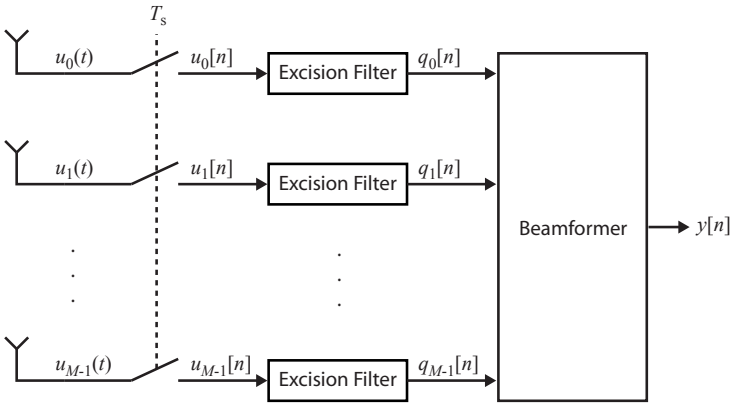

FIGURE 3.5: Dataflow diagram of a STAP beamformer with pre-excision filters

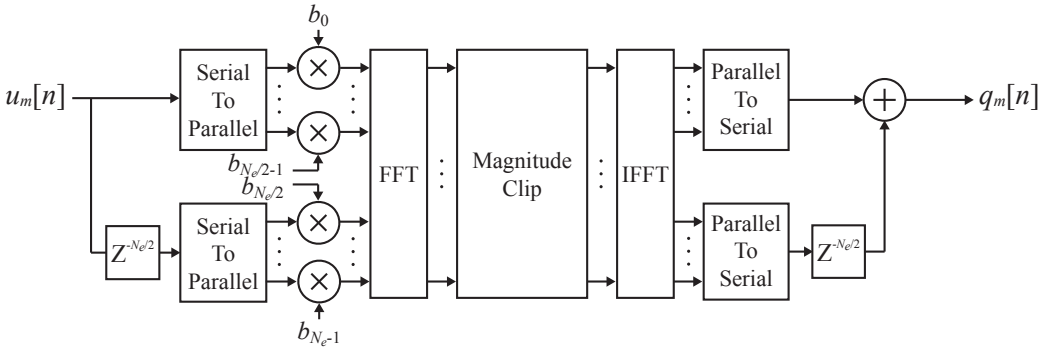

FIGURE 3.6: Dataflow diagram of a single frequency-domain excision filter

the effect whitening the signal's spectrum. This works well at removing narrowband interference which is highly correlated but will also target partialband interference as well. Furthermore, frequency-domain excision is well suited to narrowband interference suppression in DSSS systems as the DSSS signal is typically spread over a wide bandwidth [44]. Therefore, while the processing gain of the DSSS signal may not be sufficient to recover the DSSS signal to an acceptable level with interference present, after excision, the majority of the interference signal's energy should have been removed. Then, assuming that the excision process has not excised an excessive amount of the DSSS signal's energy, it should allow the DSSS signal to be recovered.

3.3.1 Front-end Excision Filters

The dataflow of a single excision filter is shown in Figure 3.6. The filter structure is based around an N_e length forward and inverse discrete Fourier (DFT/IDFT) pair which transforms blocks of samples between the sampled time-domain and the short-time discrete Fourier transform (STDFT) domain in which narrowband interferers can be identified and excised. A time-domain window $\mathbf{b} \in \mathbb{C}^{N_e \times 1}$ is applied to samples prior

to the DFT to reduce spectral leakage. This ensures that the majority of the interferer's energy is concentrated in as few bins as possible thereby minimising the number of bins, and hence portion of the spectrum, that requires excision for each interferer. To mitigate the loss incurred as a result of applying the window an $N_e/2$ sample overlap is introduced [50]. The input samples for the filter on the m^{th} channel $u_m[n]$ are processed by the filters in blocks of N contiguous samples. To simplify the description of the filter the vector notation $\mathbf{u}_m(l) \in \mathbb{C}^{N_e/2\times 1}$ for the input samples is introduced such that:

$$\mathbf{u}_m(l) = \left[u_m[\tfrac{lN_e}{2}] \quad u_m[\tfrac{lN_e}{2}+1]\ldots \quad u_m[\tfrac{(l+1)N_e}{2}-1]\right]^T$$

Firstly, the $N_e/2$ sample overlap is introduced such that the l^{th} block of overlapped samples $\tilde{\mathbf{u}}_m(l) \in \mathbb{C}^{N_e\times 1}$ is given as:

$$\tilde{\mathbf{u}}_m(l) = \begin{bmatrix}\mathbf{u}_m(l-1)\\ \mathbf{u}_m(l)\end{bmatrix} \tag{3.34}$$

The time-domain window $\mathbf{b}$ is applied to each block of samples before an N_e-point discrete Fourier transform is applied to produce a vector $\tilde{\mathbf{U}}_m(l) \in \mathbb{C}^{N_e\times 1}$ of frequency-domain samples:

$$\tilde{\mathbf{U}}_m(l) = \mathbf{F}_{N_e}\,\mathrm{diag}(\mathbf{b})\tilde{\mathbf{u}}_m(l) \tag{3.35}$$

where $\mathrm{diag}(\cdot)$ is the diagonal matrix operator, $\mathbf{F}_{N_e}$ is an $N_e \times N_e$ Vandermonde matrix such that the elements are defined by the discrete Fourier transform roots of unity:

$$[F_N]_{k,j} = \exp\left(\frac{-i2\pi kj}{N}\right) \quad \forall k,j \in \{0,1,...,N-1\} \tag{3.36}$$

where $i \triangleq \sqrt{-1}$.

Each block $\tilde{\mathbf{U}}_m(l)$ contains N_e frequency bins which represent the short-time spectrum of the signal over the N_e samples in $\tilde{\mathbf{u}}_m(l)$. At this point, bins identified as containing narrowband interference are excised from the block according to the excision function $\Gamma(\cdot)$. The excised blocks are then transformed into the time-domain by an N_e-point IDFT to produce the vector $\hat{\mathbf{q}}_m(l) \in \mathbb{C}^{N_e\times 1}$ of excised time-domain samples:

$$\hat{\mathbf{q}}_m(l) = \mathbf{F}_{N_e}^{-1}\Gamma(\tilde{\mathbf{U}}_m(l)) \tag{3.37}$$

The excision function $\Gamma(\cdot)$ either operates by zeroing or clipping the magnitude of the bin. The bins which are to be excised are specified by the N_e length mask vector $\mathbf{D} \in \{0, 1\}$. The zeroing method of excision sets bins marked for excision to zero as indicated in Eq. (3.38).

$$\Gamma_{\text{zero}}(\tilde{U}_{k,m}(l)) = \begin{cases} 0 : D_k = 1 \\ \tilde{U}_{k,m}(l) : D_k = 0 \end{cases} \tag{3.38}$$

where $\tilde{U}_{k,m}(l)$ denotes the k^{th} element i.e. frequency bin, of the vector $\tilde{U}_m(l)$ and D_k is the k^{th} element of the excision mask vector $\mathbf{D}$.

The noise clip method [50] clips the magnitude of bins marked for excision to the noise floor of the system while maintaining the phase of the bin as described by Eq. (3.39). Therefore, in order to determine the level to clip the bins to, knowledge of the noise power is required. In this thesis knowledge of the noise power is assumed however, it is noted that in practice the average noise power level can be estimated simply with minimal complexity.

$$\Gamma_{\text{clip}}(\tilde{U}_{k,m}(l)) = \begin{cases} \sqrt{2N_e\sigma_v^2}e^{j\angle\tilde{U}_{k,m}(l)} : D_k = 1 \\ \tilde{U}_{k,m}(l) : D_k = 0 \end{cases} \tag{3.39}$$

The time-domain blocks $\hat{\mathbf{q}}_m(l)$ still contain the $N_e/2$ sample overlap introduced by (3.34). In order to fully construct the output signal the last $N_e/2$ samples of the previous block must be overlapped and added to the first $N_e/2$ samples of the current block to produce the vector $\mathbf{q}_m(l+1) \in \mathbb{C}^{N_e \times 1}$ of time-domain samples:

$$\mathbf{q}_m(l) = \begin{bmatrix} \mathbf{I}_{N_e/2} & \mathbf{0}_{N_e/2} \end{bmatrix} \hat{\mathbf{q}}_m(l) + \begin{bmatrix} \mathbf{0}_{N_e/2} & \mathbf{I}_{N_e/2} \end{bmatrix} \hat{\mathbf{q}}_m(l-1) \tag{3.40}$$

where $\mathbf{I}_{N_e/2}$ is an $N_e/2 \times N_e/2$ identity matrix, $\mathbf{0}_{N_e/2}$ is an $N_e/2 \times N_e/2$ all zero matrix.

The positional relationship between the excised sample stream $q_m[n]$ on the m^{th} channel and the column vector $\mathbf{q}_m(l)$ output from the excision filter is given by the following mapping:

$$\mathbf{q}_m(l) = \begin{bmatrix} q_m[\frac{lN_e}{2}] & q_m[\frac{lN_e}{2}+1] \ldots & q_m[\frac{(l+1)N_e}{2}-1] \end{bmatrix}^T \tag{3.41}$$

The signals $q_m[n]$ for $m = 0, 1, \ldots, M-1$ are ready to be passed onto the adaptive beamformer, where the m^{th} signal forms the input to the m^{th} channel of the beamformer.

3.3.2 Effects of Pre-excision on Degrees of Freedom

The objective of pre-excision is to remove narrowband interference prior to beamforming so as to conserve degrees of freedom in the beamformer for the cancellation of partialband and broadband interference. For this to be achieved it is important that the narrowband interference is sufficiently cancelled by the pre-excision filters so as not to prompt a response from the beamformer. However, the cancellation performance of frequency-domain excision filtering is highly dependant on the window function used to suppress the sidelobe level of the narrowband interference [114]. It has already been mentioned that the discontinuous nature of block processing signals of an infinite extent in time can give rise to considerable spectral leakage. While the application of a window function does help in greatly reducing the amount of spectral leakage and hence, the sidelobe level, it will not completely eliminate it; some of the signal's power will still remain contributing to the overall noise level across the spectrum. In addition to this, the use of a window will contribute to widening the mainlobe of the interferer and as a result, increase the number of bins required to excise the interferer or, put another way, decrease the spectral resolution of the excision filter. This widening of the narrowband signal's bandwidth may be problematic for the beamformer if the narrowband interference is not sufficiently excised as the narrowband signal, with its widened bandwidth, may still consume degrees of freedom in the beamformer. Worse still, the number of degrees of freedom consumed by the signal may be more than it would otherwise have consumed without excision. However, this situation can be avoided as long as a suitable window function is used in the excision filters and a sufficient number of bins containing the interferer's energy are excised. In this way independence between the excision filtering stage and the beamforming stage maybe maintained so as reduce the complexity of the combined system.

To explore the effects of window function choice and number of bins excised on the degrees of freedom consumed, the eigenvalues of the covariance matrix of a space-time adaptive processor with a pre-excision filter on each channel are considered. The configuration used is the same as that show in Figure 3.5 and the STAP beamformer consists of $M = 4$ channels each with $K = 3$ taps where the delay between taps is equal to the sampling period T_s. The signal received by the m^{th} element is denoted $u_m(t)$ as described by Eq. (2.3.3) and is sampled at a rate relative to f_c of $f_s/f_c = 0.025$ to produce the time sampled signal $u_m[n]$. Added to the m^{th} channel at this point is the Gaussian noise process $v_m(t)$ to represent thermal noise in the receivers, the variance of the noise

on each channel is fixed at $\sigma_v^2 = 1$ and is independent and identically distributed (i.i.d.) in time as well as across elements. As described in Section 3.3.1 the time sampled signals on each channel $u_m[m]$ are processed by the excision filter on that channel to produce an excised signal $q_m[n]$ which is fed into its respective channel in the STAP beamformer. At this point it is helpful to define the vector $\tilde{\mathbf{q}}[n] \in \mathbb{C}^{MK\times 1}$ which contains the contents of each TDL in the STAP at the sampling instance n:

$$\tilde{\mathbf{q}}[n] = \begin{bmatrix} q_0[n] & q_1[n] & \dots & q_{M-1}[n] & q_0[n-1] & \dots & q_{M-1}[n-K+1] \end{bmatrix}^T \tag{3.42}$$

From Eq. (3.42) the covariance matrix of the STAP can be defined as follows:

$$\mathbf{R}_{\tilde{q}\tilde{q}} = \mathrm{E}\left\{\tilde{\mathbf{q}}[n]\tilde{\mathbf{q}}^H[n]\right\} \tag{3.43}$$

The covariance matrix $\mathbf{R}_{\tilde{q}\tilde{q}}$ can be estimated in a number of ways as discussed in Section 2.2.3, such as recursively, for example, using the RLS or LMS algorithm or directly using SMI [95]. As it is the steady state performance of the system which is of interest the SMI method is used to estimate the covariance matrix by calculating the sample average of the outer product of $\tilde{\mathbf{q}}[n]$ with its Hermitian transpose over $N_r = 200$ blocks:

$$\mathbf{R}_{\tilde{q}\tilde{q}} \approx \frac{1}{N_r}\sum_{n=0}^{N_r-1} \tilde{\mathbf{q}}[n]\tilde{\mathbf{q}}^H[n] \tag{3.44}$$

The eigenvalues of $\mathbf{R}_{\tilde{q}\tilde{q}}$ were determined by solving Eq. (3.7) numerically using the Matlab routine *eig()* which itself is based on the LAPACK eigen-decomposition routines [115].

The length of excision filter considered is $N_e = 1024$, this ensures the excision filters have a high spectral resolution while maintaining a DFT size which can be implemented efficiently in hardware using a radix-2 [116] or radix-4 [117] FFT. Initially, no explicit window function is used therefore a rectangular window is inferred: $[\mathbf{b}]_k = 1 \quad k = 0, 1, \dots, N_e - 1$. A single signal $g(t)$ in the form of a CW with a low-pass equivalent frequency f_g is incident on the array from an angle $\theta_g = 30^\circ$ with an average power P_g which is varied. Therefore, the low-pass equivalent signal on the m^{th} element of the array is given as follows:

$$u_m(t) = \sqrt{P_g}e^{j(2\pi((f_c+f_g)\tau_d(\theta_g)+tf_g/f_s)+\varphi)} + v_m(t) \tag{3.45}$$

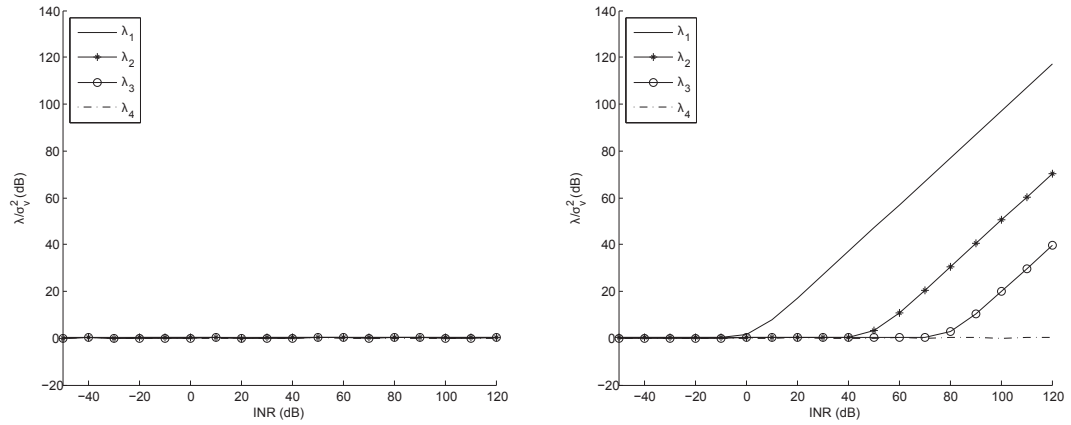

(a) $f_g/f_s = 30/1024$ (b) $f_g/f_s = 30.5/1024$

FIGURE 3.7: First four eigenvalues of $\mathbf{R}_{\tilde{q}\tilde{q}}$ for excised CW

where $\tau_d(\theta_g)$ is the inter-element delay given by Eq. (2.9) and φ is the phase component of the CW whose value is random and taken from a uniform distribution over $[0, 2\pi]$.

Two scenarios are examined: the coherent case the frequency of the CW is centred exactly over one bin so that $f_g/f_s = 30/1024$, and the incoherent case in which the CW is centred halfway between two bins so that $f_g/f_s = 30.5/1024$. The first case is chosen to ensure that the CW appears perfectly continuous to the excision filters when periodically extended; this represents the best-case spectral localisation resulting in no spectral leakage, while the second case is chosen to be maximally discontinuous thereby exacerbating the effects of spectral leakage. Excision is applied by zeroing the bin(s) around which the CW is centred. In the first case bin 30 is excised, in the second case, because the CW is halfway between two bins, both bins 30 and 31 are excised. For the excision filters to have been effective in their task of desensitising the beamformer to the CW interference signal they must reduce the effective rank of the signal subspace of $\mathbf{R}_{\tilde{q}\tilde{q}}$ from 1 to 0. Therefore, all the eigenvalues of $\mathbf{R}_{\tilde{q}\tilde{q}}$ must not be greater than the eigenvalues in the noise subspace which equal σ_v^2. The eigenvalues of $\mathbf{R}_{\tilde{q}\tilde{q}}$ are determined by solving Eq. (3.7) numerically. The first 4 eigenvalues of $\mathbf{R}_{\tilde{q}\tilde{q}}$ versus P_g/σ_v^2 due to the excised CW signal using a rectangular window for the bin centred and halfway centred cases are shown in Figure 3.7(a) and 3.7(b) respectively.

In the first case where the CW is exactly bin centred only one bin need be excised in order to reduce the effective rank of the covariance matrix to 0. This is hardly surprising as the CW signal is perfectly aligned with the rectangular DFT window of the excision filters and therefore appears perfectly periodic to the DFT thereby ensuring that all of the CW's energy is concentrated within the one bin. Therefore, when the bin is zeroed by the excision filter all of the energy associated with the CW is removed from the

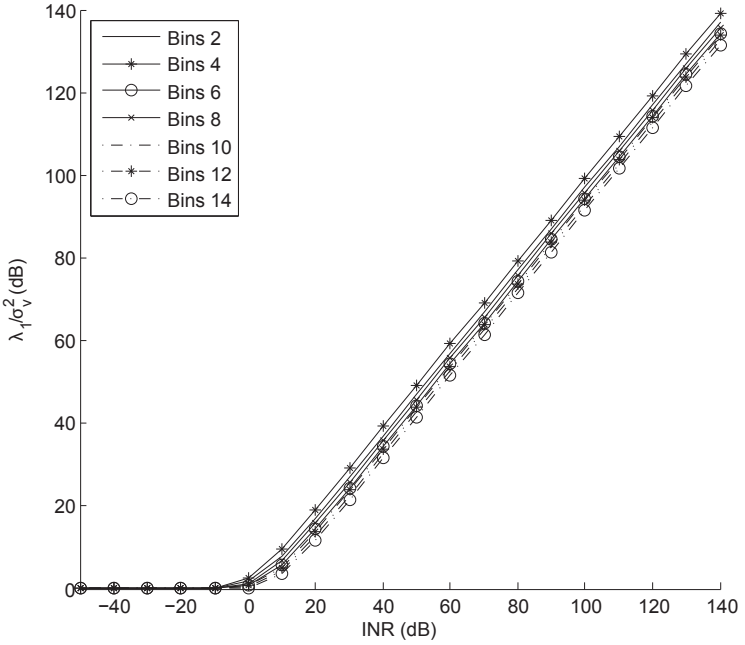

FIGURE 3.8: First eigenvalue of $\mathbf{R}_{\tilde{q}\tilde{q}}$ for excised CW using rectangular window

received signals. A very different result is obtained when excision is applied to the CW centred halfway between two bins. The effective rank of the signal's covariance matrix is increased from 1 to 3 by the excision of just one bin resulting in the residual CW signal consuming as many degrees of freedom as a broadband signal. This is to be expected as the spectral leakage resulting from the combination of the rectangular window and the CW not being bin centred has resulted in the CW's energy being spread across all of the excision filter's bins. Furthermore, the rectangular window produces a mainlobe that, while centred around bins 30 and 31, has very wide skirts i.e. the CW's energy is not well concentrated within the mainlobe. Consequently, the CW is only partially excised, the energy from the CW in the unexcised bins remains in the form of a residual signal. Worse still this residual signal no longer has a zero bandwidth which is the cause of the increased effective rank in the covariance matrix.

More of the spectrally spread CW signal's energy can be removed if a larger number of contiguous bins either side of $f_g/f_s = 30.5/1024$ is excised such that the total number of bins excised is K_b. To determine whether increasing K_b can successfully reduce the effective rank of the CW, only the first eigenvalue need be considered. Figure 3.8 shows the value of the first eigenvalue of the STAP covariance matrix for a varied number of excised bins.

It is not too surprising that increasing the number of excised bins has little effect on the value of the first eigenvalue. The width of skirts of the leakage from the mainlobe are so wide that a significant portion of the spectrum must be excised in order to remove

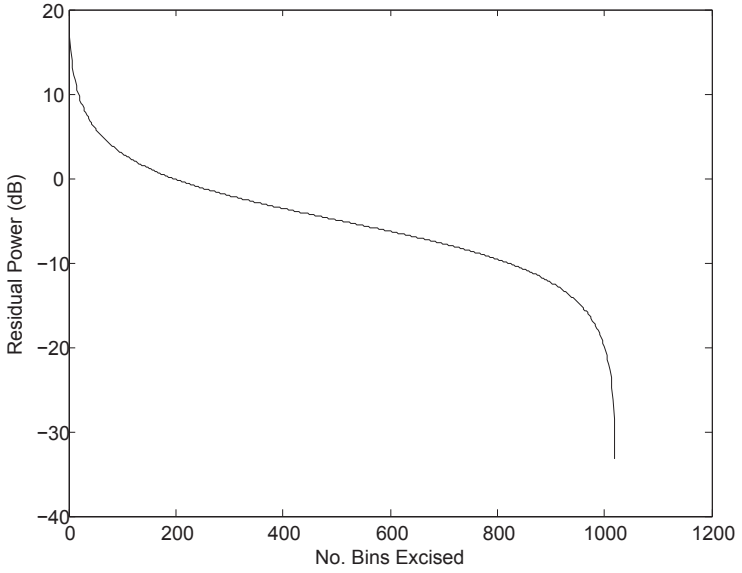

FIGURE 3.9: Residual power due to excision of CW signal with $P_g = 30$ dBW

sufficient energy from the CW signal so as to desensitise the beamformer. This can be seen in Figure 3.9 which plots the residual power of the CW signal with an average power before excision of $P_g = 30$ dBW versus number of bins excised by zeroing. In order to suppress the CW by 30 dB over a fifth of the spectrum needs to be excised.

Clearly, it would not be sensible to use the excision filters without a window to provide some level of sidelobe suppression. Indeed, the problem of spectral leakage in excision filters is well known [114]. However, the rectangular window does highlight the impact spectral leakage has on the degrees of freedom the partially excised signal consumes within the beamformer. Rather than reducing the rank of the beamformer's covariance matrix the opposite is achieved. In practice, the sidelobe level of narrowband signals would be controlled with the use of a suitable window function. One class of window function that encompasses many popular windows is the cosine series window:

$$[\mathbf{b}]_n = \sum_{l=0}^{L_w-1} (-1)^l \alpha_l \cos\left(\frac{2\pi}{N_e} ln\right) \quad n = 0, 1, \ldots, N_e - 1 \tag{3.46}$$

A large number of window functions can be described in terms of the cosine series given in Eq. (3.46), for example the Hann, Hamming, Bartlett, Nutall and Blackman windows [118]. Each window is specified by the number of cosine terms L_w and the values of the coefficients α_l for $l = 0, 1, \ldots, L_w - 1$. Of the class of cosine series windows the Blackman-Harris window is of particular interest as it is designed to minimize the maximum sidelobe level [53]. The 4-term Blackman-Harris is calculated using Eq. (3.46) with the following coefficients:

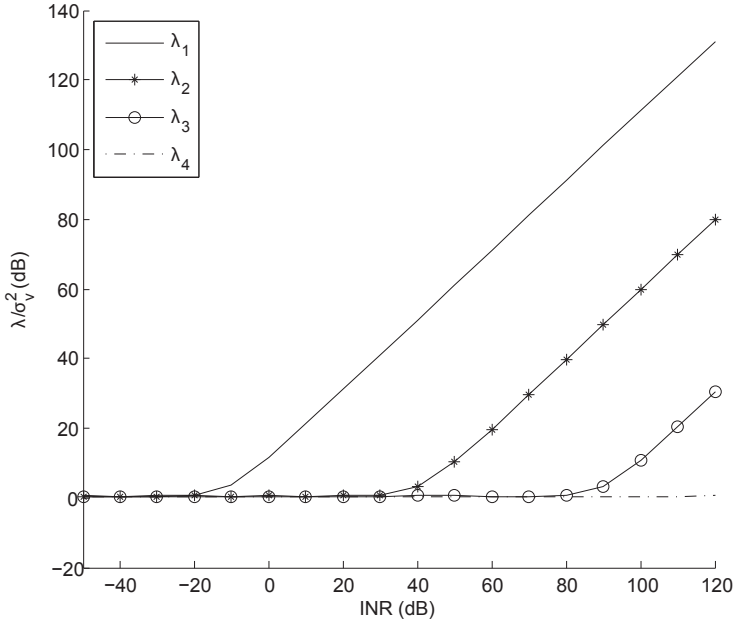

FIGURE 3.10: Eigenvalues of $\mathbf{R}_{\tilde{q}\tilde{q}}$ using Blackman-Harris window and no bins excised

$$\begin{aligned}\alpha_0 &= 0.35875\\ \alpha_1 &= 0.48829\\ \alpha_2 &= 0.14128\\ \alpha_3 &= 0.01168\end{aligned} \tag{3.47}$$

The use of the 4-term Blackman-Harris window specified by Eqs. (3.46) and (3.47) in the excision filters is now considered. In particular the effect the increased sidelobe suppression has on the eigenvalues of the beamformer's covariance matrix is of interest. The same signal model used previously with the rectangular window is retained and, in all results, the CW signal's INR is varied from -50 to 120 dB. It is important to first consider the effect the window has on the signal's rank due to the widening effect of the window with respect to the signals's bandwidth and this is shown in Figure 3.10. While the response of the first eigenvalue is almost identical to the first eigenvalue using the rectangular window with no excision, it is clear that as the INR of the signal is increased the rank of the signal is also increased as indicated by the increase in value of the remaining eigenvalues.

The effect of excising the CW using the Blackman-Harris window is now considered and in particular how many bins are required to be excised to reduce the rank of the

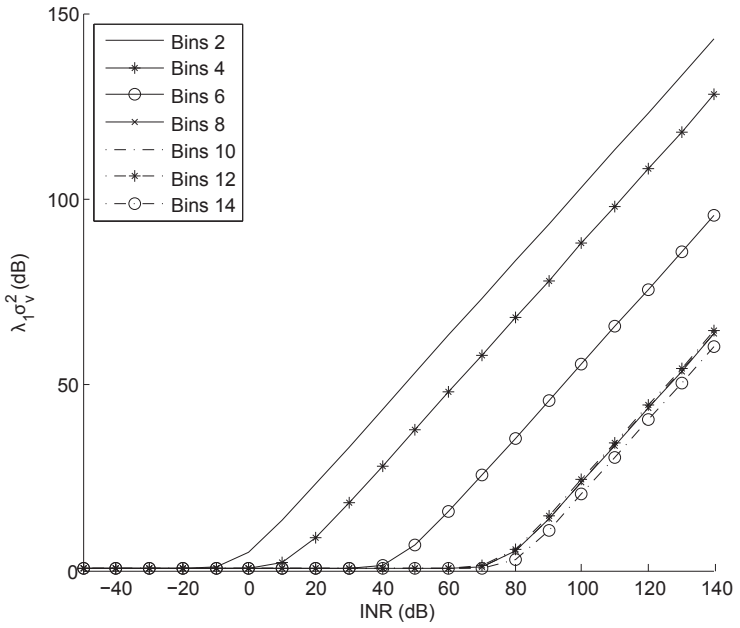

FIGURE 3.11: 1^{st} eigenvalue of $\mathbf{R}_{\tilde{q}\tilde{q}}$ using Blackman-Harris window

signal to 0. Figure 3.11 plots the first eigenvalue against INR for a varying number of contiguous bins excised. The results show the effect of the window's sidelobe suppression and hence, concentration of the CW's energy in the mainlobe. A small improvement is seen in the maximum INR which can be cancelled when the number of bins excised is increased from 2 to 4 as 4 bins is insufficient to remove all of the mainlobe. Further increasing the number of bins excised improves the cancellation more dramatically as the majority of the mainlobe is cancelled. The improvement in cancellation continues until the number of bins excised becomes greater than 8, at which point no further improvement in cancellation is achieved as the mainlobe has almost been completely cancelled.

Confirmation that the CW signal has been sufficiently cancelled by the excision filters so as not to prompt the beamformer to attempt to null the signal can be found by inspecting the beam pattern produced by a power inversion beamformer. The motivation for using the power inversion beamformer is that it provides a nulling only solution such that it places nulls in a nominally omni-directional quiescent beam pattern in the direction and across the frequency band of the interference signals it detects. The optimal weight set for the power inversion beamformer is given by:

$$\mathbf{w}_{\mathrm{PI}} = \mathbf{R}_{\tilde{q}\tilde{q}}^{-1}\mathbf{u} \tag{3.48}$$

where $\mathbf{u} = \begin{bmatrix} 1 & 0 & \dots & 0 \end{bmatrix}^T$.

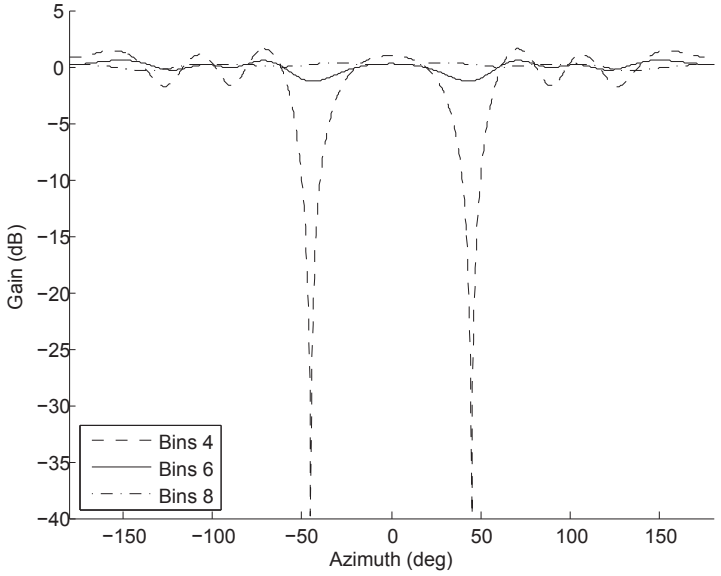

FIGURE 3.12: Beam pattern of power inversion beamformer for an excised CW

The gain of the beamformer in a given direction at a frequency f is given as follows:

$$G_b(\theta, f) = \left| \sum_{m=0}^{M-1} \left(\sum_{k=0}^{K-1} w_{mK+k} e^{-j2\pi k \frac{f}{fs}} \right) e^{j2\pi m f \tau_d(\theta)} \right|^2 \tag{3.49}$$

If the CW signal is not fully excised it is expected that the beamformer's beam pattern should contain a null co-incident with the angle of arrival of the CW signal. However, if the signal is sufficiently excised then the beamformer's beam pattern it should contain no nulls and have an omni-directional response. Figure 3.12 plots the power inversion's beam pattern in terms of gain versus azimuth angle for a CW with INR = 40 dB excised using the Blackman-Harris window and various excision widths.

The beam pattern produces a strong null in response to the signal when only 4 bins are excised. From Figure 3.11 it is clear that this is due to the signal only being partially excised as 4 bins does not provide sufficient cancellation when INR = 40 dB. However, by increasing the number of bins excised to 6 or greater the beam pattern becomes omni-directional indicating that the beamformer has been successfully desensitised to the CW signal.

Figure 3.11 indicates that the Blackman-Harris window provides sufficient suppression of the signal's sidelobes for INRs up to 70 dB. If cancellation of signals with a higher INR is needed an alternative window is required. One such window is the Dolph-Chebyshev window [119] whose function is defined in the frequency-domain:

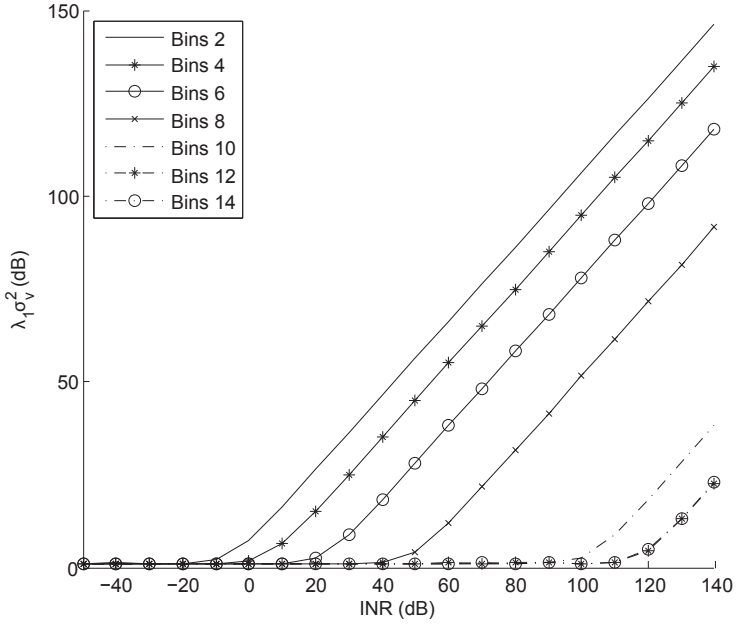

FIGURE 3.13: 1^{st} eigenvalue of $\mathbf{R}_{\tilde{q}\tilde{q}}$ using Dolph-Chebyshev window

$$\left[\tilde{\mathbf{b}}\right]_k = (-1)^k \frac{\cos(N_e \cos^{-1}(\beta \cos(\pi \frac{k}{N_e})))}{\cosh(N_e \cosh^{-1}(\beta))} \quad k = 0, 1, \ldots, N_e - 1 \tag{3.50}$$

where

$$\beta = \cosh\left(\frac{1}{N_e} \cosh^{-1}(10^{\gamma})\right) \tag{3.51}$$

The appeal of the Dolph-Chebyshev window function is two-fold: i) it is designed to give the most optimal trade-off between mainlobe width and sidelobe attenuation ii) this trade-off is adjustable by changing the value of γ. The second point is interesting as it allows the attenuation of the sidelobes to be increased at the cost of increased mainlobe width. The impact of this is seen in Figure 3.13 which plots the first eigenvalue against INR for various numbers of excised bins.

The effect of the wider mainlobe of the Dolph-Chebyshev window with $\gamma = 7.5$ compared with the Blackman-Harris window results in more bins being required to be excised in order to achieve cancellation for a given INR. For example, if the INR = 40 dB then 8 bins must be excised to cancel the signal using the Dolph-Chebyshev window compared with 6 bins using the Blackman-Harris. However, the increased sidelobe suppression of the Dolph-Chebyshev window allows for signals with much higher INRs to be cancelled. Excision of a signal with an INR = 110 dB is possible if 12 bins are excised, this appears

to be the limit as further increasing the number of excised bins does not result in more cancellation.

So far, the problem of mainlobe width on the ability of excision to desensitize the beamformer has been considered in the context of a single CW incident upon the array. However, the goal of the use of excision to pre-filter narrowband interference is to increase the cancellation capacity of the beamformer and therefore be able to pre-filter multiple narrowband signals. When multiple CWs are incident upon the array their sidelobe level due to the windowing in the excision filters becomes increasingly important. In the case of just one CW it was sufficient to ensure that the sidelobe level was suppressed to such a level so as to not prompt the beamformer to begin nulling when the mainlobe was excised. However, this condition is not necessarily sufficient when multiple CWs are present due to the combination of the CWs' sidelobes within the excision filters. This can be seen in Figure 3.14 where a varying number of CWs, all of equal power, are incident upon the array and all are removed by excising 8 bins per CW. The CWs frequencies and angles of arrival of the CWs are given in Table 3.1; the CWs are all centred halfway between frequency bins to produce worst-case spectral leakage. The length of the excision filters are 1024 bins and the Dolph-Chebyshev window with $\gamma = 7.5$ is used in all cases. The 3 plots show the value of the first eigenvalue versus the INRs of the CW (each CW has the same INR) for 1, 6 and 12 CWs. As is the case with 1 CW raising the INR of the CWs where there are multiple CWs present results in an increased sidelobe level which at a certain INR will increase the effective rank of the covariance matrix from 0. However, when multiple CWs are present this point is decreased due to the combination of sidelobe levels from each CW contributing to the overall sidelobe power level. Therefore, the beamformer will become more sensitive to the CW's INR as the number of excised CWs increases, in which case it may be necessary to increase the level of sidelobe suppression provided by the excision filters' window function to account for this so as to maintain cancellation against high INR signals.

3.4 Performance of System in Mixed Interference Environments

Having shown that frequency-domain excision filtering can be used to desensitise a beamformer to the presence of narrowband interference and hence, increase the degrees of freedom available to the beamformer, the effects of excision on the wanted signal are now considered. While the use of frequency-domain excision may help improve the overall interference cancellation in an over stressed interference environment it will introduce additional noise and distortion into the signal, therefore it is important that

CW #	f_g/f_s	θ_g
1	50.5/1024	10
2	100.5/1024	20
3	200.5/1024	30
4	300.5/1024	40
5	400.5/1024	50
6	450.5/1024	60
7	500.5/1024	70
8	-423.5/1024	80
9	-323.5/1024	90
10	-223.5/1024	100
11	-123.5/1024	110
12	-23.5/1024	120

TABLE 3.1: CW interference frequencies and angles of arrival

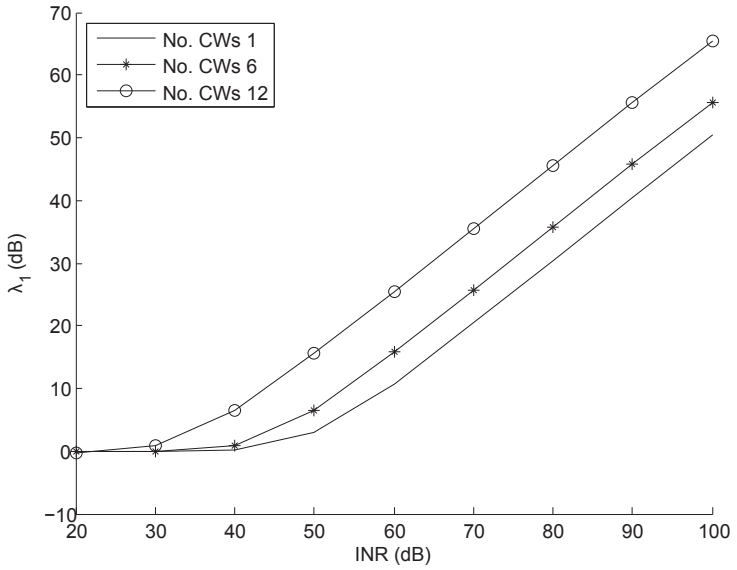

FIGURE 3.14: 1^{st} eigenvalue of $\mathbf{R}_{\tilde{q}\tilde{q}}$ using Dolph-Chebyshev window and multiple CWs

the wanted signal is still recoverable after the signal has been processed. To measure the impact that the combined system has on the wanted signal, the signal to noise ratio per bit, denoted E_b/N_0, of the wanted signal at the output of the beamformer is considered. The non-linear nature of the clipping operation applied to the signal within the pre-excision filters precludes traditional linear analysis techniques, such as considering the component parts of the received signal separately. Therefore, Monte Carlo simulations are used to determine the bit error probability of the wanted signal at the output of the beamformer, this can then be used to calculate the equivalent signal to noise ratio of the wanted signal at the output of the beamformer.

3.4.1 System Model

A combined excision STAP beamforming system is considered as shown in Figure 3.5. As the intended application of the combined excision beamforming system is small portable communication systems an antenna array with $M = 4$ elements is considered. The elements of the array are arranged in a line with half-wavelength spacing between them to form a ULA. Several signals may impinge upon the array at any one time as described in Section 2.3. At all times this includes the wanted signal, denoted $x(t)$, which is formed from a random bit source which is modulated using BPSK and then spread by a 1023 chip Gold sequence as described in Section 2.3.1. The wanted signal is received from a known direction relative to the array and at a power level $P_x = -27$dBW such that it is well below the receiver's thermal noise floor $\sigma_v^2 = 0$dBW to simulate LPI. The receiver thermal noise on each element of the array is modelled as AWGN which is i.i.d in time as well as across elements.

The remaining signals impinging upon the array are assumed to be interference signals where the i^{th} interference signal is denoted $g_i(t)$ which arrives from an unknown direction and may occupy a different portion of the receiver's spectrum depending on their classification: narrowband, partialband or broadband. Narrowband interference is then removed from the received signals on each channel in the excision filters as described in Section 3.3.1. The excised signals are then passed onto the beamformer for spatial-temporal/spatial-spectral removal of the remaining partialband and broadband interference signals.

The excision filters and STAP beamformer are setup in the same manner as described in Section 3.3.2. Each element of the array feeds an $N_e = 1024$ length excision filter (if the inclusion of excision has been specified) which uses either the zero clip or noise clip methods described in Section 3.3.1 to remove narrowband interference. The samples from the excision filters are fed into the $K = 3$ length TDL on each channel which form the structure of the STAP beamformer, such that the samples on taps of the STAP beamformer at any given sampling instance are given by Eq. (3.42). The samples on each tap of the STAP beamformer are multiplied by a corresponding complex weight contained within the weight vector $\mathbf{w} \in \mathbb{C}^{MK\times 1}$ and are then summed to produce the beamformer output:

$$y[n] = \mathbf{w}^H \tilde{\mathbf{q}}[n] \tag{3.52}$$

where the weight vector $\mathbf{w}$ is structured as follows:

$$\mathbf{w} = \begin{bmatrix} \mathbf{w}_0^T & \mathbf{w}_1^T & \dots & \mathbf{w}_{K-1}^T \end{bmatrix}^T \tag{3.53}$$

$$\mathbf{w}_k = \begin{bmatrix} w_{k,0} & w_{k,1} & \dots & w_{k,M-1} \end{bmatrix}^T \tag{3.54}$$

The weights of the beamformer are calculated using the minimum variance distortionless response (MVDR) solution based on the Weiner solution as discussed in Section 2.2.2 and, taking the covariance matrix $\mathbf{R}_{\tilde{q}\tilde{q}}$ defined in Eq. (3.43), are given as:

$$\mathbf{w}_{MVDR} = \mathbf{R}_{\tilde{q}\tilde{q}}^{-1} \bar{\mathbf{A}}_{\text{NZB}}(\theta_x, 0, B_x) \tag{3.55}$$

where $\bar{\mathbf{A}}_{\text{NZB}}(\theta, f, B) \in \mathbb{C}^{MK \times 1}$ is the matched response of the STAP beamformer's taps to a signal arriving from an angle θ_x over the bandwidth B, with a low-pass equivalent frequency f. The wanted signal is centred at f_c and is assumed to have a rectangular PSD over the bandwidth B_x, as such $\bar{\mathbf{A}}_{\text{NZB}}(\theta, f, B)$ for a signal with a rectangular PSD is given as follows:

$$\bar{\mathbf{A}}_{\text{NZB}}(\theta, f, B) = \bar{\mathbf{b}}(B, \theta) \cdot (\mathbf{S}(f) \otimes \mathbf{A}(\theta, f)) \tag{3.56}$$

where $\bar{\mathbf{b}}(B, \theta) \in \mathbf{C}^{MK \times 1}$ is a vector containing the dispersion factors due to the bandwidth of the signal.

$$\bar{\mathbf{b}}(B, \theta) = \text{sinc}(B \begin{bmatrix} 0 \\ \tau_d(\theta) \\ 2\tau_d(\theta) \\ \vdots \\ (M-1)\tau_d(\theta) \\ T_s \\ \tau_d(\theta) + T_s \\ 2\tau_d(\theta) + T_s \\ \vdots \\ \tau_d(\theta) + (K-1)T_s \end{bmatrix}) \tag{3.57}$$

As it is the steady state performance of the system which is of interest the SMI method is used to calculate the weights by direct estimation of the covariance matrix $\mathbf{R}_{\tilde{q}\tilde{q}}$. This is achieved by calculating the sample average of the outer product of $\tilde{\mathbf{q}}[n]$ with its

Hermitian transpose over N_r blocks as given by Eq. (3.44). The nulling performance of the beamformer depends on the quality of the estimate of the covariance matrix. Reed et al. [95] show that as long as $N_r \geq 2MK$ the error in the estimation of the covariance matrix will be such that the resulting loss in SINR at the output of the beamformer compared with perfect knowledge of the covariance matrix will not be greater than 3 dB.

Finally, the resulting signal at the output of the beamformer $y[n]$ is despread and demodulated as described in Section 2.3.4 and the BER, denoted ρ_e, of the wanted signal is determined. This is used to calculate the signal to thermal noise ratio per bit E_b/N_0 of the output DSSS signal which is used as the figure of merit. This is derived from the expression for the BER of a BPSK signal in the presence of AWGN as given in [109] and as is given as follows:

$$\frac{E_b}{N_0} = \text{ercfinv}(2\rho_e)^2 \tag{3.58}$$

where ercfinv$(\cdot)$ is the inverse complementary error function.

3.4.2 Numerical results

Initially, the performance of the combined excision beamformer system is considered with only the wanted signal incident upon the array and a portion of the spectrum excised. The process of excising any portion of the received signals will result in part of the wanted signal being excised at the same time. Clearly, this will adversely affect the E_b/N_0 the extent to which will depend on both the percentage of the spectrum excised as well as the excision method used [114]. As the excision filters operate independently and, therefore, do not exploit the spatial diversity of the received signals, excision of the wanted signals in portions of the spectrum in which a narrowband signal is present is unavoidable. However, if this occurs in portions of the spectrum where no interference is present then over-excision occurs. In both cases it is desirable to minimize the excision loss associated with excising part of the wanted signal.

Figure 3.15 plots the output E_b/N_0 against number of bins excised for excision filters using the noise clipping and zeroing methods of excision for the Blackman-Harris and Chebyshev (with $\gamma = 7.5$) windows detailed in Section 3.3.2. In all cases, with less than 10% of the spectrum excised, the E_b/N_0 of the DSSS signal at the output of the beamformer is between 5 and 6 dB. This gain in E_b/N_0 is due to the array gain of the beamformer since its mainlobe is steered in the direction of the wanted signal. The gain

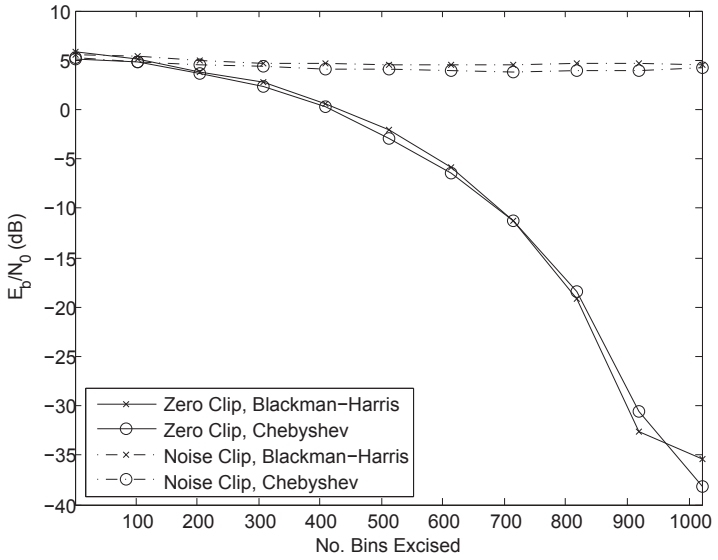

FIGURE 3.15: Excision loss due to excision of wanted signal

factor is equal to the number of elements in the array and for a 4 element linear array is 6.02 dB.

Comparing the difference in excision loss between the Blackman-Harris and the Dolph-Chebyshev windows shows that there is very little difference between them for both the zero clip and the noise clip excision method; there is a slightly greater loss seen with the Dolph-Chebyshev window, however, this is marginal. Both these windows would be suitable candidates for use in the excision filters. However, it should be noted that the wider mainlobe of the Dolph-Chebyshev window will result in the excision filters excising more bins per narrowband interferer than the Blackman-Harris. Comparing the zero clip and the noise clip excision methods the distortion loss is more marked; both methods show similar low levels of distortion loss when less than 10% of the spectrum is excised. However, when the proportion of the spectrum excised is greater than 10% it is clear that clipping to the noise floor is preferable to zeroing the signal. Therefore, less distortion loss is encountered should over-excision occur; these mirror the results Young presents in [50] for a single channel system.

The problem of unintended excision is not limited to the wanted signal since partial-band and broadband interference will also be excised if they occupy portions of the spectrum subject to excision. This is not desirable as the partialband and broadband interference can be cancelled more effectively in the beamformer if they are unexcised. Furthermore, distortion introduced by the excision filters may affect the beamformer's ability to cancel the remaining interference signal. To examine the effects of partially excising a broadband interference signal on the beamformer consider a single broadband interferer impinging upon the array from an angle $\theta_g = 60°$. The broadband interferer

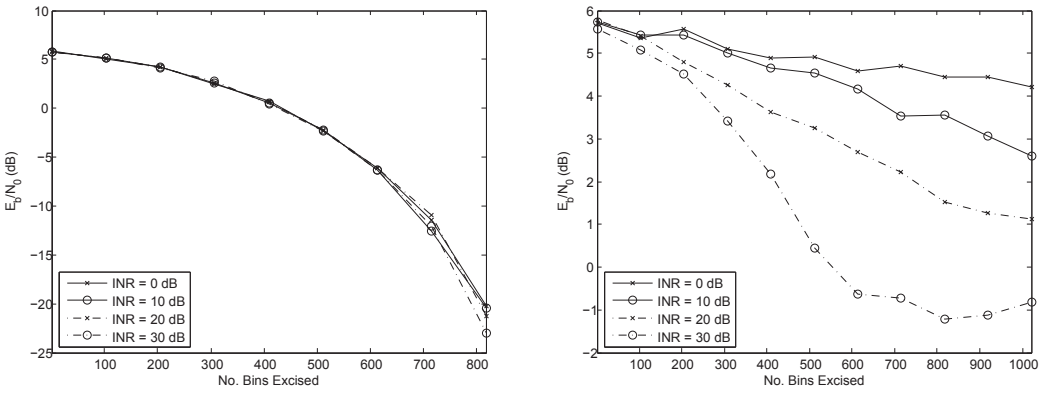

(a) Excision by zeroing bin (b) Excision by clipping bin's magnitude to noise floor

FIGURE 3.16: Partial excision of broadband interference signal

is modelled as a band-limited noise process with a flat PSD across the band $-f_s/2$ to $f_s/2$. In addition to the broadband interferer, the wanted signal arrives broadside to the array from an angle $\theta_x = 90°$.

Figures 3.16(a) and 3.16(b) plot E_b/N_0 against the number of bins excised using the the zeroing method and noise clip method respectively. In both cases the INR of the broadband interferer was varied between 0 and 30 dBW. Inspecting the results in Figure 3.16(a) for the zeroing method indicate that the loss experienced due to excision is independent of the interferer's power. In all cases as the portion of the spectrum excised is increased the loss increases until 80% of the spectrum has been excised at which point the BER from which the E_b/N_0 is calculated approaches 0.5 i.e. completely unrecoverable. In contrast, the results for the noise clip method shown in Figure 3.16(b) indicate that recovery of the DSSS signal is still possible even when large portions of the broadband signal have been excised. These results mirror those shown in Figure 3.15 however, with the broadband signal present a greater loss is seen as a result of its partial excision. As before the zero clip method shows the greatest loss as an increasing portion of the spectrum of the wanted signal is removed as the number of bins excised is increased. By constrast, using the noise clip method a reasonably high E_b/N_0 is maintained despite the partial excision of the broadband signal.

The power inversion beamformer is now briefly considered for use in conjunction with the pre-excision system. As has been mentioned in Section 2.2, the power inversion beamformer is a special case of the MVDR beamformer given by Eq. (3.55) whereby the steering vector is $\mathbf{A} = \begin{bmatrix} 1 & 0 & \dots & 0 \end{bmatrix}^T$. Besides being computationally less complex compared with other types of beamformer, if coupled with a nominally omni-directional array antenna, full coverage of the sky is achieved. The latter makes the power inversion beamformer suitable for receiving multiple, spatially diverse LPI signals simultaneously

e.g. from multiple satellites for GPS or multiple radios in a mesh network. However, the nominally omni-direction beam pattern will change as soon as any sufficiently strong signals are detected by the beamformer as it attempts to null them. This will disrupt the angular coverage of the array and so the coverage is dependant on the signals impinging upon the array. If any of the signals are narrowband then, if pre-excision is used, these signals will be removed before they reach the power inversion beamformer. As a result the power inversion beamformer should not respond to narrowband signals and, barring other wider band signals, coverage will be maintained in the direction of the narrowband signals.

To highlight the effects of coverage, Figure 3.17 shows E_b/N_0 for the wanted signal whereby the angle of arrival of the wanted signal is varied in the range of $\theta_x = 0°$ to $180°$. As the beam pattern for a ULA is symmetrical about its length, full angular coverage is provided by this range. Also impinging upon the array is a single CW signal with $P_g = 30$ dBW arriving from an angle $\theta_g = 140°$. The power inversion beamformer is used in place of the MVDR beamformer and the effect of the single CW on the coverage of the power inversion beamformer is compared with the case where pre-excision is used in conjunction with the power inversion beamformer. The plot shows that in the case where the power inversion beamformer is operating on its own, the E_b/N_0 drops quickly as θ_x approaches θ_g where the beamformer has placed a null to cancel the CW. When pre-excision is used the narrowband interference is removed before it reaches the beamformer. Therefore, the beamformer maintains its omni-directional beam pattern and full coverage of all angles of arrival for the wanted signal are maintained.

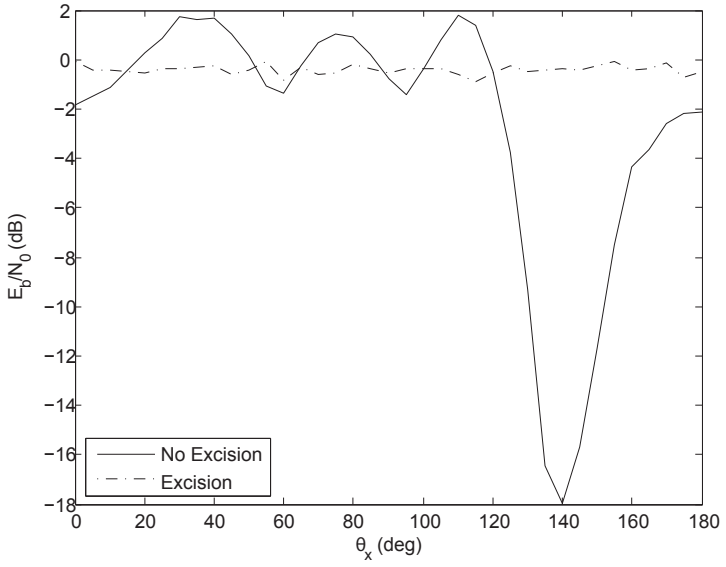

FIGURE 3.17: Improvement in coverage of the power inversion beamformer using excision

Finally, the performance of the combined excision beamforming system in an overstressed interference environment is considered. In the overstressed case, the beamformer should not have enough degrees of freedom to fully cancel all the interference signals. To ensure that the degrees of freedom in the beamformer are fully consumed, 3 broadband interference signals impinge upon the array from 30, 60 and 120 degrees each with a total power of 30 dBW. As before each of the broadband signals is modelled as a band-limited noise process with a flat PSD across the band $-f_s/2$ to $f_s/2$. To overstress the beamformer additional CW interferers also impinge on the array, in the first case just one CW is added arriving from an angle of 140 degrees, in the second case 6 CW signals impinge upon the array from angles 40, 80, 110, 140, 150 and 170 degrees. In both cases the frequency of the CW is set to be half way between two bin frequencies thereby ensuring worst-case spectral leakage. In addition to this, in the second case the frequency of each CW spaced 100 bins apart from each other. The power of all the CW signals is varied relative to the thermal noise power from -20 to 90 dB. The wanted signal impinges the array from $\theta_x = 90°$. The Dolph-Chebyshev window detailed in Section 3.3.2 is used in the excision filters and excision is performed using the noise clip method.

Figures 3.18(a) and 3.18(b) plot the results E_b/N_0 in four cases: in the first, no excision is used, then 6, 8 and 10 bins are excised per CW signal in turn. Considering Figure 3.18(a) first, the case where no excision is used and where excision is used show very similar performance while the INR of the CW signal is less than 0 dB. At very low INRs, the beamformer without excision experiences the expected 6 dB of gain due to the array while the 3 cases using excision show a 1 dB reduction in performance due to the excision. As the INR of the CW is increased, the interference environment becomes overstressed for the beamformer without the excision pre-filters, this is evident in the quick drop in E_b/N_0 as the INR of the CW exceeds 40 dB. The E_B/N_0 can be seen to be approaching an asymptote at -20 dB which is due to the BER from which the E_b/N_0 is calculated reaching 0.5. In the 3 cases where excision was used the loss experienced by the wanted signal is reduced for higher INRs. The dependence of excision performance on the interference signal's power and the number of bins excised can be clearly seen as excising a larger number of bins reduces the loss further as the INR is increased. In Figure 3.18(b) the number of CW signals impinging upon the array is increased to 6, further stressing the degrees of freedom in the beamformer. In this environment the beamformer is unable to provide sufficient suppression of all the signals even when the INR of all the CW signals is at a very low level. The advantage of pre-excising the CW signals can be clearly seen in this case where excision of 8 bins per CW allows performance to be recovered with a loss of only 1 dB for INRs of up to 60 dB for all the CW signals. As before, as the INRs of the CWs is further increased, the widening of their mainlobe that results causes the performance to drop if the number of bins

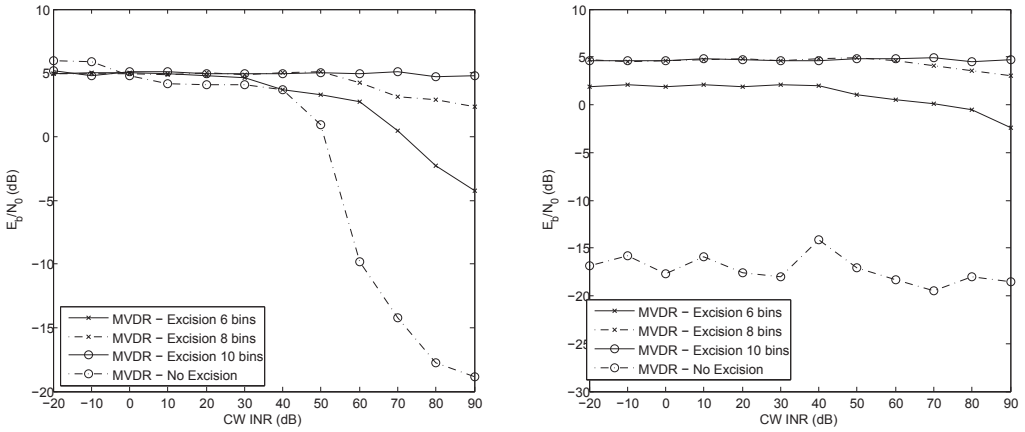

(a) 3 Broadband + 1 CW signals

(b) 3 Broadband + 6 CW signals

FIGURE 3.18: Performance of combined MVDR beamformer excision system in over-stressed environments

excised per CW is not sufficiently high. Increasing the number of bins excised from 8 to 10 compensates for the widened mainlobes of the CWs allowing the performance to be maintained at higher INRs.

3.5 Summary

In this chapter the problem of increasing the cancellation capacity of a STAP beamformer was considered. While it was noted that the complexity of increasing the number of adjustable weights in a STAP beamformer is high, adding additional time taps as opposed to channels tends to carry less of a penalty in terms of the additional hardware introduced. Therefore, the benefit of increasing the number of time taps as a method of increasing the cancellation capacity of the STAP beamformer was considered. A new expression was derived to determine how the sensitivity of the time-taps is affected by the properties of the STAP and the interference signals impinging upon it. It was shown that the use of the time-taps as a method of increasing the cancellation capacity of the STAP beamformer is too contingent on the properties of the interference signals. Interference signals with non-zero bandwidths were shown to quickly consume the beamformer's degrees of freedom due to the time-taps particularly at higher INRs. Pre-filtering narrowband interference using frequency-domain excision was also considered as a method of increasing the cancellation capacity of the STAP beamformer. eigenanalysis of the STAP's covariance matrix demonstrated the viability of this method for desensitising the STAP beamformer to the presence of narrowband interference. The ability of the excision pre-filtering method to enhance the interference protection of an LPI DSSS receiver utilising a STAP beamformer was demonstrated by simulation. In particular,

the ability to recover performance in an overstressed interference environment in the presence of CW interference was shown.

Chapter 4

Automatic Threshold Calculation for FDE Pre-filtering in Adaptive Beamformers

4.1 Introduction

In the previous chapter, the concept of using frequency-domain excision filters in front of adaptive beamformers as an efficient method of enhancing the interference suppression ability of an adaptive beamforming system was presented and investigated. In analysing the system it was assumed that the excision filters had *a priori* knowledge of the spectral location of the narrowband interferers, thus the correct bins could be selected in order to excise the interference. However, this would not be the case in a practical implementation of the system and therefore, a method of identifying bins containing narrowband interference is required.

Frequency-domain excision is well suited to the detection of narrowband signals which are clearly identifiable in the frequency-domain. However, when excision filtering is used in the manner proposed in Section 3.3, the problem faced in the process of identifying narrowband interference signals is in the avoidance of detecting other forms of interference present in the spectrum which should not be excised. Therefore, the identification process must be able to discriminate between the narrowband forms of interference, which should be excised, and partialband or broadband signals which should be left for the adaptive beamformer to remove. Given that frequency-domain excision has thus far been used predominantly as a method of interference suppression in single channel systems, the algorithms proposed in the literature for identifying interference within the

excision filter do not possess the ability to discriminate between interference of differing bandwidths. These methods are typically based on a uniform threshold across the spectrum whose magnitude is compared with the magnitude of the value in each bin to determine whether or not the bin should be excised [44]. By using the same threshold value for all the bins in a given spectrum it is likely that all interference present in the received signal will be identified and excised, therefore, making this approach unsuitable for the proposed application.

In this chapter, a novel method for the automatic identification of bins containing narrowband interference is proposed. The technique is based on the image processing technique of *opening* which, when applied to 1-dimensional signals, can be implemented efficiently. The benefit of the proposed system is its ability to identify bins containing narrowband interference in the presence of other forms of interference. This includes situations where another interference signal may partially occlude the narrowband signal. The performance of the proposed technique is evaluated in the combined excision adaptive beamforming system by BER simulation of an LPI DSSS receiver. Two different types of broadband adaptive beamformer are compared with the proposed system: Frost's [85] LCMV STAP and a sub-optimal sub-band SFAP. A variety of interference environments are considered containing a mix of narrowband, partialband and broadband interference.

4.2 System Model

A beamformer attached to an M element antenna array is used to provide protection to a DSSS receiver from several high power interference sources. The wanted DSSS signal is received from a known direction relative to the array at a power level that is well below the receiver's thermal noise floor. Each of the interference sources impinges the array from an unknown direction and may occupy a different portion of the receiver's spectrum depending on its classification: narrowband, partialband or broadband as described in Section 2.3.2.

The combined excision and adaptive beamformer system is based on the model described in Section 3.3 and is shown in Figure 4.1. As before an M element ULA antenna receives and down-converts the signals impinging upon it. Likewise, each channel contains an N_e length excision filter of the arrangement described in Section 3.3.1 to remove narrowband interference prior to the signals entering the beamformer. The key addition to this model is the inclusion of a method to automatically determine which bins contain narrowband interference and should therefore be excised. The threshold calculation is determined based on the spectrum received from one of the channels according to the algorithm

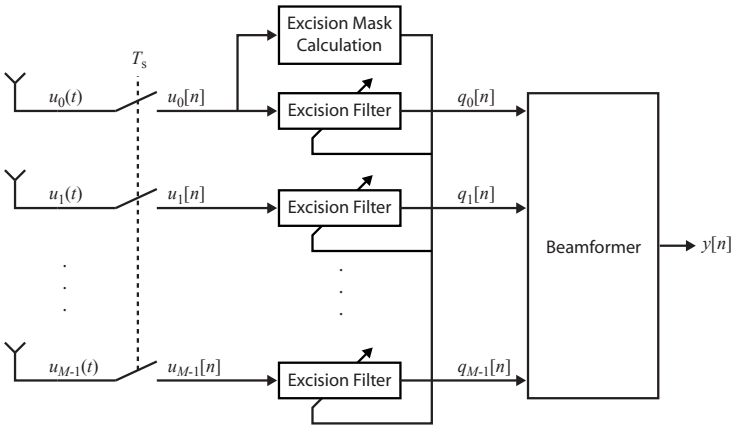

FIGURE 4.1: Dataflow diagram of a beamformer with pre-excision filters

described later in Section 4.3. The calculated threshold is then used by the excision filters on all the channels in order for them to determine which bins should be excised. Therefore, excision is applied separately to each channel in order to reduce the overall system complexity, this is discussed in further detail in Section 4.4. The excision filters are followed by the beamformer, two differing broadband adaptive beamformers are considered: the first is the STAP beamformer where the weights are determined using Frost's LCMV solution [85], the second is a sub-optimal sub-band adaptive beamformer.

4.2.1 Space-time Adaptive Processor

The STAP is formed of M channels each containing a K sample tap delay line (TDL). The input of the TDL on the m^{th} channel is fed by the respective excision filter output $q_m[n]$, which is described in Section 3.3 such that samples on the STAP at the sampling instance n are given by $\tilde{\mathbf{q}}[n]$ as defined in Eq. (3.42).

The weights are calculated using Frost's LCMV optimization criterion which aims to minimize the output power of the beamformer subject to K linear constraints [85]. This is well suited to LPI systems where the angle of arrival of the wanted signal is known or can be determined *a priori*, for example a GPS (global positioning system) receiver, as the constraints can be used to maintain a desired response in the direction of the wanted signal. Given the LCMV criterion the weight set can be shown to be as follows:

$$\mathbf{w} = \mathbf{R}_{\tilde{q}\tilde{q}}^{-1}\mathbf{C}\left[\mathbf{C}^H\mathbf{R}_{\tilde{q}\tilde{q}}^{-1}\mathbf{C}\right]^{-1}\mathbf{f} \tag{4.1}$$

where the weight set $\mathbf{w}$ takes the form given in Eq. (3.54) and the covariance matrix $\mathbf{R}_{\tilde{q}\tilde{q}}$ is defined in Eq. (3.43).

The K linear constraints are specified by the constraint matrix $\mathbf{C} \in \mathbb{C}^{MK \times K}$ and response vector $\mathbf{f} \in \mathbb{C}^{K \times 1}$ such that their relationship with the weight set produced by Eq. (4.1) is as follows:

$$\mathbf{C}^H \mathbf{w} = \mathbf{f} \tag{4.2}$$

Each column of $\mathbf{C}$ along with the corresponding element of $\mathbf{f}$ form a single constraint. To ensure unity gain in the direction of the wanted signal, given by θ_x, K constraints are specified across the band of interest at frequencies specified by $\hat{f}_k$ for $k = 0, 1, \ldots, K-1$. To achieve this each element of the response vector $\mathbf{f}$ was set to 1 to specify unity gain and the k^{th} column of the constraint matrix $\mathbf{C}$ is defined as:

$$\mathbf{c}_k = \hat{\mathbf{F}}(\hat{f}_k) \otimes \mathbf{A}(\theta_x, \hat{f}_k) \tag{4.3}$$

$$\mathbf{C} = \begin{bmatrix} \mathbf{c}_0 & \mathbf{c}_1 & \ldots & \mathbf{c}_{K-1} \end{bmatrix} \tag{4.4}$$

where f_c is the tuned frequency of the antenna array, $\hat{f}_k$ is the frequency at which the k^{th} constraint should apply, $\mathbf{A}(\theta, f)$ is the steering vector in Eq. (3.12) and $\hat{\mathbf{F}}(f)$ is defined as follows:

$$\hat{\mathbf{F}}(f) = \begin{bmatrix} 1 & e^{-j2\pi f} & e^{-j2\pi 2f} & \ldots & e^{-j2\pi(K-1)f} \end{bmatrix}^T \tag{4.5}$$

As it is the steady state performance of the system that is of interest the SMI method is used to calculate the weights by direct estimation and inversion of the covariance matrix $\mathbf{R}_{\tilde{q}\tilde{q}}$. This method also has the advantage of the convergence time being invariant to the eigenspread of the signals received. Therefore, $\mathbf{R}_{\tilde{q}\tilde{q}}$ is estimated by calculating the sample average of the outer product of $\tilde{\mathbf{q}}[n]$ with its Hermitian transpose over N_r as given by Eq. (3.44).

4.2.2 Space-Frequency Adaptive Processor

An alternative approach to space-time beamforming is to use sub-band decomposition. This approach decomposes the received signal on each element into one of K separate sub-bands using a suitable analysis filter bank, in this way the signal in each sub-band

can be processed by the beamformer independently before being reconstructed using a synthesis filter bank [71]. One advantage of sub-band decomposition based beamforming is that each sub-band may be considered as a narrow-band signal and as such lower complexity algorithms may be used as the beamformer does not have to consider the the co-variances between signals of different sub-bands. This assumes that the analysis filter bank behaves as a series of brick-wall filters for each sub-band. As this is not the case in reality the assumption is not completely valid and as a result this approach is sub-optimal compared with the LCMV beamformer described in Section 4.2.1. However, the sub-band based beamforming is of interest as the DFT may be used as the analysis and synthesis filter banks to form a SFAP, in this case the beamformer can be realised efficiently in hardware using the FFT, particularly for high values of K [72].

Firstly, the output of the excision filters on each channel must be redefined in terms of blocks of $K/2$ contiguous signals. To this end the vector notation $\hat{\mathbf{y}}_m(l) \in \mathbb{C}^{K/2\times 1}$ is introduced such that:

$$\hat{\mathbf{y}}_m(l) = \left[q_m[\tfrac{lK}{2}] \quad q_m[\tfrac{lK}{2}+1]\ldots \quad q_m[\tfrac{(l+1)K}{2}-1]\right]^T$$

As with the excision filters an overlap in the sample blocks is introduced, in this case a $K/2$ sample overlap to produce the column vector $\tilde{\mathbf{y}}_m[l] \in \mathbb{C}^{K\times 1}$:

$$\tilde{\mathbf{y}}_m(l) = \begin{bmatrix} \hat{\mathbf{y}}_m(l-1) \\ \hat{\mathbf{y}}_m(l) \end{bmatrix} \tag{4.6}$$

A time-domain window $\hat{\mathbf{b}} \in \mathbb{C}^{K\times 1}$ is then applied to each block before it is transformed into the frequency-domain, resulting in the vector $\tilde{\mathbf{Y}}(l) \in \mathbb{C}^{K\times 1}$:

$$\tilde{\mathbf{Y}}(l) = \mathbf{F}_K \,\mathrm{diag}(\hat{\mathbf{b}})\tilde{\mathbf{y}}_m(l) \tag{4.7}$$

where $\mathbf{F}_K$ is a $K \times K$ Fourier transform matrix whose elements are given by Eq. (3.36).

The l^{th} block of output samples $\mathbf{y}(l) \in \mathbb{C}^{K\times 1}$ from the SFAP beamformer can then be expressed as follows:

$$\mathbf{y}(l) = \mathbf{F}_K^{-1} \sum_{m=0}^{M-1} \mathrm{diag}\left(\left[W_{m,0} \quad W_{m,1}\ldots \quad W_{m,K-1}\right]\right) \tilde{\mathbf{Y}}(l) \tag{4.8}$$

where $W_{m,k}$ is an element of the beamformer weight matrix $\mathbf{W} \in \mathbb{C}^{M\times K}$.

Given that the sub-band beamformer operates as K parallel narrowband beamformers the weight sets are calculated on each sub-band independently using frequency-domain samples from all the elements. Furthermore, the narrowband signal assumption allows a look direction constraint to be applied in the form of the narrowband steering vector $\mathbf{A}(\theta_x, \tilde{f}_k)$ as defined by Eq. (3.12) and Eq. (2.10), where $\tilde{f}_k$ is the low-pass equivalent frequency of the k^{th} sub-band centre frequency. The weight set for the k^{th} sub-band, denoted $\hat{\mathbf{W}}_k \in \mathbb{C}^{M\times 1}$, form the k^{th} column of the beamformer's weight matrix $\mathbf{W}$ such that:

$$\mathbf{W} = \begin{bmatrix} \hat{\mathbf{W}}_0 & \hat{\mathbf{W}}_1 & \dots & \hat{\mathbf{W}}_{K-1} \end{bmatrix} \tag{4.9}$$

where the weights for the k^{th} sub-band $\hat{\mathbf{W}}_k$ are given as follows:

$$\hat{\mathbf{W}}_k = \frac{\mathbf{R}_k^{-1}\mathbf{A}(\theta_x, \tilde{f}_k)}{|(\mathbf{R}_k^{-1}\mathbf{A}(\theta_x, \tilde{f}_k))^H \mathbf{A}(\theta_x, \tilde{f}_k)|}, \quad k = 0, 1, ..., K-1 \tag{4.10}$$

where $\mathbf{R}_k \in \mathbb{C}^{M\times M}$ is the covariance matrix between the frequency-domain samples on each element for the k^{th} sub-band and is calculated as follows:

$$\mathbf{R}_k = \mathrm{E}\left\{\mathbf{Y}_k(l)\mathbf{Y}_k^H(l)\right\} \tag{4.11}$$

where $\mathbf{Y}_k(l) \in \mathbb{C}^{M\times 1}$ is a vector containing the frequency-domain samples over all the antenna elements for the k^{th} sub-band and is defined as follows:

$$\mathbf{Y}_k(l) = \begin{bmatrix} \tilde{Y}^*_{0,k}(l), & \tilde{Y}^*_{1,k}(l), & \dots, & \tilde{Y}^*_{M-1,k}(l) \end{bmatrix}^T \tag{4.12}$$

where $\tilde{Y}_{m,k}(l)$ is the k^{th} element of the vector $\tilde{\mathbf{Y}}_m(l)$ as defined in Eq. (4.7).

The covariance matrix for each sub-band $\mathbf{R}_k$ is estimated by calculating the sample average of the outer product of $\mathbf{Y}_k(l)$ with its Hermitian transpose over N_r blocks. Every other block is used in approximating $\mathbf{R}_k$ to remove the effect of the overlap introduced in Eq. (4.6). The covariance matrix for the k^{th} sub-band is approximated as follows:

$$\mathbf{R}_k \approx \frac{1}{N_r}\sum_{l=0}^{N_r-1} \mathbf{Y}_k(2l)\mathbf{Y}_k^H(2l) \tag{4.13}$$

The estimated covariance matrices are directly inverted in the same manner as was used for the STAP processor. As the SFAP beamformer is, in essence, K parallel, independent narrowband (single tap) beamformers, whose covariance matrices are constructed from M independent observation variables, $N_r \geq 2K$ is sufficient to gain a good estimate of the covariance matrix for each sub-band.

The relationship between the n^{th} output sample $y[n]$ of the SFAP beamformer and the output vector $\mathbf{y}(l)$ given by Eq. (4.8) is given by the following mapping:

$$\mathbf{y}(l) = \left[y[\tfrac{lK}{2}] \quad y[\tfrac{lK}{2}+1] \ldots \quad y[\tfrac{(l+1)K}{2}-1] \right]^T \tag{4.14}$$

4.3 Threshold Calculation

The identification and excision of narrowband interferers is performed in the frequency-domain in the pre-excision filters described in Section 3.3.1. The identification process operates on each block of N_e frequency-domain samples contained within $\tilde{\mathbf{U}}_m(l)$ (see Eq. (3.35)) independently, producing a per bin threshold $r_k(l)$ value for each block. It should be noted that the threshold value for any given bin k in a block l of frequency-domain samples is shared between each excision filter in the M channel beamformer, therefore, each excision filter does not require its own independent interference identification module. This simplification is possible because the spectra of the received signals on each channel should not differ significantly in magnitude and therefore, the threshold value produced from the samples recorded on one channel can be used as the threshold values for the remaining channels.

The threshold is calculated using two morphological operations used in image processing called *opening* & *closing* [120]. The closing operation produces a spectral envelope that follows the composite spectral profile of all the signals contained within each spectral block while the opening operation removes impulsive elements in the spectral mask produced by narrowband interferers. Both opening and closing are composite functions, opening is made up of an *erosion* followed by a *dilation* operation while closing is the reverse. When treating 1-D signals, erosion and dilation operations can be computed using a min() or max() rank ordered filter respectively. Both filters operate by sliding a window across the samples from each block, in each case the centre sample is replaced by the minimum or maximum value within the window.

To define the process for calculating the threshold first let $\hat{\mathbf{U}}(l) = \tilde{\mathbf{U}}_0(l)$, as defined by Eq. (3.35), and note that $\hat{U}_k(l)$ is the k^{th} element of $\hat{\mathbf{U}}(l)$. The threshold value $r_k(l)$ for

the k^{th} bin of the l^{th} block can now be determined by applying the following 4 steps in order:

$$\hat{r}_k(l) = max(|\hat{U}_{k-(K_c-1)/2}(l)|, \ldots, |\hat{U}_k(l)|, \ldots, |\hat{U}_{k+(K_c-1)/2}(l)|) \quad \text{for } k = 0, 1, \ldots, N_e - 1 \quad (4.15)$$

$$\acute{r}_k(l) = min(\hat{r}_{k-(K_c-1)/2}(l), \ldots, \hat{r}_k(l), \ldots, \hat{r}_{k+(K_c-1)/2}(l)) \quad \text{for } k = 0, 1, \ldots, N_e - 1 \quad (4.16)$$

$$\tilde{r}_k(l) = min(\acute{r}_{k-(K_o-1)/2}(l), \ldots, \acute{r}_k(l), \ldots, \acute{r}_{k+(K_o-1)/2}(l)) \quad \text{for } k = 0, 1, \ldots, N_e - 1 \quad (4.17)$$

$$r_k(l) = max(\tilde{r}_{k-(K_o-1)/2}(l)), \ldots, \tilde{r}_k(l)), \ldots, \tilde{r}_{k+(K_o-1)/2}(l))) \quad \text{for } k = 0, 1, \ldots, N_e - 1 \quad (4.18)$$

The first pair of max() and min() operations given in Eq. (4.15) and Eq. (4.16) perform the closing operation using K_c length filters. The remaining two filtering operations given in Eq. (4.17) and Eq. (4.18) perform the opening operation using K_o length filters. The length of the filters will depend on the maximum bandwidth of interferer that should be excised but it has been found empirically that for $N_e = 1024$ a value of 7 for K_c and K_o is suitable for the removal of continuous wave interferers. The threshold values $r_k(l)$ produced by Eq. (4.15) through Eq. (4.18) for a given block l are used by the excision function $\Gamma(\cdot)$ (see Eq. (3.38) and (3.39)) to determine whether the sample in the k^{th} bin should be excised or not.

The novelty of the proposed approach is that it allows narrowband interferers to be identified and excised whilst leaving partialband and broadband interferers to pass through the filter as is shown in Figure 4.2. This is important as traditional frequency-domain excision filters would attempt to whiten the signal and therefore would excise all non-white forms of interference present in the signal. Not only would this render the beamformer

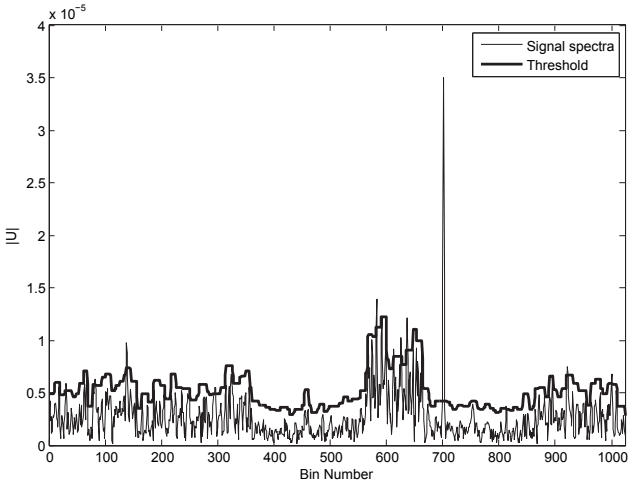

FIGURE 4.2: Excision variable threshold for a spectrum containing 1 CW interferer and several partial/broadband interferers

redundant but would also introduce excessive distortion into the signal where larger bandwidth interferers had been excised.

4.4 Computational Complexity

The computational complexity of the combined pre-excision beamformer system is clearly split between the complexity of the pre-excision filters and the complexity of the beamformer. The complexity of STAP versus sub-band beamformers have already been discussed in Section 2.2.1, so instead the additional complexity that the pre-excision filters add to the system is considered. The bulk of the computational complexity of the pre-excision filters lays mainly in the filter structures themselves; this is dominated by the DFT and IDFT operations. A radix-2 implementation of the fast Fourier transform (FFT) can be implemented efficiently such that it requires $N_e/2 \log_2 N_e$ complex multiplies to transform N_e samples [116, 121], so together the DFT and IDFT can be implemented with a combined complexity of $N_e \log_2 N_e$ complex multiplies per block of N_e samples using FFTs. In addition to this $2N_e$ real multiplications are required per block of N_e samples to apply the window to the time-domain samples. It is helpful to express the complexity in terms of multiplications required per sample processed; as $N_e/2$ new samples are processed per transform, due to the $N_e/2$ overlap, the number of complex multiplications per sample processed is $2\log_2 N_e$ and the number of real multiplications per sample is 4. One excision filter is required per channel, therefore the computational complexity of the pre-excision filters in an M channel system with N_e frequency bins is:

$M\,(2\log_2 N_e)$ Complex multiplications

$4M$ Real multiplications

The complexity of the adaptive algorithm to determine the excision threshold is shared among the excision filters as the threshold value of one adaptive block can be used by all M excision filters. The algorithm requires 2 real multiplications per sample processed to calculate the magnitude-squared spectrum of the signal. Calculation of the threshold value requires 2 running min() and 2 running max() functions, each of which operates over a window size of K_o or K_c. The complexity of the running min() and max() functions are identical; each function can be implemented using K comparators operating in parallel and in polyphase to each other, where each comparator produces a result every k^{th} sample. This leads to a requirement of $K_o + K_c$ comparators per sample processed per min/max function, therefore, a total of $2K_o + 2K_c$ comparators are required to implement all 4 functions. As such, the complexity of the adaptive algorithm for the pre-excision filters is only sensitive to the window size K_o and K_c used by the opening and closing operations respectively.

Compared with a traditional frequency-domain excision filter, such as the noise clip presented by Young [44], the complexity only differs in terms of the algorithm used to calculate the threshold as the filter structures are the same. The proposed scheme requires $2K_o + 2K_c$ comparators to determine the threshold per bin while the noise clip method just requires knowledge of the noise floor. However, the noise clip method has no means of distinguishing between narrowband and broadband interference and, therefore, removes all interference making it unsuitable for use in front of beamformers. Another popular form of narrowband interference suppression is the linear prediction error filter. This uses a FIR filter structure in either a single or double-sided configuration. If a one single-sided LPE filter were placed on each channel of the beamformer in place of the pre-excision filters then MN_e complex multiplications would be required per sample to calculate the output of the filters. In addition to this, each LPE filter, if implemented using the conventional LMS algorithm, would require N_e additional real multiplies per sample to update the weights. Clearly, the computational complexity of the pre-excision filter scales much better than the LPE filter as N_e increases. Furthermore, the requirements of the adaptive component of the pre-excision method are far simpler than the adaptive component of the LMS algorithm as the main requirement of the algorithm are the comparators whose number do not increase with N_e and only one adaptive unit is required for all M pre-excision filters.

Interferer	Type	P_{g_i}/σ_x^2	θ_i	f_{g_i}/f_s	B_{g_i}/f_s
A	Partial	50	60°	0.1	0.5
B	Broad	50	30°	0	1
C	Partial	50	120°	-0.4	0.1
D	CW	20 to 90	140°	0.1841	-
E	CW	50	90°	-0.2504	-

TABLE 4.1: Simulated interference signal parameters

4.5 Simulations

4.5.1 Methodology

Monte Carlo computer simulations were used to evaluate the performance of the STAP and SFAP beamformer with pre-excision in a variety of different interference scenarios. Without loss of generality, all signals and filters were simulated using their low-pass equivalents as described in Section 2.3. To model a system suitable for compact mobile deployment a 4 element ULA was used. The performance of each beamformer system was measured in terms of the BER of a BPSK DSSS signal with a 1023-chip Gold spreading sequence received from an angle of $\theta_x = 90°$ relative to the direction of the array antenna. The average power of the wanted signal was fixed at $P_x = -30$ dBW. The average thermal noise power on each channel of the beamformer was varied to produce BER results versus E_b/MN_0 which is the SNR per bit normalised by the array gain factor M. Normalising of the SNR per bit by the array gain factor allowed the BER results to be directly compared with the theoretical single channel BER performance of a BPSK modulated signal in an AWGN channel which is given as [122]:

$$\text{BER} = \frac{1}{2}\,\text{erfc}\left(\sqrt{\frac{E_b}{N_0}}\right) \tag{4.19}$$

where erfc$(\cdot)$ is the complementary error function.

The variance of the AWGN on each channel was normalised by the processing gain of the DSSS signal, given by L_s, and the array gain of the antenna, given by M, such that: $\sigma_v^2 = (P_x L_s)/(E_b/MN_0)$ and E_b/MN_0 was varied between 0 and 8 dB. Several different signals were used to simulate high power interference received by the array from various directions. These are summarized in Table 4.1, where the parameters refer to the models described in Section 2.3.2 which, for the i^{th} interferer are given in terms of its: interference to signal ratio (ISR) which is expressed as P_{g_i}/P_x, the direction of arrival θ_i in degrees, the low-pass equivalent centre frequency f_{g_i} and the bandwidth normalised to the sampling rate.

The beamformer weights were calculated and fixed for each simulation run using the first 1024 samples per channel. For the purposes of setting the beamformer steering constraints it was assumed that the direction of the wanted signal was known *a priori*. A Kaiser window with $\beta = 10.0613$ [53] was used in this series of simulations however, it is noted that greater performance may have been achieved, particularly against higher INR CWs, if a window with higher sidelobe suppression had been used such as the Backman-Harris or Dolph-Chebyshev windows studies in Section 3.3.2. The SFAP window function was given by $\left[\hat{\mathbf{b}}\right]_k = \sin^2(\pi\frac{2k+1}{2K}) \; \forall \; k \in \{0, 1, \ldots, K-1\}$. These were chosen as they showed good performance in simulation compared with other windowing functions. Other window functions may also be considered but a comparison is beyond the scope of this thesis. In both cases a windowing function that minimises distortion to the signal is important, in the case of the excision filters a window with high sidelobe suppression is important to reduce the amount of unexcised interference signal power introduced into the signal. The choice of window for the SFAP must minimise the width of the mainlobe so as to ensure that each sub-band is spectrally decorrelated in order for the assumption that each sub-band can be treated as a narrowband signal is valid.

4.5.2 Numerical Results

Initially, the ability of the pre-excision system to recover BER performance when a single CW interferer was causing the number of available degrees-of-freedom in the beamformer to be exceeded was studied. Three interference sources were chosen that together consumed, but did not exceed, the beamformer's degrees of freedom, these were interferers A, B & C as given in Table 4.1. The BER performance[1] was then simulated using the STAP beamformer and the sub-optimal SFAP beamformer, the results are shown in Figures 4.3 and 4.4 respectively. In each case the curve closely follows the theoretical BPSK performance which, after adjusting for the array gain factor, is as expected.

A single CW interference signal (interferer D) was then added to the interference scenario, its ISR was varied from 20 to 40 dB and the BER performance for both systems was simulated. The results, also shown in Figures 4.3 and 4.4, show that both beamformers are unable to fully cancel all four interferers and, as the ISR of the CW is increased, the BER performance progressively degrades. Comparing the performance of the two beamformers with each other shows that the BER performance of the SFAP degrades to a much greater extent than the STAP and achieves no cancelling above an ISR of 40 dB.

[1] In some cases the results in the figures in this exhibit deviation at low BERs, this was due to the simulation terminating after 10,000 trials in order to limit the run-time of the simulation.

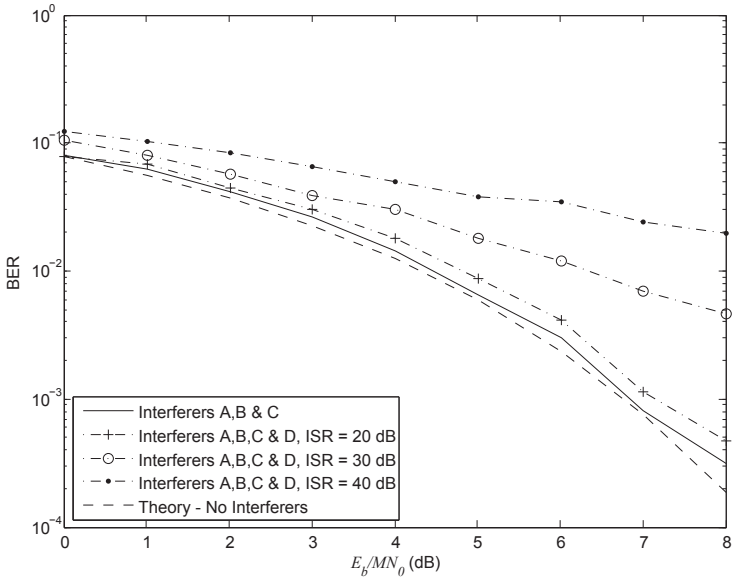

FIGURE 4.3: BER performance of STAP beamformer with no pre-excision

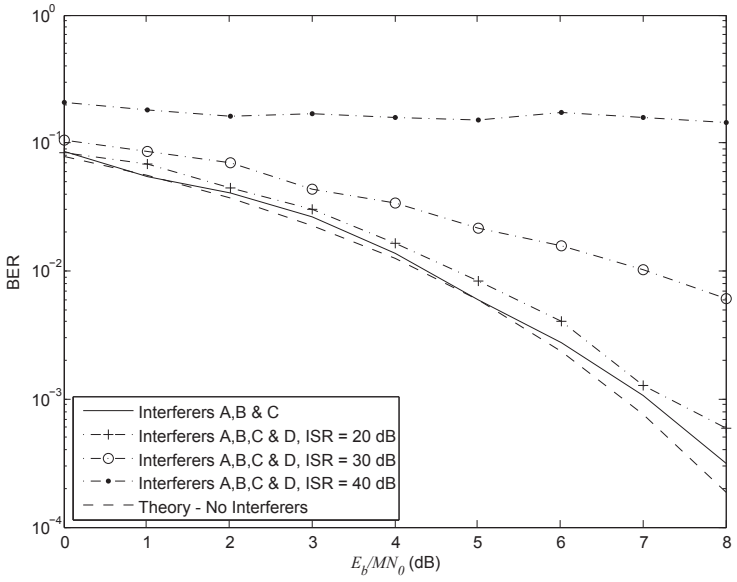

FIGURE 4.4: BER performance of SFAP beamformer with no pre-excision

The BER performance when pre-excision is employed is now considered. As with the previous experiment interferers A, B, C & D were used against both beamformers equipped with excision filters. This time a higher range of ISRs was used for the CW interferer D ranging from 70 to 90 dB as the pre-excision filters are expected to provide the cancellation required to maintain a good BER. The results for the STAP and SFAP beamformers are shown in Figures 4.5 and 4.6 respectively. Clearly, in both cases the pre-excision of the CW interferer improves the BER performance of the receiver for ISRs up to 70 dB with less than 1 dB loss compared with theoretical performance in the absence of interference. The small loss incurred by using pre-excision is due to the unexcised power from

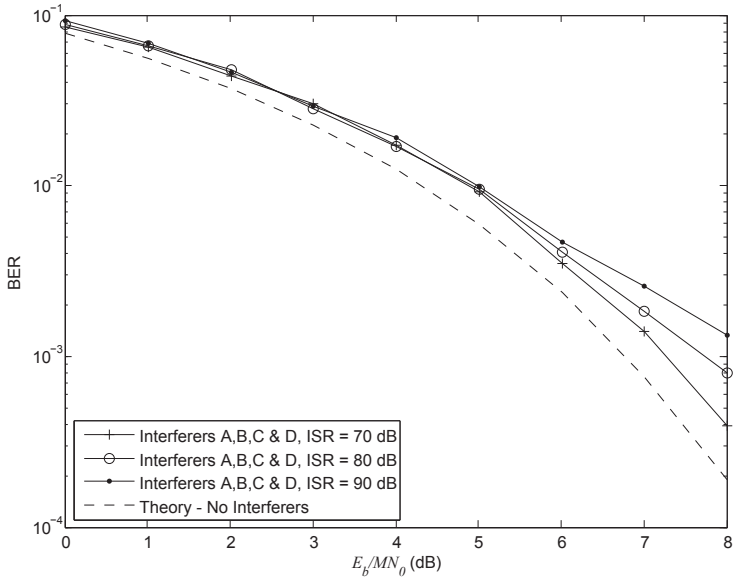

FIGURE 4.5: BER performance of STAP beamformer with pre-excision

the portion of the interferer below the clip value (as given by Eq. (3.39)) of the excised bins and the unexcised power contained within the interferer's sidelobes. The amount of remaining interference power will be a function of the interferer's power before excision as this will affect both the level power contained within the sidelobes and the width of the mainlobe. In addition to this, the bandwidth of non-CW narrowband interferers will contribute toward increasing the size of the section of the mainlobe below the clip value. In practice, assuming a window with good sidelobe suppression is used, the amount of power left unexcised will be small compared with the total power of the interferer. For both beamformers the BER performance began to degrade as the CW ISR was increased beyond 70 dB indicating that the excision was limited by the leaked power. However, below this ISR both the STAP and SFAP beamformer with pre-excision show similar levels of performance.

Next, the effect of narrowband interference arriving at such an angle that it falls within the beamformer's mainlobe is considered. In this scenario a sufficiently strong narrowband interferer should degrade the BER performance of the receiver regardless of the number of available degrees-of-freedom in the beamformer because the look direction constraint will force unity gain in the direction of the wanted signal. This is highlighted in Figure 4.7 where a single CW interferer E is located in exactly the same direction as the wanted signal, only two other interferers A & B are present in the received signal such that the degrees of freedom of the beamformer are not exceeded. The results show that without pre-excision both beamformers are unable to provide sufficient cancellation however, by pre-excising the CW in the excision filters the receiver is able to successfully recover the signal albeit with a small loss in BER performance due to the unexcised

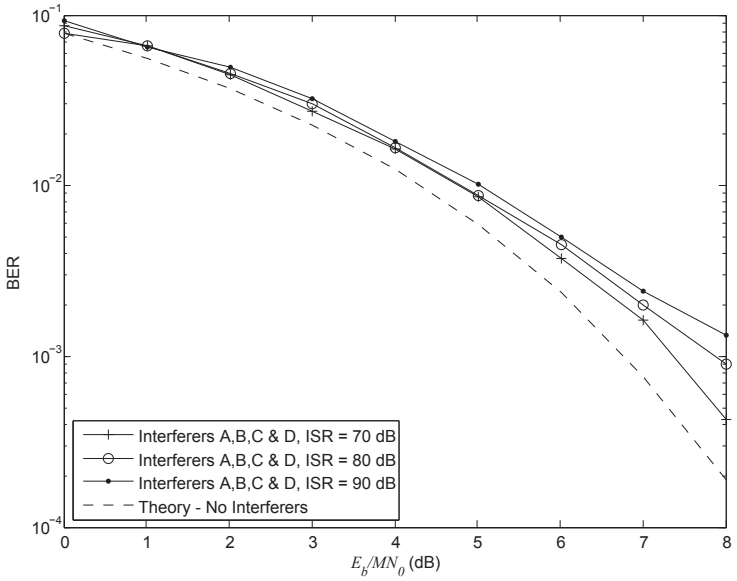

FIGURE 4.6: BER performance of SFAP beamformer with pre-excision

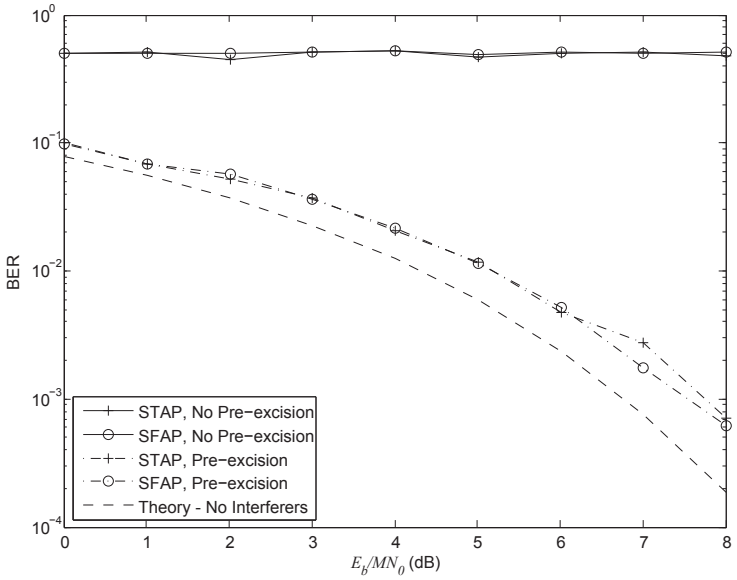

FIGURE 4.7: BER performance with interferers A, B and E where the wanted signal and interferer E are co-located

leaked power present in the mainbeam.

Finally, the performance of the pre-excision approach in a scenario containing multiple CW interferers as well as broadband interferers is considered. As with the first scenario a mix of three partialband/broadband interferers (interferers A, B & C) were used to consume the beamformer's degrees of freedom. Alone, these 3 interferers should not degrade the BER performance as per the results in Figures 4.3 and 4.4. However, 4 spatially and spectrally diverse CW interferers were also introduced into the interference

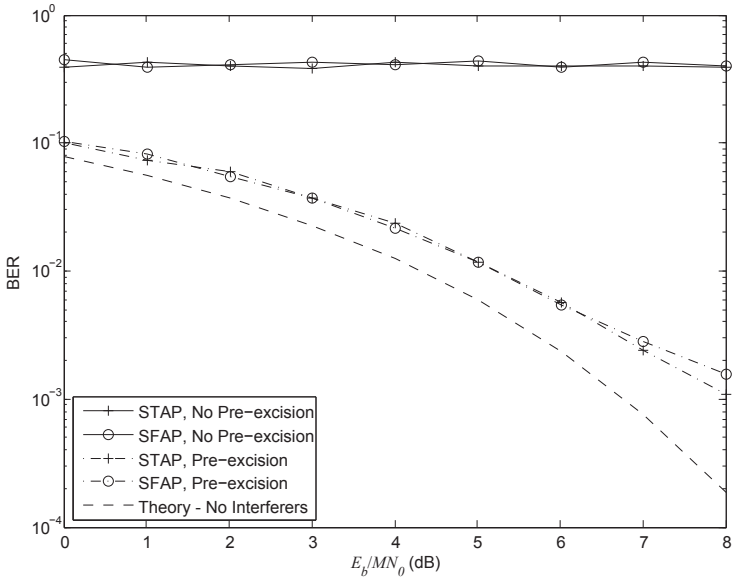

FIGURE 4.8: BER performance with interferers A, B, C and 4 CWs

environment such that full cancellation of all 7 interferers was not possible by either beamformer on its own. The ISR of all the CWs was fixed to 50 dB but the direction of arrivals were set to: 45°, 75°, 100° & 140° and the normalised low-pass equivalent centre frequencies were: 0.0376, 0.4771, 0.103 & 0.1841 respectively. The centre frequencies of the CWs were chosen so that the CW would appear exactly halfway between two bins in the excision filters to simulate worst-case spectral leakage. The results shown in Figure 4.8 indicate that with pre-excision both the STAP and SFAP beamformers are able to cancel all 7 interferers to a sufficient level to provide a BER with only a small amount of loss. Without pre-excision, the addition of the 4 CWs renders the signal completely unrecoverable.

4.6 Summary

A novel frequency-domain excision filter for use in front of broadband adaptive array antenna systems has been presented which increases the interference suppression capability of the overall system. Using image processing techniques, a method of setting a non-uniform threshold value across the bins of each spectral record has been proposed so that only narrowband interfering signals are excised. The performance of the pre-excision method was demonstrated by Monte Carlo simulation using a space-time adaptive processor and a sub-optimal space-frequency adaptive processor. It was shown that for a given size of array antenna, pre-excision can be used to provide enhanced protection to both the STAP and SFAP beamformers when their degrees-of-freedom were exceeded by the presence of continuous wave interference. It was noted that the

SFAP, due to the sub-optimality of its weight setting algorithm, experienced the greater improvement in performance compared with the STAP beamformer when pre-excision was used. Additionally, it was shown that pre-excision provided protection against CW interferers spatially located within the mainlobe of the beamformer and in scenarios containing multiple CW interferers.

Chapter 5

Channel Mismatch Compensation For Space-Time Adaptive Processors

5.1 Introduction

It is well known that the cancellation performance against non-zero bandwidth signals of adaptive beamformers can be reduced by frequency dependant gain and phase mismatches between each of the analogue receive channels in the beamformer [64, 68, 72]. The mismatches have the effect of decorrelating the signals across the beamformer's channels making it more difficult for the beamformer to cancel. This was the concern of ERA Technology Ltd. (trading as Cobham Technical Services) who had developed a technology demonstrator (TD) STAP beamformer. These mismatches can arise due to the differences in electrical characteristics of the components in the RF front-ends of each channel of the beamformer. In particular, the use of surface acoustic wave (SAW) filters in the analogue down-conversion modules (ADMs) of the ERA Technology TD were identified as a source of high frequency ripple across the frequency responses of the channels and, therefore, a cause of channel mismatching. Although the use of better matched components can help reduce the mismatches, they cannot eliminate them completely and higher tolerance components may increase the overall cost of the system. Additionally, the components' responses may vary over time due to environmental factors such as temperature or age, thereby removing the benefit of attempting to match the channels during manufacture. Therefore, in order to achieve good interference rejection, these mismatches must be compensated for in an adaptive manner. However,

changes of this nature tend to be slow over time and therefore constant tracking of the mismatches tend not to be necessary, instead periodic re-calibration is usually sufficient.

The problem of compensating for interchannel mismatches in beamforming systems has been approached in various ways in literature. One approach is to add additional temporal (or spectral) degrees of freedom to the beamformer such that the beamformer's response can be adjusted across the bandwidth of interest as well as spatially. Broadband adaptive beamformers such as the STAP and the SFAP possess this ability by virtue of the tap-delay lines, in the case of STAP beamformers, and sub-bands, in the case of SFAP beamformers. Therefore, one approach to compensating for the interchannel mismatches is to ensure that the beamformer contains sufficient temporal or spectral degrees of freedom to reverse the effects of decorrelation introduced by the mismatches [68] [64]. The improvement in cancellation performance using this approach will depend on the extent of the decorrelation experienced by the signals between channels and the number and resolution of the temporal or spectral degrees of freedom in the beamformer. However, the computational complexity of even a modest number of adjustable weights in the beamformer can be high and it does not scale well as the number is increased. Therefore, this approach is not suitable if a large number of taps is required to achieve the required level of compensation between channels. In particular, this may occur if high frequency ripples are present in the responses of any of the devices in the RF front-ends [123].

The high computational cost of compensating for the mismatches within the beamformer have lead others to propose that the compensation be performed prior to beamforming [123, 124]. In [124] the authors propose the use of FIR filters on each channel of the beamformer which adaptively adjust their weights using a weighted RLS algorithm in order to match the channel's response with an arbitrary desired response. As the filters operate independently of one another the complexity of calculating the filter weights is reduced compared with increasing the number of adjustable weights in the beamformer. However, given that the complexity of each FIR filter structure is $O(N)$ for N taps they may not be suitable when a large number of taps is required. The authors suggest the use of the RLS algorithm to determine the weight sets for each filter which has a complexity of $O(N^2)$. It may seem that computationally less complex algorithms, such as the LMS algorithm with $O(N)$ complexity, may be more suitable in a design where low computational complexity is the aim. However, it has already been noted that the front-end channel responses don't change quickly enough over time to warrant continual tracking. Therefore, the weights can be adapted at a much slower rate than the sample rate of the system such that it is the complexity of the FIR filtering structure that dominates the real-time complexity of the algorithm.

The problem of interchannel mismatches has been approached from the point of view of calibrating the array [125–127]. Instead of compensating for the mismatches by directly altering the received signals on each channel, these approaches collect calibration information about the channel responses in order to correct array manifold information used by the beamformer. The manifold data is typically used to produce steering vector information for beam-steering or direction of arrival estimation (DoA), therefore accurate knowledge of the array manifold is necessary to avoid point-steering or DoA estimate errors. As no compensation is applied directly to the received data these approaches are typically not suitable for improving the cancellation performance of the beamformer where it is limited by interchannel mismatches.

In this chapter, two new efficient methods of compensating for the mismatches between channels in adaptive beamformers are presented based on frequency-domain techniques. Frequency-domain filtering allows for very efficient linear filter structures to be realised compared with time-domain filtering structures, such as FIR filtering, when a larger number of taps is required. Longer filters lengths are typically necessary in order to achieve a sufficiently high level of matching between channels in order to provide strong rejection of high power broadband interferers [123]. To avoid the complexity of compensating for the mismatches within the beamformer itself, both of the proposed interchannel mismatch compensation schemes utilise frequency-domain filtering independently on each channel prior to beamforming. This is crucial in high performance beamforming systems which utilise computationally complex adaptive algorithms such as the SMI [95] or RLS algorithms [97]. Both mismatch compensation algorithms are simulated in software using measured ADM channel responses from the ERA Technology STAP TD to evaluate their improvement in broadband cancellation performance and SINR using a simulated STAP beamformer. The performance of both algorithms were then demonstrated using the ERA Technology STAP TD and software-in-the-loop methods to realise the algorithms.

5.2 System Model

Consider the M channel adaptive beamforming system depicted in Figure 5.1. Rather than having an ideal flat amplitude and zero phase response each channel has a transfer function denoted $H_m(f)$ $m = 0, 1, \ldots, M-1$ where $H_m(f)$ is the low-pass equivalent combination of all the transfer functions of all the components on the m^{th} channel. Therefore, the signal received by each element of the array $u_m(t)$ $m = 0, 1, \ldots, M-1$ will be distorted by the corresponding channel response transfer function. The differences in transfer functions between each of the channels will have the effect of decorrelating

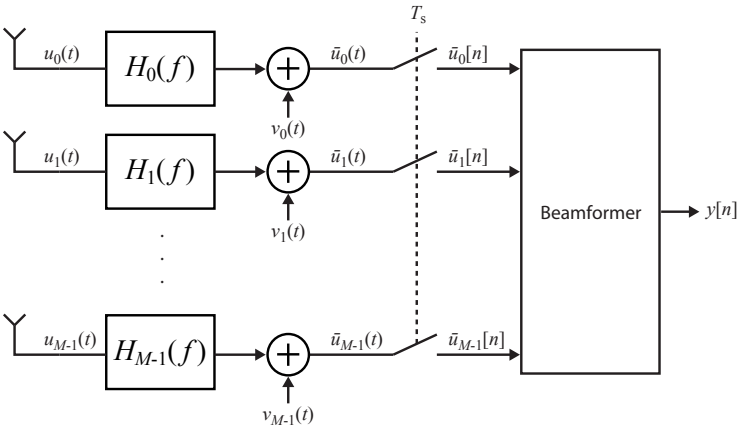

FIGURE 5.1: STAP beamformer with mismatched channel responses

the signals received by each element. This decorrelation makes it more difficult for the beamformer to null non-zero bandwidth signals. The channel response transfer functions are assumed to be linear time-invariant (LTI) and so can be modelled as filters whose time-domain impulse responses are denoted $h_m(t)$ $m = 0, 1, \ldots, M-1$ such that the signal prior to sampling on the m^{th} channel is given as follows:

$$\hat{u}_m(t) = \int_{-\infty}^{\infty} h_m(\tau) u_m(t-\tau) d\tau \tag{5.1}$$

The signal $\hat{u}_m(t)$ on each channel is sampled every T_s seconds. Therefore, the channel impulse responses can be replaced by FIR filters such that $h_{m,k}$ is the k^{th} sample of the discrete-time response of $h_m(t)$. In this way the time-sampled signal on each channel is given as follows:

$$\hat{u}_m[n] = \sum_{k=0}^{L_c-1} h_{m,k} u_m(nT_s - k) \tag{5.2}$$

where L_c is the length of the FIR filters approximating the responses of each channel.

5.2.1 Frequency-Domain Mismatch Compensation Filters

To compensate for the mismatches in responses between channels it is proposed that a frequency-domain filter be placed on each channel in front of the beamformer inputs as shown in Figure 5.2. The frequency-domain filters operate independently of one another to reduce the difference in the responses of each channel in the frequency-domain. The frequency-domain filters are equivalent to a linear time-domain filtering process however, greater computational efficiency is achieved as the convolution operation between

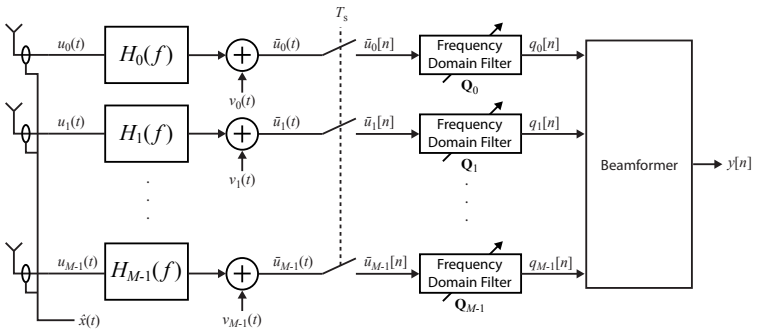

FIGURE 5.2: STAP with proposed channel mismatch compensation scheme

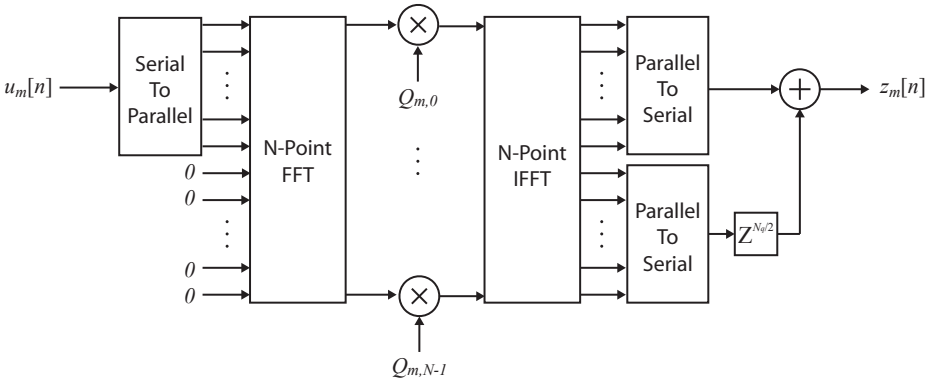

FIGURE 5.3: Dataflow of a single mismatch compensation filter

the signal and the filter coefficients required in time-domain filters is replaced by a multiplication in the frequency-domain. However, in order for the signals to be filtered in the frequency-domain it is necessary to transform them from the time-domain and then back again after filtering has been applied as shown in Figure 5.3. Therefore, the bulk of the complexity of frequency-domain filters is in the forward and inverse discrete Fourier transform pair required for this purpose. However, by realising the DFT/IDFT using the computationally efficient FFT algorithm the combined complexity of the transform pair and complex multiplication used to apply the filter coefficients can still be less than the equivalent length time-domain filter. This typically occurs when the length of the filter exceeds 32 taps [128] however, as the length of the filter is increased the efficiency savings of the frequency-domain filter compared with the time-domain filter become more marked.

It has already been mentioned that multiplication in the frequency-domain is equivalent to convolution in the time-domain. However, this is not strictly true as the form of convolution produced by frequency-domain multiplication is circular as opposed to linear convolution produced by time-domain filtering. The difference is that circular convolution performs the convolution operation with a periodicity equal to the length of the DFTs. This means that in the time-domain the convolution wraps around at the

end of the sequence back to the beginning which can introduce aliasing into the result if this effect is not taken into consideration. To prevent aliasing and ensure that the frequency-domain filtering appears linear in the time-domain it is necessary to employ either an overlap & add or overlap & save scheme [118].

To help describe the frequency-domain filtering process the vector notation $\mathbf{u}_m(l) \in \mathbb{C}^{N_q/2\times 1}$ is used to denote the l^{th} block of input samples $\hat{u}_m[n]$ on the m^{th} channel:

$$\mathbf{u}_m(l) = \left[\hat{u}_m[\tfrac{lN_q}{2}], \quad \hat{u}_m[\tfrac{lN_q}{2}+1], \ldots, \quad \hat{u}_m[\tfrac{(l+1)N_q}{2}-1]\right]^T \tag{5.3}$$

The length of each block of samples is doubled by appending $N_q/2$ zeros to form the vector $\breve{\mathbf{u}}_m(l) \in \mathbb{C}^{N_q\times 1}$. This forms the first part of the overlap & add process required to ensure that the frequency-domain filtering process appears linear rather than circular in the time-domain.

$$\breve{\mathbf{u}}_m(l) = \begin{bmatrix} \hat{\mathbf{u}}_m[l] \\ \hat{\mathbf{0}} \end{bmatrix} \tag{5.4}$$

where $\hat{\mathbf{0}}$ is an $N_q/2$-length all zero column vector.

The zero-padded sample blocks are transformed into the frequency-domain using an N_q-point DFT on each channel, where the DFT operation is performed by the pre-multiplication of the $N_q \times N_q$ Vandermonde matrix $\mathbf{F}_{N_q}$ which contains the DFT coefficients as defined in Eq. (3.36). This results in the frequency-domain samples which, for the l^{th} block on the on the m^{th} channel, are given as follows:

$$\breve{\mathbf{U}}_m(l) = \mathbf{F}_{N_q}\breve{\mathbf{u}}_m(l) \tag{5.5}$$

At this point the complex channel mismatch compensation filter weights $\mathbf{Q}_m$ are applied to the frequency-domain samples in each block on each channel. The weights for the m^{th} channel are contained in the vector $\mathbf{Q}_m \in \mathbb{C}^{N_q\times 1}$ as follows:

$$\mathbf{Q}_m = \begin{bmatrix} Q_{m,0} & Q_{m,1} & \ldots & Q_{m,N_q-1} \end{bmatrix}^T \tag{5.6}$$

Once the weights have been applied the compensated samples are transformed back into the time-domain using an N_q-point IDFT by the pre-multiplication of the weights samples with the inverse of $\mathbf{F}_{N_q}$. This yields blocks of time-domain samples for which

compensation has been applied where the l^{th} block of compensated time-domain samples is given as follows:

$$\hat{\mathbf{z}}_m(l) = \mathbf{F}_{N_q}^{-1} \operatorname{diag}(\mathbf{Q}_m)\breve{\mathbf{U}}(l) \tag{5.7}$$

While the weights have been applied to the blocks of samples on each channel the time-domain samples contained within the vectors $\hat{\mathbf{z}}_m(l)\ \forall\ l$ still require one final processing stage in order for the process to replicate linear convolution. This involves removing the overlap by taking the last $N_q/2$ samples of the previous block and overlapping and adding them to the first $N_q/2$ samples of the current block:

$$\mathbf{z}_m(l) = \begin{bmatrix}\mathbf{I}_{N_q/2} & \mathbf{0}_{N_q/2}\end{bmatrix} \hat{\mathbf{z}}_m(l) + \begin{bmatrix}\mathbf{0}_{N_q/2} & \mathbf{I}_{N_q/2}\end{bmatrix} \hat{\mathbf{z}}_m(l-1) \tag{5.8}$$

where $\mathbf{I}_{N_q/2}$ is an $N_q/2 \times N_q/2$ identity matrix, $\mathbf{0}_{N_g/2}$ is an $N_g/2 \times N_g/2$ all zero matrix and $\mathbf{z}_m(l)$ is a $N_g/2$ column vector containing the equalised samples.

The positional relationship between the equalised sample stream $z_m[n]$ on the m^{th} channel the column vector $\mathbf{z}_m(l)$ is given by the following mapping:

$$\mathbf{z}_m(l) = \begin{bmatrix} z_m[\frac{lN_q}{2}] & z_m[\frac{lN_q}{2}+1]\ldots & z_m[\frac{(l+1)N_q}{2}-1]\end{bmatrix}^T \tag{5.9}$$

5.2.2 Mismatch Equaliser Weights

The weight set $\mathbf{Q}_m$ of each of the channel mismatch compensation filters must be calculated so that they reduce the mismatch between the frequency responses $H_m(f)$ of each channel thereby reducing the decorrelation experienced between the signals on each channel. This objective can be achieved either by minimising the differences between the channel responses relative to one another or by minimising the response of each individual channel relative to a desired response for the channels. The first approach, which will be termed *relative compensation*, minimises the differences between channel responses relative to each other. This can be achieved most efficiently if the differences are minimised relative to one chosen channel termed the *reference* channel. This is subtly different from minimising the differences in channel responses relative to one another as only the responses of the current channel and the reference channel are used to determine the current channel's weights as opposed to finding the optimal weights for all the channels simultaneously. The second approach, which will be termed *absolute compensation*, behaves more like an equaliser and may be used where control of the final response of each channel is required.

Beginning with the relative mismatch compensation scheme, a channel is designated as the reference channel. For the purposes of this discussion channel 0 is selected, however any of the channels may be used. As the remaining channels will be compensated such that their frequency responses match that of the reference channel, it is not necessary to include a mismatch compensation filter on the reference channel. Therefore, the per frequency bin error in response between the m^{th} channel and the reference channel is defined as follows:

$$\mathbf{e}_m = \mathbf{H}_0 - \text{diag}(\mathbf{H}_m)\mathbf{Q}_m \tag{5.10}$$

where $\mathbf{H}_m$ is a column vector containing the discrete frequency response of the m^{th} analogue front-end channel:

$$\mathbf{H}_m = \left[H_m(0), H_m(\tfrac{f_s}{N_q}), H_m(\tfrac{2f_s}{N_q}), ..., H_m(\tfrac{(N_q-1)f_s}{N_q})\right]^T \tag{5.11}$$

The objective of the mismatch compensation filters is to minimise $\mathbf{e}_m$ by adjusting the complex weights $Q_{m,k}$ for $k = 0, 1, \ldots, N_q - 1$. Minimisation of the per bin error leads to a solution that is analogous to the zero-forcing equalizer. However, rather than using a weight set which is the inverse of the transfer function of the channel the weights are adjusted relative to the reference channel:

$$\mathbf{Q}_m = \text{diag}(\mathbf{H}_m)^{-1}\mathbf{H}_0 \tag{5.12}$$

It is typical in the equalisers of digital receivers to use the minimum-mean squared error (MMSE) criterion to determine the optimal weight set so as to minimise the difference between the received signal and the desired signal [129]. Receivers operating in a mobile environment and therefore, prone to rapid fading, benefit from improved performance using an equaliser based on the MMSE criterion compared with a zero-forcing solution as the MMSE criterion compensates for possible noise enhancement which may occur using a zero-forcing solution. However, in this application, the deep drops in gain caused by fading which lead to noise enhancement are not expected as, despite the mismatches, the transfer functions of the RF front-ends are relatively flat. Therefore, in this case, there is no great advantage to using the MMSE solution and as such, the zero-forcing solution should suffice.

The absolute channel mismatch compensation scheme can be described in a similar way as the relative channel mismatch scheme. In this case the per bin error is defined in terms

of a specified channel response given by the vector $\hat{\mathbf{G}} \in \mathbb{C}^{K\times 1}$ such that the mismatch error vector for the m^{th} channel is given as:

$$\mathbf{e}_m = \hat{\mathbf{G}} - \text{diag}(\mathbf{H}_m)\mathbf{Q}_m \tag{5.13}$$

where $\hat{\mathbf{G}} = \left[\hat{G}_0, \quad \hat{G}_1, \quad \ldots, \quad \hat{G}_{N_q-1}\right]^T$ is a vector of the desired frequency response of all the channels.

This leads to the weight set solution which minimises the per bin error given by the absolute mismatch compensation criterion which is given as follows:

$$\mathbf{Q}_m = \text{diag}(\mathbf{H}_m)^{-1}\hat{\mathbf{G}} \tag{5.14}$$

Calculation of the frequency-domain weights requires knowledge of the front-end channel responses $\mathbf{H}_m$ for $m = 0, 1, \ldots, M-1$. As they are unknown to the mismatch compensation filters *a priori* they must be estimated. This is achieved by injecting a calibration symbol $\hat{x}[n]$ into each channel input simultaneously. The calibration symbol is formed of N_q samples so that it appears periodic to the mismatch compensation filters' DFTs. The calibration symbol should have as near uniform power spectral density as possible so each bin receives a comparable amount of power, one such sequence with this property is the constant modulus Chu sequence [130] which is used here. Let the calibration signal be defined in vector notation: $\hat{\mathbf{x}} = [\hat{x}[0], \hat{x}[1], \ldots, \hat{x}[N_q-1]]^T$. Then the m^{th} channel's discrete frequency response is given as follows:

$$\mathbf{H}_m(l) = E\{\text{diag}(\mathbf{F}_{N_q}\hat{\mathbf{x}})^{-1}\mathbf{F}_{N_q}\hat{\mathbf{u}}_m(l)\} \tag{5.15}$$

where the vector $\hat{\mathbf{u}}_m$ contains the N_q samples of the calibration symbol as received by the m^{th} channel just after:

$$\hat{\mathbf{u}}_m = \left[u_m[lN_q], \quad u_m[lN_q+1], \ldots, \quad u_m[(l+1)N_q-1]\right]^T \tag{5.16}$$

To ensure that a good estimate of the channel responses is made, either a calibration signal with a sufficiently high signal to thermal noise ratio may be used or the estimate can made over a series of successive calibration symbols to achieve a high SNR by coherent averaging over N_a captures of the calibration signal:

$$\mathbf{H}_m \approx \frac{1}{N_a} \sum_{l=0}^{N_a-1} \text{diag}(\mathbf{F}_{N_q}\hat{\mathbf{x}})^{-1}\mathbf{F}_{N_q}\hat{\mathbf{u}}_m(l) \tag{5.17}$$

5.2.3 Beamformer

For the purposes of evaluating the mismatch compensation scheme a STAP beamformer where the weights are determined using Frost's LCMV solution [85] is used. The beamformer is formed of M channels where the m^{th} channel is fed by the output of the mismatch compensation filter of the same channel given by $z_m[n]$. Each channel of the beamformer contains K taps as shown in Figure 2.2, such that the samples on the STAP's taps at the sampling instance n is given as follows:

$$\bar{\mathbf{z}}[n] = (z_1[n], z_2[n], \ldots, z_M[n], z_1[n-1], \cdots, z_M[n-(K-1)])^T$$

Given the weight set $\mathbf{w}$ structured in the manner given in Eq. (3.54) and the taps on the beamformer $\bar{\mathbf{z}}[n]$ the output of the STAP is as follows:

$$y[n] = \mathbf{w}^H\bar{\mathbf{z}}[n] \tag{5.18}$$

The weight set is calculated using Frost's LCMV solution [85] such that the $\mathbf{w}$ is defined as follows:

$$\mathbf{w} = \mathbf{R}_{\bar{z}\bar{z}}^{-1}\mathbf{C}\left[\mathbf{C}^H\mathbf{R}_{\bar{z}\bar{z}}^{-1}\mathbf{C}\right]^{-1}\mathbf{f} \tag{5.19}$$

where $\mathbf{R}_{\bar{z}\bar{z}}$ is the covariance matrix of the equalised samples on each tap of the STAP:

$$\mathbf{R}_{\bar{z}\bar{z}} = \text{E}\left\{\bar{\mathbf{z}}[n]\bar{\mathbf{z}}^H[n]\right\} \tag{5.20}$$

As only the steady-state cancellation performance of the beamformer is of interest, the weight set is calculated using the SMI method described by Reed *et al.* in [95] rather than recursively. Therefore, the covariance matrix must be estimated by taking the sample average of the outer product of $\bar{\mathbf{z}}[n]$ with its Hermitian transpose over N_r blocks:

$$\mathbf{R}_{\bar{z}\bar{z}} \approx \frac{1}{N_r} \sum_{n=0}^{N_r-1} \bar{\mathbf{z}}[n]\bar{\mathbf{z}}^H[n] \tag{5.21}$$

The look direction constraint is defined over K frequencies $\hat{f}_k$ for $k = 0, 1, \ldots, K-1$ specified by the $K \times MK$ constraint matrix $\mathbf{C}$ and the K length column vector $\mathbf{f}$. The formation of both $\mathbf{C}$ and $\mathbf{f}$ are detailed in Section 4.2.1.

5.2.4 Complexity

The complexity of the channel mismatch compensation scheme can be divided between the complexity of the frequency-domain filters used to apply the compensation weights and the adaptive process used to calculate the weights. The complexity of the frequency-domain filters is found mainly in the DFT and IDFT pair required to transform samples between the time-domain and frequency-domain. By implementing these using the FFT a complexity of $1/2 \log_2 N_q$ complex multiplies per transform per N_q samples [116, 121] can be achieved. However, as the input samples must be zero padded by $N_q/2$ samples the efficiency of each transform is reduced by a factor of 2. In addition to this, one complex multiplication is required per sample to apply the weights to the frequency-domain samples. Therefore, the total number of complex multiplications required per channel mismatch filter is given as follows:

$$\text{Complex multiplies} = 2\log_2 N_q \tag{5.22}$$

Both the relative and absolute channel mismatch algorithms required to calculate the weights are also simplified by operating in the frequency-domain. In both cases the channel responses must be estimated by capturing the DFT of the calibration symbol as received by each channel. The DFT in this case can be a shared DFT used by each channel mismatch filter to transform samples into the frequency-domain and, therefore, no extra complexity is added. In order to calculate the channel response estimates, the calibration symbol must be removed from the captured signals which requires one complex division per weight. However, depending on the algorithm, the channel response estimates may not need to be directly computed. In the case of absolute channel mismatch compensation, the reciprocal of each channel response is required rather than the direct channel estimate. As the weights are calculated on a per bin basis this requires one complex division per weight. If a non-unity gain, non zero-phase response is specified as the required absolute response then an additional complex multiply per weight is required to apply the response. In the case of relative mismatch compensation the direct

channel estimate of the reference channel is required while the reciprocal of the channel estimate is required from the remaining channels. However, estimation of both the channel response and inverse channel response is not explicitly required as the weights for each channel can be calculated by the complex division of the captured calibration symbol from each channel, requiring only one complex division per channel per weight.

5.3 Simulation

5.3.1 Methodology

A STAP beamformer with mismatches in its channel responses was simulated so that the performance of the proposed channel mismatch compensation schemes could be verified and studied. In order to predict whether the proposed schemes would be of benefit to the ERA Technology TD the measured front-end channel responses from the ADM channels were used in the simulation as the model for the channel responses. The measured responses for 3 ADM channels was supplied by ERA Technology in the form of magnitude and phase data as shown in Figures 5.4 and 5.5 respectively. Before the measured channel responses could be used in the simulation it needed to be processed to produce filter coefficients suitable for convolution in the channel response filters of the model [107]. The first stage of this required the resampling and interpolation of the magnitude and phase using cubic spline methods to obtain magnitude and phase data at the desired frequency intervals of the simulation. The channel response filter coefficients could then be calculated by taking the IDFT of the resampled and interpolated amplitude and phase data; a IDFT of 512-points was found empirically to provide a suitably close match between the measured response data and processed response data. Each impulse response of the channel response filter coefficients was centred and then a Blackman-Harris window applied to de-emphasis the effects of the ripple in the tails of the impulse responses so as to avoid Gibb's phenomenon [131].

A 3 element ULA antenna with half a wavelength spacing between elements was used to match the number of channels for which measured ADM data was available. Each element was assumed to have an isotropic radiation pattern. Impinging upon the array are two signals: the wanted signal $x(t)$ from an angle $\theta_s = 45°$ and an broadband interference signal $g(t)$ from an angle $\theta_g = 90°$. Given that the interference signal arrives broadside, to the array the decorrelation it experiences is entirely due the interchannel mismatches as opposed to the effects of dispersion. Both the wanted signal $x(t)$ and the interfering signal $g(t)$ were modelled as complex zero-mean Gaussian processes band-limited to the central third of the system bandwidth to match the pass-band of the

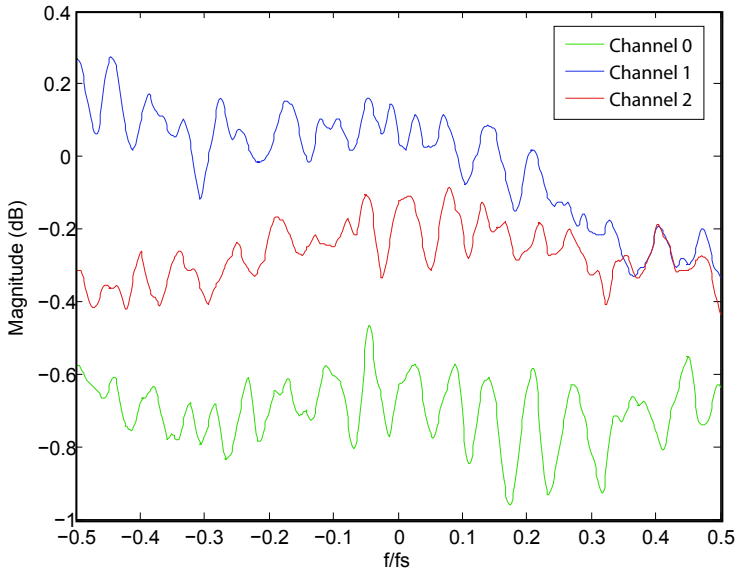

FIGURE 5.4: Magnitude response of beamformer's analogue front-end

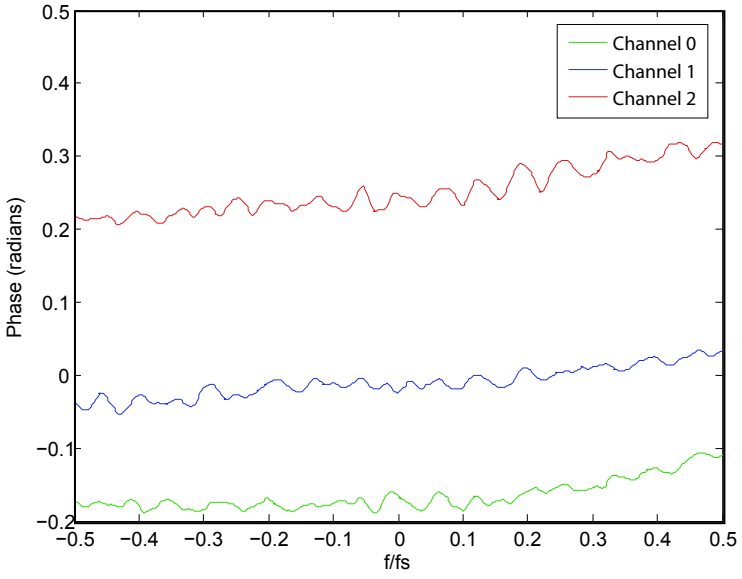

FIGURE 5.5: Phase response of STAP beamformer's analogue front-end

ERA Technology TD. The SNR of the wanted signal $x(t)$ was fixed at $P_x/\sigma_v^2 = -30$ dB to simulate an LPI signal while the INR of the interference signal $g(t)$ was varied as indicated later.

A N_q point frequency-domain filter as described in Section 5.2.1 was used on each channel to remove the channel mismatches. The weight set for each channel mismatch filter was calculated using both the relative or the absolute mismatch compensation methods described in Section 5.2.2. The space-time adaptive processor included $K = 5$ time taps per channel to provide 5 frequency constraints on the STAP weight solution given by Eq.

(5.19). These frequencies were equispaced across the bandwidth of the wanted signal such that the normalised constrained frequencies were at -0.2, -0.1, 0, 0.1, 0.2 relative to the sampling frequency.

The performance of the beamformer with interchannel mismatches was evaluated both with and without the proposed channel mismatch compensation scheme. In each case the cancellation ratio (CR) [68] was used to measure the amount of the interference signal's power that was suppressed by the beamformer. The CR is defined as the ratio of the power's output power over the power of the interference signal:

$$\mathrm{CR} = \frac{E\{|y|^2\}}{E\{|g|^2\}} \tag{5.23}$$

where y is the output signal of the beamformer (see Eq. 5.18) and g is the received interference signal.

Additionally, the SINR was measured at the beamformer's output to measure the effect the mismatch compensation filters had on the wanted signal. Typically, the SINR is determined by measuring the average power of the individual components of the signal at the output of the system. However, this measure does not take into account distortion which may be introduced into the wanted signal by the various elements of the system. Therefore, the following estimator which uses the cross-correlation between the transmitted signal and the output signal to account for decorrelation of the wanted signal is used to determine the SINR [107]:

$$\mathrm{SINR} = \frac{E\{yx^*\}^2}{E\{|y|^2\}E\{|x|^2\} - E\{yx^*\}^2} \tag{5.24}$$

where y is the output of the beamformer and x is the wanted signal.

Finally, the improvement in SINR is used to show the SINR performance of the beamformer when channel mismatch compensation is used relative to the SINR performance when channel mismatch compensation is not used. The SINRs in both cases are measured using Eq. (5.24) and the improvement factor is given as follows:

$$\mu = \frac{\mathrm{SINR}_{mm}}{\mathrm{SINR}_{eq}} \tag{5.25}$$

where SINR_{mm} is the SINR when no compensation is used and SINR_{eq} is the SINR when compensation is used.

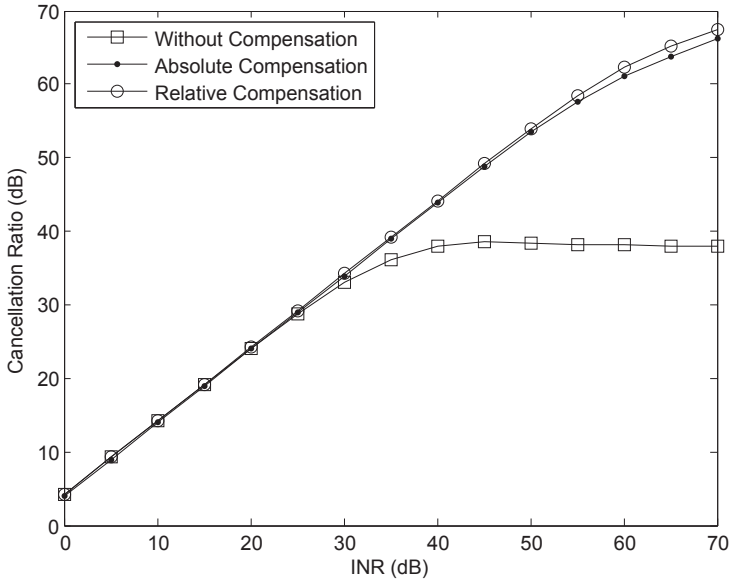

FIGURE 5.6: CR vs. INR with and without channel mismatch compensation

5.3.2 Numerical Results

Initially, the cancellation ratio achieved by the beamformer both with and without channel mismatch compensation was considered. In the first instance, channel mismatch compensation was performed using $N_e = 512$ point frequency-domain equalisers on each channel using both the relative and absolute mismatch compensation schemes. In both cases, perfect knowledge of the channel mismatches was assumed in order to determine an upper limit on the performance of the system. The results comparing INR versus cancellation ratio are shown in Figure 5.6. In all three cases the beamformer is able to null the interferer as fully as possible (i.e. to the thermal noise floor of the system) up to an INR of 25 dB as indicated by the linear relationship between INR and cancellation ratio up to this point. Therefore, for lower levels of interference, the presence of the channel mismatches does not impact on the nulling performance of the beamformer. As the INR is increased beyond 25 dB, the uncompensated system's cancellation ratio quickly asymptotes showing that, in this case, the maximum interference level which can be cancelled is limited to 38 dB. However, with channel mismatch compensation the beamformer is able to fully cancel the interferer up to an INR of 50 dB as indicated by the linear portion of the plots for both relative and absolute mismatch compensation. This confirms that the nulling performance against higher power interferers of the beamformer with mismatches in its channels can be greatly improved by using the channel mismatch compensation scheme. The performance of relative and absolute mismatch compensation are closely matched suggesting that from a nulling only point of view, absolute mismatch compensation does not present any advantage over relative mismatch compensation.

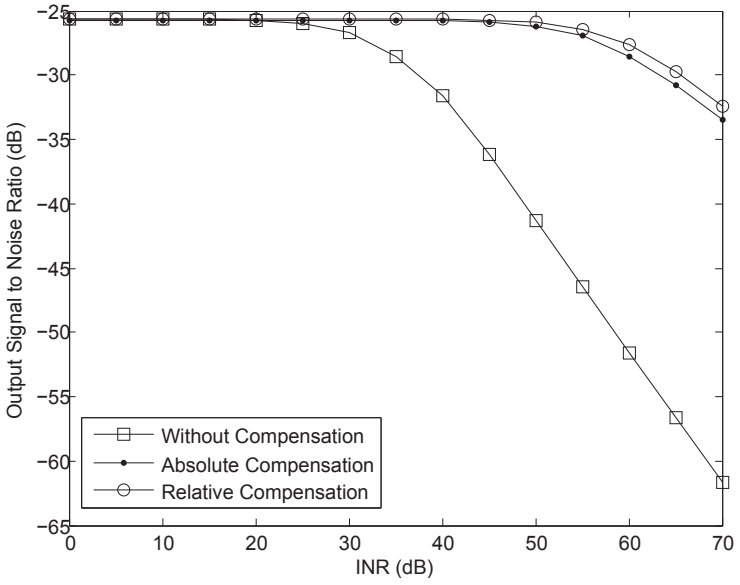

FIGURE 5.7: Output SINR vs. INR with and without mismatch compensation

While the cancellation ratio is a good indicator of the nulling performance of a beamformer it does not take into account any distortion in the wanted signal due to channel mismatches or the subsequent mismatch compensation. Therefore, the output SINR (as defined in Eq. (5.24)) of the beamformer was also measured for the simulation described previously and the results are presented in Figure 5.7. These results follow the cancellation ratio results very closely, indicating that the interference is the main source of SINR degradation as opposed to any distortion being introduced by the channel mismatch or channel compensation. Again the performance of the relative and absolute channel mismatch compensation schemes are very similar.

The performance of the beamformer was considered for different lengths of mismatch compensation filter. The results are shown in Figure 5.8 where the output SINR gain (given by Eq. (5.25)) is used as the figure of merit. The plot show that up to an INR of 50 dB the length of the filter has little effect. As the INR is increased further the SINR improvement of system using $N_q = 512$ length mismatch compensation filters falls off indicating that the beamformer is no longer able to fully cancel the interference signal. In contrast, where mismatch compensation filters with lengths $N_q = 1024$ and $N_q = 2048$ were used full cancellation of the interference signal was possible at higher INRs. This suggests that in the second two cases the longer filter lengths enabled the mismatch compensation filters to achieve a higher level of matching between channels and hence, allowed the beamformer to fully cancel the broadband interferer. For the range of INRs considered increasing the filter length beyond $N_q = 1024$ did not show any improvement.

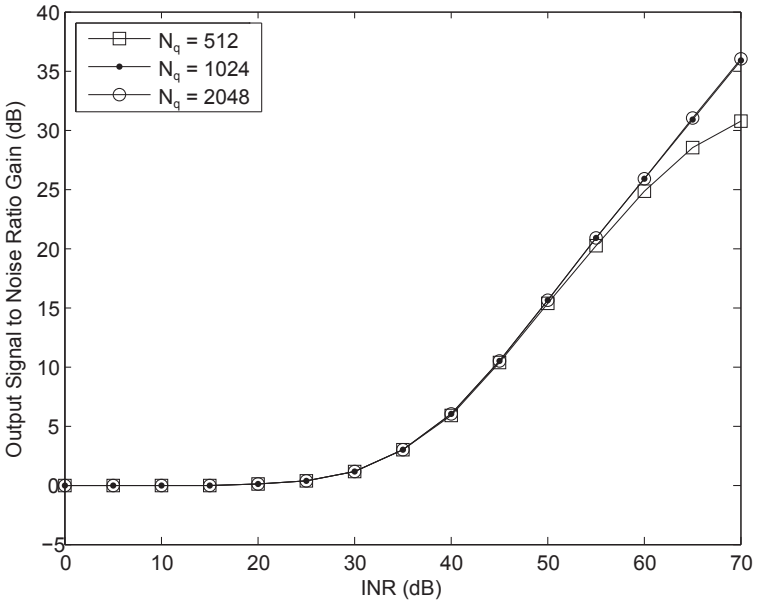

FIGURE 5.8: Output SINR gain vs. INR for various filter lengths

The performance of the system without perfect channel knowledge was also studied; the channel responses were estimated from a single N_q sample calibration symbol at various calibration symbol SNRs. The results for $N_q = 1024$ are shown in Figure 5.9. It should first be noted that in all cases the performance of the relative scheme (denoted Rel) was almost identical to the absolute scheme (denoted Abs). At CNR = 60 dB the SINR gain is almost identical to the performance in Figure 5.8 where perfect channel knowledge was assumed. Reducing the CNR to 40 dB yields a corresponding drop in the beamformer's output SINR gain, thereby reducing the level of interference that can be successfully nulled and hence, lowering the improvement provided by channel mismatch compensation. This is followed further as the CNR is decreased to 20 dB.

5.4 Hardware Experiments

The proposal of the channel mismatch compensation scheme described in Section 5.2.1 was motivated by the development of a STAP technical demonstrator (TD) system at ERA Technology Ltd. An area of interest was highlighted to see if the cancellation performance of the ERA Technology TD could be improved against broadband interference. While the ERA TD showed very high nulling performance against high power narrowband interferers the level of nulling achieved against broadband interferers became limited as the interference level was increased. As mentioned, an area of concern that was identified was in the use of SAW filters in the ADM front-end of the ERA TD. In [123] the problems of ripple in the frequency response of SAW filters and the

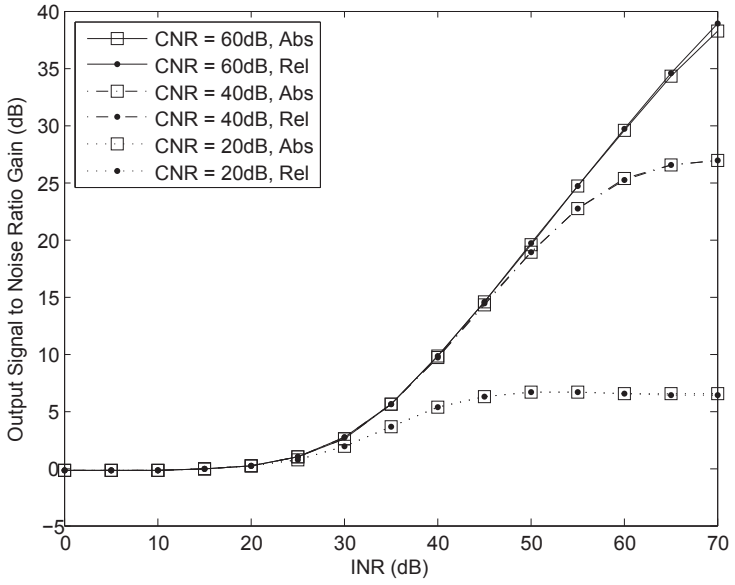

FIGURE 5.9: Output SINR gain vs. INR for various CNRs, N = 1024

associated effects on null depth performance in STAP beamformers was highlighted. Therefore, recognising that simulations can only go so far to show the effectiveness of a particular scheme, it was important to prove the channel mismatch compensation scheme on the TD hardware. In this section, the methodology used to test the channel mismatch compensation scheme in conjunction with the ERA Technology TD is detailed and measured results presented.

5.4.1 System Overview

The TD STAP unit developed by ERA Technology Ltd. is a 4 channel system with 5 time taps per channel. Each channel includes an ADM which mixes radio frequency (RF) L-band signals down to an intermediate frequency (IF). The IF signal on each channel is sampled and quantized before being down-converted to baseband digitally in the digital down-converter (DDC) modules. The sampled data is then spatially and temporally filtered by the STAP weights which are adaptively calculated over blocks of 100 samples per channel. The beamformed data is finally up-converted to the IF frequency suitable for the external receiver module before being output. In order to integrate the channel mismatch compensation scheme with the TD hardware a software-in-the-loop approach was used whereby the channel mismatch compensation scheme was implemented in Matlab and hosted on a PC connected to the TD hardware (Figure 5.10). This was facilitated by the design of the TD unit, which has the ability to capture 32k samples of baseband data per channel from each of the 4 RF input channels simultaneously which can subsequently be transferred to a PC via a JTAG connection.

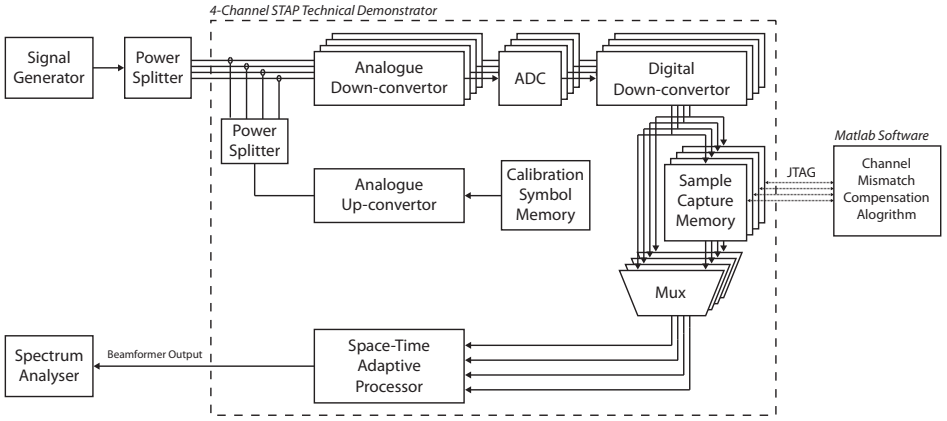

FIGURE 5.10: Experimental setup for TD STAP channel mismatch compensation

Furthermore, data from a PC can be loaded into the 32k sample memories and played back through the beamformer instead of live data.

The TD unit already contained provision for generating, up-converting and injecting a calibration signal into the RF inputs of the ADMs. This is comprised of a 16-bit 4k memory for storing the calibration symbol at an IF of 17.295 MHz and a synthesizer up-conversion module (SUCM) to mix the calibration signal from IF to RF. A power splitter internally distributes the calibration signal to each of the 4 ADM channel RF inputs where it is injected via a coupler. The timing of the various modules of the TD, such as the ADMs and SUCMs, are controlled by a PLL network. This ensures there is no timing drift between the output of the calibration symbol from the calibration memory and the sampling of the channel data at the output of the ADMs.

In order to evaluate the performance of the channel mismatch compensation scheme in conjunction with ERA Technology's TD an experimental setup was assembled as per Figure 5.10. The first step in the channel mismatch compensation process involves estimating the frequency response of each of the ADM channels in order for the weights of the mismatch compensation filters to be calculated. A 512 sample long Chu sequence was generated on the host PC and then loaded into the TD unit's calibration symbol memory. The calibration signal was then played out through each of the 4 ADMs and the signal from each channel captured using the 32k sample channel capture memory. The captured samples from each channel could then be used to estimate each channel's frequency response either by selecting 512 samples from each capture or by coherent averaging over a number of captures of the calibration symbol.

The channel mismatch compensation filter weights required to remove mismatch between the ADM channel responses are calculated on the host PC using the estimated channel responses. Two procedures for calculating the filter weights were detailed in Section 5.2.2 *relative compensation* and *absolute compensation*. As previously noted the first method

aims to match the channels' frequency responses relative to a reference channel, while the second method matches the channels' frequency response to a predetermined response. However, during the course of testing it was noted that the electrical delay experienced by the calibration signal complicated the calculation of filter weights using the absolute compensation method. This is particularly problematic if coherent addition is to used to average over contiguous calibrations symbols in order to improve the calibration signal to thermal noise ratio and would require the delay to be estimated an compensated for. However, this is not the case if the relative channel mismatch compensation scheme is used as the weights are calculated relative to one of the other channels and as such, the effect of the electrical delay is cancelled out as long as the electrical delay for each channel is similar. Given that the simulations in Section 5.3.2 showed little difference in the null depth improvement achieved using absolute mismatch compensation compared with relative mismatch compensation, only the later method was used for this series of experiments.

A signal generator was used to generate a broadband interference signal in the form of an orthogonal frequency-division multiplexing (OFDM) signal with sub-carriers of a uniform magnitude over a 20 MHz band. The interference signal was injected into the 4 ADM RF channel inputs via a power splitter to simulate the interferer arriving from broadside so as to minimise the effects of broadband dispersion due to angle of arrival. The received signal containing the interferer was captured in 32k sample memories of the 4 channels of the TD and transferred to the PC host via the JTAG link for mismatch compensation filtering to be applied in Matlab. At this point the captured interferer data for each ADM channel will have been distorted by the channel response of each respective ADM channel. Channel mismatch compensation filtering was then applied to the captured samples using the relative mismatch compensation weights calculated using the earlier estimate of the ADM channel responses. The compensated data samples of the interference signal were then loaded back into the DDC sample memory of each of the 4 channels and replayed to the beamformer.

The performance of the channel mismatch compensation system was measured in terms of the improvement in null depth, denoted ψ, achieved by the TD unit while adapting against the broadband interferer. The TD beamformer can operate in a number of different beamforming modes of which two were used in the measurement of the null depth improvement. The first mode termed *omni* is a non-adaptive state in which the beamformer produces a fixed omni-directional reception pattern. The second mode termed *omni-adapt* adaptively adjusts the beamformer's weights to produce a power inversion solution so as to provide a nominally omni-directional reception pattern into which nulls are adaptively placed to cancel any received interference. Using both these modes, the null depth improvement, ψ was calculated as the ratio of null depth achieved

using the mismatch compensation filters over the null depth achieved without using the mismatch compensation filters. In each case the null depth was determined by measuring the average power at the output of the TD using a spectrum analyser with the TD beamformer operating in omni mode and then in omni-adapt mode. Therefore, the final improvement in null depth can be given as follows:

$$\psi = \frac{P_{\mathrm{co}} P_{\mathrm{ma}}}{P_{\mathrm{ca}} P_{\mathrm{mo}}} \tag{5.26}$$

where the output power of the TD is given as: P_{mo} for no compensation in omni mode, P_{ma} for no compensation in omni-adapt mode, P_{co} for mismatch compensation in omni mode and P_{ca} for mismatch compensation in omni-adapt mode.

5.4.2 Measured Results

The results of experiments using the ERA Technology TD STAP in conjunction with the proposed channel mismatch compensation scheme are presented in this section. Initially, an example of the magnitude and phase responses of the 4 ADM channels are presented both with and without relative channel mismatch compensation having been applied. In the case of the magnitude responses Figure 5.11(a) plots the ADM responses without any mismatch compensation while Figure 5.11(b) plots the magnitude responses after mismatch compensation. A ripple across the band is evident in both the uncompensated and compensated magnitude responses however, in the uncompensated case further differences between the channels can be observed, these are minimised after compensation has been applied. The phase response of each channel is shown in Figures 5.12(a) before mismatch compensation has been applied and in Figure 5.12(b) after compensation has been applied. In both cases because the mismatch compensation has been applied relative to the first channel perturbations across the band still exist however, rather than differing between channels the mismatch compensation has matched the channels relative to the first channel.

Initially, the effect of the length of the channel mismatch compensation filters on null depth improvement was studied. 4 lengths of filter were considered: 512, 1024, 2048 and 4096, in each case a calibration symbol of equal length was used. It is noted that filter lengths of less than 512 samples were considered however, these resulted in severely distorted estimates of the channel responses. Further investigation of this showed that it was due to the manner in which the TD hardware up-converts the calibration symbol. The calibration symbol memory and up-converter were designed to operate at the same IF as the beamformer in the TD which is at 17.295 MHz. Therefore, the frequency

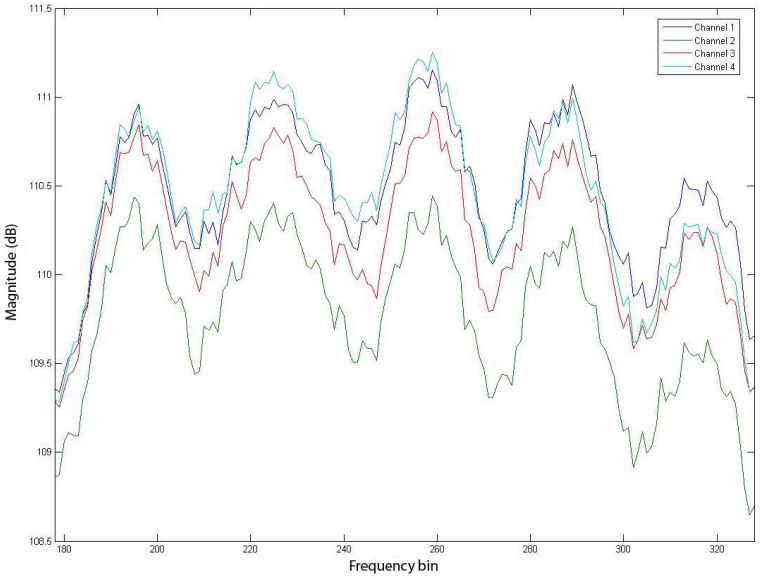

(a) Before mismatch compensation

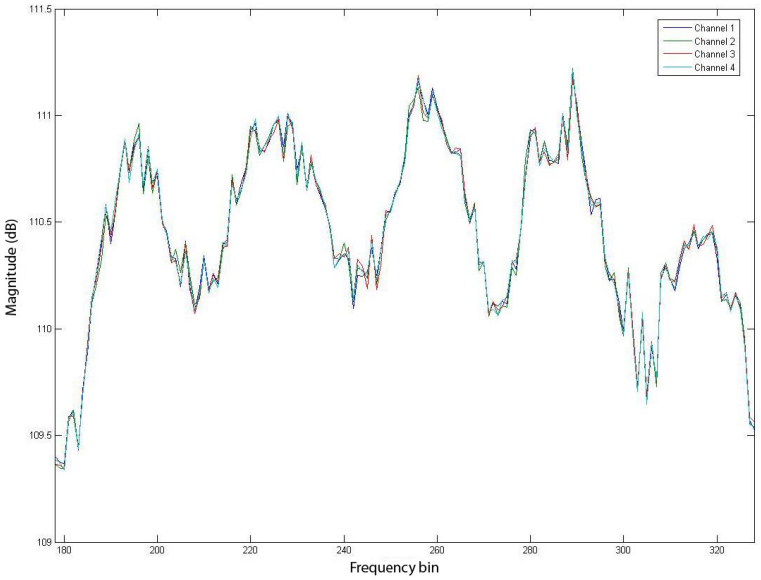

(b) After mismatch compensation

FIGURE 5.11: Magnitude response of ADM channels

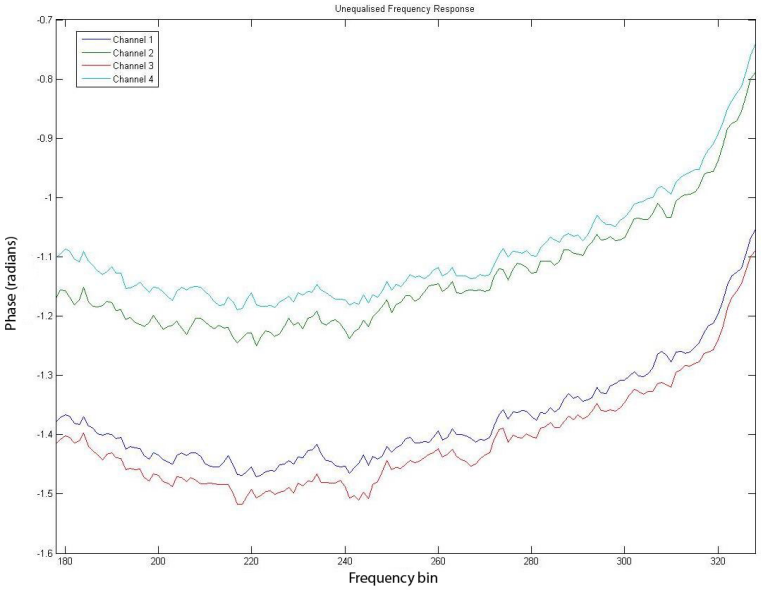

(a) Before mismatch compensation

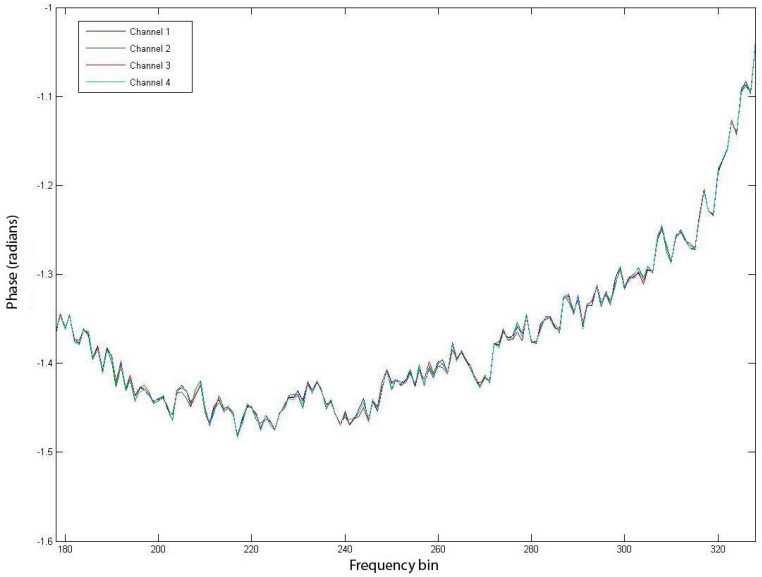

(b) After mismatch compensation

FIGURE 5.12: Phase response of ADM channels

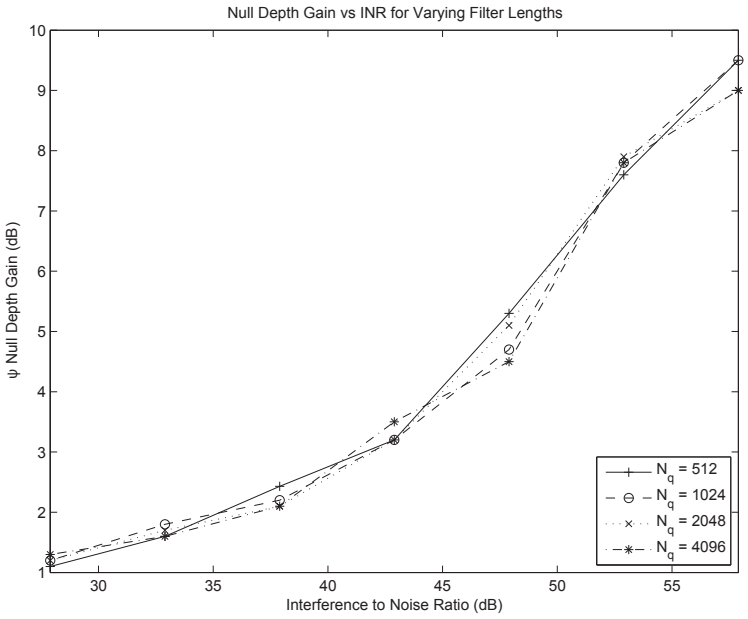

FIGURE 5.13: Interference power vs. null depth gain for varying filter orders

translation experienced by the calibration symbol from IF to RF and then down to baseband in the ADMs resulted in a fractional misalignment of the calibration symbol with the FFTs within the channel compensation filters.

Figure 5.13 shows the improvement in null depth achieved using relative mismatch compensation versus the INR of the broadband interference signal. For these results the ADM channel responses were estimated using a calibration symbol with an SNR of 59 dB - the maximum achievable power into the ADM channels without saturating the analogue to digital converters. For the lengths of filter considered, the improvement in null depth achieved by the mismatch channel compensation filters are similar across the range of INRs. As was evident in the simulation results, the increase in improvement in null depth is small while the INR of the interferers remains low. However, as the INR is further increased the beamformer finds it increasingly difficult to cancel the additional interference power with the mismatches present in the channel responses. It is at this point that the mismatch compensation filters have a greater impact on the null depth achieved by the beamformer as is evidenced by the null depth improvement.

The effect of varying the calibration symbol signal power and hence, the calibration symbol SNR, was investigated to determine its relationship with null depth. The same OFDM symbol used in the previous investigation was used as the broadband interference source. However, the SNR was fixed at 57 dB. As there was little difference in performance when the channel mismatch compensation filter length was varied, a filter length of $N_q = 512$ was used. The SNR of the calibration symbol signal was varied from 27 to 59 dB to obtain ADM channel estimates of differing accuracies from which

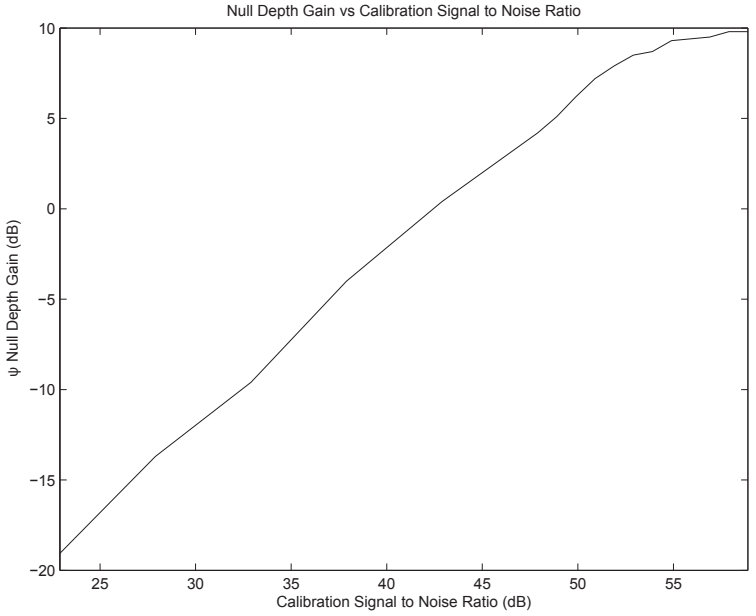

FIGURE 5.14: Calibration SNR vs. null depth gain

the relative channel mismatch compensation weights were calculated and applied to the captured interference signal data. The results shown in Figure 5.14 illustrate the importance of the calibration symbol SNR in achieving good channel matching for improved broadband nulling. At calibration symbol SNRs below 43 dB, the level of thermal noise relative to the calibration symbol is sufficiently high to prevent a sufficiently accurate estimate of the ADM channel responses to be made. This leads to the channel mismatch compensation filters introducing additional distortion into the received signal resulting in further decorrelation of the received signal rather than better channel matching. Increasing the calibration symbol SNR shows that the null depth improvement is linearly proportional to the SNR of the calibration symbol up to a calibration SNR of 52 dB. Beyond this point the null depth improvement asymptotes at 10 dB indicating that there is no further advantage to increasing the calibration symbol SNR. While the source of this limit was not determined, it may well be due to other limiting factors of the hardware, such as precision within the beamformer and would require further investigation.

5.5 Summary

In this chapter, two efficient methods for the compensation of interchannel mismatches in adaptive beamformers have been presented based on frequency-domain filtering. The use of frequency-domain equalisers as opposed to time-domain equalisers allows for larger filter lengths to be realised in hardware and enables the calculation of the weights to be greatly simplified. This is important as longer filter lengths are often necessary to

provide sufficient channel matching to produce deep nulls against broadband interferers. The performance of the scheme was demonstrated using software simulations as well as with a hardware space-time adaptive processor. It was shown that the null depth produced by the STAP beamformer with mismatches against high power interferers could be significantly improved by employing channel mismatch compensation.

Chapter 6

Conclusions and Further Work

In this thesis the protection of LPI DSSS receivers from high levels of interference received from multiple sources simultaneously was considered. Broadband adaptive beamforming was focused upon due to its high interference suppression capability, in particular, its ability to simultaneously cancel multiple sources of interference which are spatially diverse from the wanted signal. However, it was noted that the hardware complexity of broadband adaptive beamforming is typically high, particularly for systems with a high number of channels. Therefore, for small, mobile deployments adaptive beamformers with a limited number of channels are desirable in order to reduce the size, weight and power requirements of the system. However, it was noted that this would limit the degrees of freedom in the beamformer and hence, the cancellation capacity of the number of interference sources which can be simultaneously cancelled by the beamformer. Furthermore, the properties of the received signals such as power and bandwidth also impact upon the number of interferers which can be simultaneously cancelled. Therefore, in order to increase a beamformer's cancellation capacity, while avoiding the cost of adding channels, the benefit of increasing the number of time-taps in a STAP beamformer was studied. A new expression was derived to determine how readily the degrees of freedom due to the additional time taps are consumed by interference with a non-zero bandwidth. It was shown that the use of the time-taps as a method of increasing the cancellation capacity of the STAP beamformer is highly contingent on the properties of the interference. In particular, the sensitivity of the time-taps to the bandwidth of the interference signal with respect to the sampling rate of the taps was noted. It was shown that, at higher INRs, interference signals with relatively small non-zero bandwidths compared with the bandwidth of the STAP were shown to quickly consume all the degrees of freedom due to the time-taps.

This motivated the search for other methods of efficiently increasing the cancellation capacity of adaptive beamforming based interference suppression systems. To this end, a split interference suppression system was considered where frequency-domain excision is used to pre-filter each channel of the beamformer before the adaptive beamforming is applied. The aim of this approach was to remove narrowband interference leaving only partialband and broadband interference to be removed by the beamformer. This method was shown to successfully desensitise the beamformer to the presence of narrowband interference in the form of continuous wave signals by eigenanalysis of the beamformer's covariance matrix. Issues relating to the performance of frequency-domain excision, such as choice of window function, were discussed in relation to the impact this had on the beamformer's performance. Simulation of the system using an LPI DSSS signal was also used to demonstrate the improved interference capacity of the combined system. In particular, the benefit of pre-filtering by frequency-domain excision was demonstrated in an over-stressed environment and also in terms of coverage improvement when used in conjunction with a power inversion beamformer.

It was noted that current algorithms for interference detection in the excision filters are unsuitable for use as pre-filters in adaptive beamformers. A need for the interference detection algorithm to discriminate between narrowband and other forms of interference was identified. A novel interference detection algorithm based on the image processing technique of *opening* for use in the excision filters was presented. The new technique allows for narrowband interferers to be identified for excision while ignoring the presence of partialband or broadband interference. The performance of the frequency-domain excision pre-filters using this algorithm was demonstrated in combination with a STAP beamformer as well as a sub-optimal SFAP beamformer by BER simulation. It was shown that in an overstressed interference environment, in which the beamformer's degrees of freedom were exceeded by the presence of a CW interferer in addition to partialband and broadband interferers, the frequency-domain excision pre-filtering system was able to restore the performance of an LPI DSSS receiver from a completely unrecoverable BER, i.e. 0.5, to within 1 dB of the expected theoretical performance of the receiver in an AWGN only environment. It was noted that the SFAP beamformer, due to the sub-optimality of its weight setting algorithm, experienced the greater improvement in performance compared to the STAP beamformer when frequency-domain excision pre-filtering was used. A further advantage of the frequency-domain excision pre-filtering system was demonstrated in so far as it can provide protection from CW interference in arriving in the mainlobe of the beamformer's beam pattern. In this case it was shown that without pre-filtering a CW interferer could render the output of the beamformer unrecoverable in the demodulator even though the beamformer has sufficient degrees of freedom available to cancel it. However, by employing frequency-domain excision

pre-filters in the beamformer performance was restored to within 1 dB of the theoretical performance.

The problem of degraded cancellation of non-zero bandwidth signals in broadband adaptive beamformers due to interchannel mismatches was also considered. It was noted that additional temporal or spectral degrees of freedom are often required to compensate for these mismatches but at the cost of increased complexity in the beamformer. Therefore, rather than compensate for interchannel mismatches in beamformer it is more efficient to compensate for the mismatches before beamforming is applied to the received signals. Using this approach, two new interchannel mismatch compensation schemes were presented based on efficient frequency-domain methods. The performance of both compensation methods was demonstrated by simulation as well as on a hardware space-time adaptive processing system using a software-in-the-loop approach to implement the algorithms. In each case mismatch compensation was shown to improve the cancellation performance of the beamformer against broadband interference signals.

6.1 Future Work

For communications systems operating in stressed interference environments it is clear that there will always be a drive towards greater interference cancellation performance and capacity. Furthermore, the ability to realise these systems in smaller, more mobile solutions will enable the use of more sophisticated interference suppression in systems where before it was not practical. This goal will be achieved, in part, by advances in the technology of the components themselves allowing for greater miniaturisation as well as better power efficiency but also by improvements in the algorithms through the invention of more efficient methods of implementing those algorithms. To this end it is observed that their is potential for greater efficiency in the implementation of the frequency-domain techniques presented in this thesis. Frequency-domain techniques operating on each channel of an adaptive beamformer have been used for the cancellation of narrowband interference as well as the removal interchannel mismatches. The combination of both of these functions into a single filter seems an obvious one. However, there is further potential for the reduction of hardware if space-frequency adaptive beamforming is used. This leads to the possibility of integrating the interchannel mismatch compensation, narrowband excision and spatial/spectral beamforming into the same DFT/IDFT datapath and avoid the multiple transforms back and forth between time and frequency-domain if they were implemented separately. What is problematic in this suggestion is the difference in spectral resolutions used by the mismatch compensation and excision filters compared with the SFAP beamforming algorithm. Increasing the

number of sub-bands in the SFAP beamformer to match those of the mismatch compensation and excision filters would make the beamforming algorithm prohibitively complex and not realisable in hardware. Therefore, a multi-resolution approach may be possible whereby the signal is initially processed at a higher resolution for the mismatch compensation and excision filters but is then converted down to a lower resolution for the SFAP beamforming algorithm.

The analysis of interference suppression systems is made difficult by the multitude of different forms of interference which may be encountered. Assumptions about the nature of the interference have to be made in order to analyse the problem. An assumption that was made in this thesis was that all interference signals are wide-sense stationary so that the steady state performance of the interference suppression systems could be determined. This is a reasonable enough assumption in an interference environment which changes very slowly with time. However, in reality it is likely that an interference suppression system may encounter interference for which the wide-sense stationarity assumption can not be made. In particular, time varying signals may be pulse modulated or swept in frequency at fast rates. Time varying signals of this nature can pose a problem for adaptive beamforming systems in so far as the signal can adversely modulate the response of beamformer. As frequency-domain excision filtering operates in an open-loop manner it can respond very quickly to changes in the interference environment. Therefore, there is an opportunity for the pre-filtering method to further enhance the interference suppression capabilities of the adaptive beamformer by removing any time-varying narrowband signals. A package of future work would consider non-stationary forms of interference in order to determine the performance of the combined excision beamforming system in such scenarios.

References

[1] N. Tisdale, T. J. Kazmierski, and D. Brooks. A bandwidth selective frequency domain excision filter for use in front of adaptive array antennas. *Proceedings of the IEEE Military Communications Conference*, pages 1–6, October 2007.

[2] N. Tisdale, T. J. Kazmierski, and D. Brooks. Bandwidth selective filter for the pre-excision of narrowband interference in broadband beamformers. *IET Communications Journal*, 4:201–212, 2010.

[3] N. Tisdale, T. J. Kazmierski, and D. Brooks. Channel mismatch compensation for space-time adaptive processors. In *Proceedings on IEEE Military Communications Conference*, pages 1–7, November 2008.

[4] I. Otung. *Communication engineering principles*. Palgrave Macmillan, 2001.

[5] R. Pickholtz, D. Schilling, and L. Milstein. Theory of spread-spectrum communications–a tutorial. *IEEE Transactions on Communications*, 30(5):855–884, 1982.

[6] L. L. Gutman and G. E. Prescott. System quality factors for LPI communications. In *Proceedings of the IEEE International Conference on Systems Engineering*, pages 475–478, August 1989.

[7] USAF Space and Missile Systems Organization. Specification for the NAVSTAR global positioning system. Technical report, United States Air Force, 1977.

[8] R. J. Landry, V. Calmettes, and M. Bousquet. Impact of interference on a generic GPS receiver and assessment of mitigation techniques. In *Proceedings of the IEEE 5th International Symposium on Spread Spectrum Techniques and Applications*, volume 1, pages 87–91, September 1998.

[9] J. J. Spilker. GPS signal structure and performance characteristics. *Journal of the Institute of Navigation*, 25(2):121–145, 1978.

[10] M. K. Simon. *Spread spectrum communications handbook*. McGraw-Hill Education, 2001.

[11] L. Pap. A general jamming model of spread-spectrum systems. In *Proceedings of the IEEE International Conference on Communications*, volume 1, pages 473–477, Geneva, May 1993.

[12] S. G. Glisic. *Advanced wireless communications - 4G technologies.* John Wiley and Sons Ltd, 2004.

[13] M. Spellman. A comparison between frequency hopping and direct spread PN as antijam techniques. *IEEE Communications Magazine*, 21(2):37–42, 1983.

[14] J. D. Laster and J. H. Reed. Interference rejection in digital wireless communications. *IEEE Signal Processing Magazine*, 14(3):37–62, 1997.

[15] H. Meyr, M. Moeneclaey, and S. Fechtel. *Digital communication receivers: synchronization, channel estimation, and signal processing.* John Wiley & Sons, Inc., New York, NY, USA, 1997. ISBN 0471502758.

[16] L. Milstein and R. Iltis. Signal processing for interference rejection in spread spectrum communications. *IEEE Acoustics, Speech and Signal Processing Magazine*, 3(2):18–31, 1986.

[17] L. B. Milstein. Interference rejection techniques in spread spectrum communications. *Proceedings of the IEEE*, 76(6):657–671, 1988.

[18] M. Bouvier Jr. The rejection of large CW interferers in spread spectrum systems. *IEEE Transactions on Communications*, 26(2):254–256, 1978.

[19] M. Abu-Regheff, N. K. Al-shamma, A. N. Sleiman, and W. A. Al-gailani. Cancellation of a sweeping CW interferer in direct sequence spread spectrum signals. In *Proceedings of the Electrotechnical Conference*, pages 399–401, April 1989.

[20] L. D. Gottesman and L. B. Milstein. The performance of a direct sequence spread spectrum acquisition system employing a linear prediction filter. In *Proceedings of the IEEE Global Telecommunications Conference*, volume 3, pages 1597–1601, November 1989.

[21] E. Masry and L. Milstein. Performance of DS spread-spectrum receiver employing interference-suppression filters under a worst-case jamming condition. *IEEE Transactions on Communications*, 34(1):13–21, 1986.

[22] J. Ketchum and J. Proakis. Adaptive algorithms for estimating and suppressing narrow-band interference in PN spread-spectrum systems. *IEEE Transactions on Communications*, 30(5):913–924, 1982.

[23] F. Hsu and A. Giordano. Digital whitening techniques for improving spread spectrum communications performance in the presence of narrowband jamming and interference. *IEEE Transactions on Communications*, 26(2):209–216, 1978.

[24] N. Levinson. The Wiener RMS (root-mean-square) error criterion in filter design and prediction. *Review of the International Statistical Institute*, 28:233–244, 1960.

[25] J. Durbin. The fitting of time series models. *Journal of Mathematical Physics*, 25: 261–278, 1947.

[26] J. P. Burg. Maximum entropy spectral analysis. In *Proceedings of the 37th Meeting of the Society of Exploration Geophysicists*, 1967.

[27] L. Loh-Ming and L. Milstein. Rejection of narrow-band interference in PN spread-spectrum systems using transversal filters. *IEEE Transactions on Communications*, 30(5):925–928, 1982.

[28] L. Loh-Ming and L. Milstein. Rejection of pulsed CW interference in PN spread-spectrum systems using complex adaptive filters. *IEEE Transactions on Communications*, 31(1):10–20, 1983.

[29] M. Morf, B. Dickinson, T. Kailath, and A. Vieira. Efficient solution of covariance equations for linear prediction. *IEEE Transactions on Acoustics, Speech and Signal Processing*, 25(5):429–433, October 1977.

[30] C. Wang and L. B. Milstein. Rejection of multiple narrow-band interference in both BPSK and QPSK DS spread-spectrum systems. *IEEE Transactions on Communications*, 36(2):195–204, 1988.

[31] G. Saulnier, P. Das, and L. Milstein. An adaptive digital suppression filter for direct-sequence spread-spectrum communications. *IEEE Journal on Selected Areas in Communications*, 3(5):676–686, 1985.

[32] L. Loh-Ming and L. Milstein. Rejection of CW interference in QPSK systems using decision-feedback filters. *IEEE Transactions on Communications*, 31(4):473–483, 1983.

[33] L. Loh-Ming and L. Milstein. Correction to "rejection of CW interference in QPSK systems using decision-feedback filters". *Communications, IEEE Transactions on*, 31(9):1116–1116, 1983.

[34] J. F. Doherty. Linearly constrained interference rejection for improved spread spectrum performance. In *Proceedings on IEEE International Conference on Communications*, volume 3, pages 1257–1261, June 1992.

[35] J. F. Doherty. Linearly constrained direct-sequence spread-spectrum interference rejection. *IEEE Transactions on Communications*, 42(234):865–872, 1994.

[36] D. S. Roberts and M. G. Amin. Linear vs. bilinear time-frequency methods for interference mitigation in direct sequence spread spectrum communication systems. In *Conference Record of the Twenty-Ninth Asilomar Conference on Signals, Systems and Computers*, volume 2, pages 925–929, October 1995.

[37] M. G. Amin, A. R. Lindsey, and C. Wang. On the application of time-frequency distributions in the excision of pulse jamming in spread spectrum communication systems. In *Proceedings of the IEEE Signal Processing Workshop on Statistical Signal and Array Processing*, pages 152–155, June 1996.

[38] M. G. Amin. Interference mitigation in spread spectrum communication systems using time-frequency distributions. *IEEE Transactions on Signal Processing*, 45 (1):90–101, 1997.

[39] C. Wang and M. G. Amin. Performance spectrum analysis of interference excisions in spread communications based on instantaneous frequency estimation. In *Proceedings of the Fourth International Symposium on Signal Processing and Its Applications*, volume 2, pages 638–641, August 1996.

[40] C. Wang and M. G. Amin. Performance analysis of instantaneous frequency-based interference excision techniques in spread spectrum communications. *IEEE Transactions on Signal Processing*, 46(1):70–82, 1998.

[41] M. G. Amin, C. Wang, and A. R. Lindsey. Optimum interference excision in spread spectrum communications using open-loop adaptive filters. *IEEE Transactions on Signal Processing*, 47(7):1966–1976, 1999.

[42] L. Milstein and P. Das. An analysis of a real-time transform domain filtering digital communication system–part ii: wide-band interference rejection. *IEEE Transactions on Communications*, 31(1):21–27, 1983.

[43] R. C. DiPietro. An FFT based technique for suppressing narrow-band interference in PN spread spectrum communications systems. In *Proceedings of the IEEE International Conference on Acoustics, Speech, and Signal Processing*, pages 1360–1363, May 1989.

[44] J. A. Young and J. S. Lehnert. Analysis of DFT-based frequency excision algorithms for direct-sequence spread-spectrum communications. *IEEE Transactions on Communications*, 46(8):1076–1087, 1998.

[45] X. Ouyang and M. G. Amin. Performance analysis of the DS/SS communications receiver implementing a short time Fourier transform interference excision system. In *Proceedings of the IEEE International Symposium on Time-Frequency and Time-Scale Analysis*, pages 393–396, October 1998.

[46] J. Gevargiz, P. Das, O. McKee, and J. Moran. Implementation of a 200 MHz transform domain processing spread spectrum receiver with narrow-band adaptive interference exciser. In *Proceedings of the IEEE Ultrasonics Symposium*, pages 108–113, 1985.

[47] L. Milstein and P. Das. An analysis of a real-time transform domain filtering digital communication system–part ii: narrow-band interference rejection. *IEEE Transactions on Communications*, 28(6):816–824, 1980.

[48] R. Rifkin. Comments on "narrow-band interference rejection using real-time Fourier transforms". *IEEE Transactions on Communications*, 39(9):1292–1294, 1991.

[49] R. F. Guertin, R. C. Johnson, and D. A. Wamsley. Monte Carlo analysis of matched-filter performance after narrowband interference suppression. In *Proceedings of the IEEE Military Communications Conference*, volume 3, pages 1161–1166, September 1990.

[50] J. A. Young and J. S. Lehnert. Sensitivity loss of real-time DFT-based frequency excision with direct sequence spread-spectrum communication. In *Proceedings of the Tactical Communications Conference*, volume 1, pages 409–420, May 1994.

[51] P. T. Capozza, B. J. Holland, T. M. Hopkinson, and R. L. Landrau. A single-chip narrow-band frequency-domain excisor for a global positioning system (GPS) receiver. *IEEE Journal of Solid-State Circuits*, 35(3):401–411, 2000.

[52] S. Davidovici and E. G. Kanterakis. Radiometric detection of direct-sequence spread-spectrum signals using interference excision. *IEEE Journal on Selected Areas in Communications*, 7(4):576–589, 1989.

[53] F. J. Harris. On the use of windows for harmonic analysis with the discrete Fourier transform. *Proceedings of the IEEE*, 66(1):51–83, 1978.

[54] D. B. Ruth and M. A. Wickert. A time varying transform domain excision filter for interference rejection in direct-sequence spread-spectrum. In *Proceedings of the IEEE Military Communications Conference*, volume 3, pages 908–912, October 1992.

[55] P. Daryani, E.G. Kanterakis, and S. Davidovici. The effect of spectral shaping on the probability of detection of a DS-SS in the presence of CW interference. In *Proceedings of the IEEE Military Communications Conference*, volume 2, pages 335–339, October 1989.

[56] M. J. Medley, G. Saulnier, and P. Das. Applications of the wavelet transform in spread spectrum communications systems. *Proceedings of SPIE - Wavelet Applications*, pages 54–68, 1994.

[57] M. Mettke, M. J. Medley, G. J. Saulnier, and P. Das. Wavelet transform excision using IIR filters in spread spectrum communication systems. In *Proceedings of the IEEE Global Telecommunications Conference*, volume 3, pages 1627–1631, November 1994.

[58] S. Barbarossa, A. Scaglione, S. Spalletta, and S. Votini. Adaptive suppression of wideband interferences in spread-spectrum communications using the Wigner-Hough transform. In *Proceedings of the IEEE International Conference on Acoustics, Speech, and Signal Processing*, volume 5, pages 3861–3864, April 1997.

[59] J. Vartiainen, J. Lehtomaki, H. Saarnisaari, and M. Juntti. Interference suppression in several transform domains. In *Proceedings of the IEEE Military Communications Conference*, volume 4, pages 2294–2300, October 2005.

[60] J. J. Lehtomaki, J. Vartiainen, and H. Saarnisaari. Domain selective interference excision and energy detection of direct sequence signals. In *Proceedings of the 6th Nordic Signal Processing Symposium*, pages 216–219, 2004.

[61] S. Aromaa, P. Henttu, and M. Juntti. Transform-selective interference suppression algorithm for spread-spectrum communications. *IEEE Signal Processing Letters*, 12(1):49–51, 2005.

[62] B. Allen and M. Ghavami. *Adaptive array systems: fundamentals and applications.* John Wiley and Sons, 2005. ISBN 0470861894.

[63] X. Ping, M. J. Medley, and S. N. Batalama. Spatial and temporal processing for global navigation satellite systems: the GPS receiver paradigm. *IEEE Transactions on Aerospace and Electronic Systems*, 39(4):1471–1484, 2003.

[64] R. T Compton Jr. *Adaptive antennas: concepts and performance.* Prentice Hall, 1988.

[65] R. T. Compton Jr. The bandwidth performance of a two-element adaptive array with tapped delay-line processing. *IEEE Transactions on Antennas and Propagation*, 36(1), January 1988.

[66] M. Zatman. How narrow is narrowband? *IEE Proceedings on Radar, Sonar and Navigation*, 145(2):85–91, April 1998.

[67] B. Widrow, P. E. Mantey, L. J. Griffiths, and B. B. Goode. Adaptive antenna systems. *Proceedings of the IEEE*, 55(12):2143–2159, December 1967.

[68] R. A. Monzingo and T. W. Miller. *Introduction to adaptive arrays*. John Wiley & Sons, 1980.

[69] R. T. Compton Jr. The relationship between tapped delay-line and FFT processing in adaptive arrays. *IEEE Transactions on Antennas and Propagation*, 36(1):15–26, January 1988.

[70] R. G. Lyons. *Understanding digital signal processing*. Prentice Hall, 2004.

[71] C. L. Koh and S. Weiss. Performance and complexity comparison of broadband beamforming structures. In *Sensor Array and Multichannel Signal Processing Workshop Proc.*, pages 124–128, July 2004.

[72] R. L. Fante and J. J. Vaccaro. Wideband cancellation of interference in a GPS receive array. *IEEE Transactions on Aerospace and Electronic Systems*, 36(2): 549–564, April 2000.

[73] C. L. Koh, S. Weiss, and W. Liu. A comparison of adaptive beamforming implementations for wideband scenarios. In *Proceedings of the 2nd IEE/EURASIP Conference on DSP Enabled Radio*, page 9, September 2005.

[74] P. Howells. Explorations in fixed and adaptive resolution at GE and SURC. *IEEE Transactions on Antennas and Propagation*, 24(5):575–584, September 1976.

[75] S. Applebaum. Adaptive arrays. *IEEE Transactions on Antennas and Propagation*, 24(5):585–598, September 1976.

[76] S. W. W. Shor. Adaptive technique to discriminate against coherent noise in a narrow-band system. *Acoustical Society of America Journal*, 39:74, 1966.

[77] R. T. Compton Jr. The power-inversion adaptive array: concept and performance. *IEEE Transactions on Aerospace and Electronic Systems*, 15(6):803–814, November 1979.

[78] C. L. Zahm. Application of adaptive arrays to suppress strong jammers in the presence of weak signals. *IEEE Transactions on Aerospace and Electronic Systems*, 9(2):260–271, March 1973.

[79] S. Haykin. *Adaptive filter theory*. Prentice Hall, fourth edition, September 2001. ISBN 0130901261.

[80] J. Capon. High-resolution frequency-wavenumber spectrum analysis. *Proceedings of the IEEE*, 57(8):1408–1418, August 1969.

[81] C. A. Baird and C. L. Zahm. Performance criteria for narrowband array processing. In *Proceedings of the IEEE Conference on Decision and Control*, volume 10, pages 564–565, December 1971.

[82] H. Cox. Optimum arrays and the Schwartz inequality. *Acoustical Society of America Journal*, 45:228–232, 1969.

[83] D. J. Edelblute. Criteria for optimum-signal-detection theory for arrays. *Acoustical Society of America Journal*, 41:199–205, 1967.

[84] H. Cox. Resolving power and sensitivity to mismatch of optimum array processors. *Acoustical Society of America Journal*, 54:771–785, 1973.

[85] O. L. Frost. An algorithm for linearly constrained adaptive array processing. In *Proceedings of the IEEE*, volume 60, pages 926–935, August 1972.

[86] L. Griffiths and C. Jim. An alternative approach to linearly constrained adaptive beamforming. *IEEE Transactions on Antennas and Propagation*, 30(1):27–34, January 1982.

[87] B. D. Van Veen. Minimum variance beamforming with soft response constraints. *IEEE Transactions on Signal Processing*, 39(9):1964–1972, September 1991.

[88] B. D. Van Veen and K. M. Buckley. Beamforming: a versatile approach to spatial filtering. *IEEE Acoustics, Speech and Signal Processing Magazine*, 5(2):4–24, April 1988.

[89] S. Chen, N. N. Ahmad, and L. Hanzo. Adaptive minimum bit-error rate beamforming. *IEEE Transactions on Wireless Communications*, 4(2):341–348, March 2005.

[90] S. Wei and M. G. Amin. A self-coherence anti-jamming GPS receiver. *IEEE Transactions on Signal Processing*, 53(10):3910–3915, 2005.

[91] B. Widrow. *Aspects of network and system theory*, chapter Adaptive Filter, pages 563–587. Holt, Rinehart and Winston, 1970.

[92] K. D. Senne and L. L. Horowitz. New results on convergence of the discrete-time LMS algorithm applied to narrowband adaptive arrays. In *Proceedings of the IEEE Conference on Decision and Control including the 17th Symposium on Adaptive Processes*, volume 17, pages 1166–1167, January 1978.

[93] P. S. R. Diniz. *Adaptive filtering: algorithms and practical implementation.* Kluwer Academic Publishers, second edition, 2002.

[94] K. J. Suen. A study of eigenvalue behaviour in adaptive arrays. Master's thesis, ElectroScience Lab. Ohio State University, Columbia, USA, 1981.

[95] I. S. Reed, J. D. Mallett, and L. E. Brennan. Rapid convergence rate in adaptive arrays. *IEEE Transactions on Aerospace and Electronic Systems*, 10(6):853–863, November 1974.

[96] I. S. Reed, J. D. Mallett, and L. E. Brennan. Sample matrix inversion technique. In *Proceedings of the Adaptive Antenna Systems Workshop*, volume 1, pages 219–222, March 1974.

[97] C. A. Baird. Recursive processing for adaptive arrays. In *Proceedings of the Adaptive Antenna Systems Workshop*, pages 163–182, March 1974.

[98] R. L. Walke, R. W. M. Smith, and G. Lightbody. Architectures for adaptive weight calculation on ASIC and FPGA. In *Conference Record of the Thirty-Third Asilomar Conference on Signals, Systems, and Computers*, volume 2, pages 1375–1380, 1999.

[99] H. T. Kung and C. E. Leiserson. Systolic arrays (for VLSI). In *Proceesings on Sparse Matrix, Society of Applied Mathematics*, pages 256–282, 1978.

[100] W. M. Gentleman and H. T. Kung. Matrix triangularization by systolic arrays. In *Proceedings of the Society of Photo-Optical Instrumentation Engineers Conference Series*, volume 298, pages 19–26, January 1981.

[101] I. Gupta. Effect of jammer power on the performance of adaptive arrays. *IEEE Transactions on Antennas and Propagation*, 32(9):933–938, September 1984.

[102] W. E. Rodgers and R. T. Compton. Adaptive array bandwidth with tapped delay-line processing. *IEEE Transactions on Aerospace and Electronic Systems*, 15(1): 21–28, January 1979.

[103] F. W. Vook and R. T. Compton Jr. Bandwidth performance of linear adaptive arrays with tapped delay-line processing. *IEEE Transactions on Aerospace and Electronic Systems*, 28(3):901–908, July 1992.

[104] T. D. Moore and I. J. Gupta. The effect of interference power and bandwidth on space-time adaptive processing. In *Proceedings of the IEEE Antennas and Propagation Society International Symposium*, volume 1, pages 53–56, June 2003.

[105] L. Y. Materum and J. S. Marciano Jr. Wideband nulling capability estimate of a tapped delay line beamformer. In *Proceedings of the IEEE Topical Conference on Wireless Communication Technology*, pages 386–387, 2003.

[106] C. Yeh, Y. J. Hong, and D. R. Ucci. Use of the tapped delay line adaptive array to increase the number of degrees of freedom for interference suppression. *IEEE Transactions on Aerospace and Electronic Systems*, 23(6):809–813, November 1987.

[107] M. Jeruchim, P. Balaban, and K. Shanmugan. *Simulation of ommunication systems*. Applications of Communications Theory. Plenum Press, New York, 1992.

[108] Matlab. www.mathworks.com.

[109] J. Proakis. *Digital communications*. McGraw Hill Higher Education, fourth edition, 2000.

[110] R. Pickholtz, D. Schilling, and L. Milstein. Revisions to "theory of spread-spectrum communications–a tutorial". *IEEE Transactions on Communications*, 32:211–212, 1984.

[111] W.D. White. Wideband interference cancellation in adaptive sidelobe cancellers. *IEEE Transactions on Aerospace and Electronic Systems*, 19(6):915–925, November 1983.

[112] J. E. Hudson. *Adaptive array principles*. IEE Electromagnetic Wave Series 11. IEE, first edition, 1981. ISBN 0863412475.

[113] J. O. Smith III. *Mathematics of the discrete Fourier transform (DFT): with audio applications*. W3K Publishing, second edition, 2007.

[114] J. A. Young and J. S. Lehnert. Performance metrics for windows used in real-time DFT-based multiple-tone frequency excision. *IEEE Transactions on Signal Processing*, 47(3):800–812, 1999.

[115] E. Anderson, Z. Bai, C. Bischof, S. Blackford, J. Demmel, J. Dongarra, J. Du Croz, A. Greenbaum, S. Hammarling, A. McKenney, and D. Sorensen. *LAPACK user's guide*. SIAM, Philadelphia, third edition, 1999.

[116] S. He and M. Torkelson. Design and implementation of a 1024-point pipeline FFT processor. In *Proceedings of the IEEE Custom Integrated Circuits Conference*, pages 131–134, May 1998.

[117] J. A. Vite-Frias, R. J. Romero-Troncoso, and A. Ordaz-Moreno. Vhdl core for 1024-point radix-4 FFT computation. In *In Proceedings of the IEEE Computer*

Society International Conference on Reconfigurable Computing and FPGAs, pages 4 pp.–24, September 2005.

[118] A. V. Oppenheim, R. W. Schafer, and J. R. Buck. *Discrete-time signal processing.* Prentice-Hall, Inc., Upper Saddle River, NJ, USA, second edition, 1999.

[119] C. L. Dolph. A current distribution for broadside arrays which optimizes the relationship between beam width and side-lobe level. *Proceedings of the IRE*, 34 (6):335–348, June 1946.

[120] M. J. Ready, M. L. Downey, and L. J. Corbalis. Automatic noise floor spectrum estimation in the presence of signals. In *Conference Record of the Thirty-First Asilomar Conference on Signals, Systems & Computers*, volume 1, pages 877–881, November 1997.

[121] S. He and M. Torkelson. A new approach to pipeline FFT processor. In *Proceedings of the 10th International Parallel Processing Symposium*, pages 766–770, April 1996.

[122] J. Proakis, M. Salehi, and G. Bauch. *Contemporary communication systems using MATLAB.* Brooks Cole, second edition, 2003.

[123] The MITRE Corporation. On the number of time-taps needed for high anti-jam STAP for GPS system. Technical report, The MITRE Corporation, 2006.

[124] S. Wu and Y. Li. Adaptive channel equalization for space-time adaptive processing. *Proceedings of the IEEE International Radar Conference*, pages 624–628, May 1995.

[125] H. Xue, V. Kezys, and J. Litva. Smart antenna calibration for beamforming. In *Proceedings of the IEEE Antennas and Propagation Society International Symposium*, volume 3, pages 1458–1461, June 1998.

[126] A. Kortke. A new calibration algorithm for smart antenna arrays. In *Proceedings of the 57th IEEE Semi-annual Vehicular Technology Conference*, volume 2, pages 1030–1034, April 2003.

[127] L. Wu, G. Liao, and L. Zhang. A blind calibration method for smart antenna system. In *Proceedings on the IEEE Region 10 Conference on Computers, Communications, Control and Power Engineering*, volume 2, pages 1031–1034, October 2002.

[128] D. Falconer, S. L. Ariyavisitakul, A. Benyamin-Seeyar, and B. Eidson. Frequency domain equalization for single-carrier broadband wireless systems. *IEEE Communications Magazine*, 40(4):58–66, April 2002.

[129] S. U. H. Qureshi. Adaptive equalization. *Proceedings of the IEEE*, 73(9):1349–1387, September 1985.

[130] D. Chu. Polyphase codes with good periodic correlation properties (corresp.). *IEEE Transactions on Information Theory*, 18(4):531–532, July 1972.

[131] C. Pan. Gibbs phenomenon removal and digital filtering directly through the fast Fourier transform. *IEEE Transactions on Signal Processing*, 49(2):444–448, February 2001.